博士論文

Stray-corrosion-free surface texturing through electrochemical machining with electrolyte absorbed in a porous solid ball

多孔質固体ボールに吸収された電解液を用いた電解加工による漂遊腐食のない表面テクスチャリング

September, 2022

東京農工大学　大学院工学府

機械システム工学専攻

Wang Jiankang　（王 建康）

Content

Chapter 1 Introduction 1
1.1 Principle, background, and processing method of ECM 1
1.1.1 Principle of ECM 1
1.1.2 Background of ECM 3
1.1.3 Processing method of ECM 5
1.2 Several necessary devices of ECM 7
1.2.1 Power supply 7
1.2.2 Tool electrode 8
1.2.3 Electrolyte, electrolyte supply and filter system 8
1.2.4 Workpiece 9
1.3 Advantages and disadvantages of ECM 10
1.3.1 Advantages of ECM 10
1.3.2 Disadvantages of ECM 11
1.3.3 Solutions about reduce stray-corrosion 13
1.4 Research purpose and significance 20
1.5 Dissertation structure 23
Chapter 2: Processing method, mechanism, and experimental verification 27
2.1 Introduction 27
2.2 Experimental equipment 28
2.2.1 Workpiece and electrolyte 28
2.2.2 Power supply 29
2.2.3 Waveform generator 30
2.2.4 CNC machine 30
2.3 Measurement equipment 32
2.3.1 3D measurement device 32
2.3.2 Cross-section measurement device 33
2.4 Selection and trying of electrolyte absorption materials 34
2.4.1 Attempting with diatomaceous earth 34
2.4.2 Attempting with MFS-ball 37
2.5 Introduction of MFS-ball 42
2.6 Electrolyte absorption principle of MFS-ball 45
2.7 Processing mechanism and Experimental method 48
2.7.1 Electrode with a V-shaped cross-section track 48
2.7.2 Processing method 49
2.7.3 Experimental procedure 50

2.8 Experimental result 53
2.8.1 Mechanical grinding effect of MFS-ball 53
2.8.2 Experimental result and measurement result 54
2.9 Discussion about processed result 57
2.9.1 Discussion about electrolyte distribution 57
2.9.2 Discussion about machining current paths 59
2.10 Conclusion 65
Chapter 3 Simulation and verification of processed result of ECM 67
3.1 Introduction 67
3.2 Concept and geometry model for simulation 68
3.3 Multiphysics formulations 71
3.4 Simulation results 72
3.4.1 Simulation results of potential, current density distribution, and processed result 72
3.4.2 Simulation by changing electrical conductivities of MFS-ball 76
3.5 Discussion of experimental results with simulation results 79
3.5.1 Point processing method and result 79
3.5.2 Discussion and comparison between point processing result and simulation result 81
3.6 Discussion of groove processing and point processing in ECM 83
3.6.1 Discussion between point processing and groove processing 84
3.6.2 Verification of point processing and groove processing 86
3.7 Conclusion 88
Chapter 4 Influence of processing parameters and optimal parameters selection 89
4.1 Introduction 89
4.2 Influence of pressure between workpiece and MFS-ball 90
4.3 Influence of electrolyte flow rate 93
4.4 Influence and necessity of pre-scanning 96
4.4.1 Influence of pre-scanning 96
4.4.2 Necessity of pre-scanning 98
4.5 Influence of machining current and selection of optimal machining current value 101
4.5.1 Influence of different machining current value 101
4.5.2 Selection of optimal machining current value 102
4.6 Influence of machining time 104
4.7 Influence of workpiece moving speed 106
4.8 Influence of MFS-ball's size difference and solution 109
4.8.1 Influence of MFS-ball's size difference 109
4.8.2 Solution of MFS-ball's size difference 112

4.9 Conclusion 117
Chapter 5 Applications of this ECM method 119
5.1 Introduction 119
5.2 Processing of wide groove 120
5.2.1 Processing method 120
5.2.2 Processing result of wide groove 123
5.2.3 Comparison between wide groove measurement result and calculation result and analysis 129
5.3 Metal marking processing with universal moving unit 131
5.3.1 Introduction of metal marking 131
5.3.2 Introduction of universal moving unit and processing principle 133
5.3.3 Processing method of metal marking 136
5.3.4 Processing result of metal marking 139
5.3.5 Discussion about metal marking 140
5.4 Oil pocket processing 142
5.4.1 Introduction of oil pocket and its processing method 142
5.4.2 Experimental equipment and groove processing method 146
5.4.3 Groove processing result of ON 10 mm / OFF 10 mm 150
5.4.4 Groove processing grocessing result of different groove lengths 151
5.4.5 Groove processing result of different moving speed 152
5.4.6 Discussion of groove processing 154
5.5 Conclusions 156
Chapter 6 Shortcomings, future issues and conclusions 157
6.1 Shortcomings and future issues 157
6.2 Conclusions 158
Renference 165
Acknowledgements 174
Published papers related to this dissertation 176

Chapter 1 Introduction

1.1 Principle, background, and processing method of ECM

1.1.1 Principle of ECM

Electrochemical machining (ECM) [1-6] is a non-conventional machining method, which is basing on the principle of electrolysis to remove metallic materials at the atomic level.

As the basic principle of ECM, electrolysis is a chemical etching process, during which, electric currents pass electrolyte solutions of the working gas between the tool electrode and the workpiece with a certain gap distance [5, 6]. The tool electrode is connected with the negative pole of the power supply to be used as the cathode of ECM, and the electrode is usually made of copper, brass, or stainless steel. Used as the anode, the workpiece, which need to be processed into the desired shape, is connected with the positive pole of the power supply. In ECM processing, workpiece materials must be metallic bonded material, otherwise, electrolysis will not occur. To ensure that there are electrolytes existing in the working gap, the workpiece and the tool electrode are normally are immersed in the electrolyte, which is contained by the electrolyte tank combining with a filtering system.

The electrolyte solution is another necessary component in ECM [4, 5], because it plays the role of carrying the machining current and removing ECM by-products at the working gap. The electrolyte must be low corrosive, low toxic, high conductivity, and well electrochemical stable. It can be aqueous solutions such as sodium (NaCl) or sodium nitrate (NaNO3). When processing some special materials like tungsten materials [7], NaOH solution or KOH solution will be used as the electrolyte.

When being diluted, the electrolyte will contain ions of salt and water. Sodium chloride is the most common electrolyte used in ECM because it is useful for machining stainless steel with a very shiny surface. And it does not produce the passive film on the stainless steel surface while letting the workpiece be processed quickly [8]. When the sodium chloride is put into water, it

will dissociate into sodium ions (Na^+) and chloride ions (Cl^-). At the same time, water (H_2O) will be dissociated into hydrogen ions (H^+) and hydroxyl ions (OH^-).

When there is a potential difference provided by the power supply existing between the workpiece and the electrode, these ions of the electrolyte solution move in the working gap. During which, the cations of OH^- move toward the workpiece surface, while the anions of H^+ move toward the anode due to the action of the electric field. As shown in the schematic of the electrochemical machining principle in Figure 1.1, since hydrogen ions have higher ionic mobility than sodium ions, hydrogen ions will move to the surface of the electrode to produce hydrogen gas of H_2. Meanwhile combining with the hydroxyl ions in the electrolyte, sodium ions will form sodium hydroxide.

$$NaCl \rightarrow Na^+ + Cl^- \quad (1)$$

$$H_2O \rightarrow H^+ + OH^- \quad (2)$$

$$2H^+ + 2e^- \rightarrow H_2\uparrow \quad (3)$$

On the workpiece surface, metal ions from the workpiece will be released as Fe^{2+}, and then, the Fe^{2+} will combine with hydrogen ions to form $Fe(OH)_2$, which will be precipitated in the form of sludge.

$$Fe \rightarrow Fe^{2+} + 2e^- \quad (4)$$

$$Fe^{2+} + 2OH^- \rightarrow Fe(OH)_2\downarrow \quad (5)$$

Though there are electrochemical reactions occur inside of the electrolyte, the electrolyte material of NaCl is not consumed at all, due to it is not involved in electrochemical reactions.

Hence, just adding the water into the electrolyte solution to maintain the electrolyte solubility, the ECM can be carried out continuously.

Finally, the workpiece is processed to be the target shapes, such as holes, robs, and grooves.

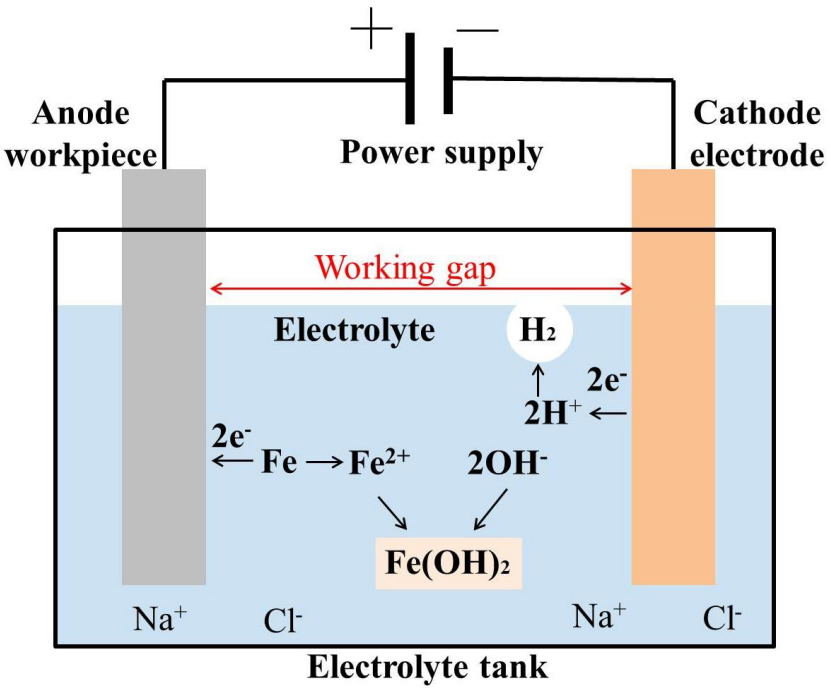

Figure 1.1 Schematic of electrolysis in ECM processing.

1.1.2 Background of ECM

The principle of electrolysis was discovered and established by one of the greatest researchers: Michael Faraday (1791-1867) [9].

After that, as a kind of technological method, the ECM was originated firstly from the electrolytic polishing processing by a Russian chemist: E. Shpitalsky in 1911. In 1929, a Russian researcher: W. Gusseff developed and used the electrolytic process to machine metal anodically [10].

At the beginning of the 20th century, researchers in Russia, Western Europe, and the USA

offered various ways and technological schemes of ECM application for dimensional processing of parts, mainly on operations of contouring and internal push broaching of various forms [11]. Much more researches about the ECM were carried out from the 1950s to 1970s in the aircraft and aerospace industries, such as being used to process blades of the aero-engine in Figure 1.2. In 1959, the Anocut Engineering Company of the USA introduced into production the traditional ECM model of using the direct current at the production run equipment for the first time. And ECM technologies were developed during this period, and lots of famous companies like Philips, Mitsubishi, Hitachi, etc. focused on ECM technologies [11].

Though the rising of electric discharge machining (EDM) in some periods slowed the development of ECM, the processing of ECM is based on electrochemical corrosion to remove materials at the atomic level, and there are no thermal and mechanical stresses remained on the workpiece surface. Hence the ECM process is usually used in various fields, such as engine turbine blade processing, steam turbine blade processing, biomedical tool processing, etc.

Figure 1.2 Schematic of aero-engine. [12]

1.1.3 Processing method of ECM

As shown in Figure 1.3, the tool electrode, which is pre-shaped before being used, the workpiece, the electrolyte solution, and the power supply are necessary. During processing, the tool electrode is positioned close to the workpiece surface extremely. The purpose is to increase the amount of dissolution and decrease the Ohmic voltage drop between the workpiece and the electrode as much as possible [13].

In addition, a high current density of about 30~200 A/cm^2, low-voltage of about 10~25V are used generally to corrode materials from the metallic workpiece [11]. At the same time as processing, the electrolyte flows through the working gap between the electrode and the workpiece to remove the ECM by-products, such as bubbles and the sludge mentioned before. Without that, it is easy to cause the generation of discharge in the working gap, and the temperature rise of the electrolyte because of the Joule heating [14].

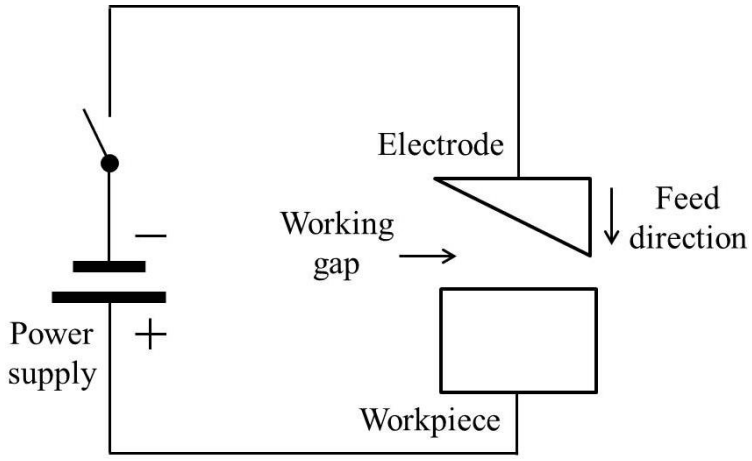

(a) ECM electrical circuit and workpiece before processed.

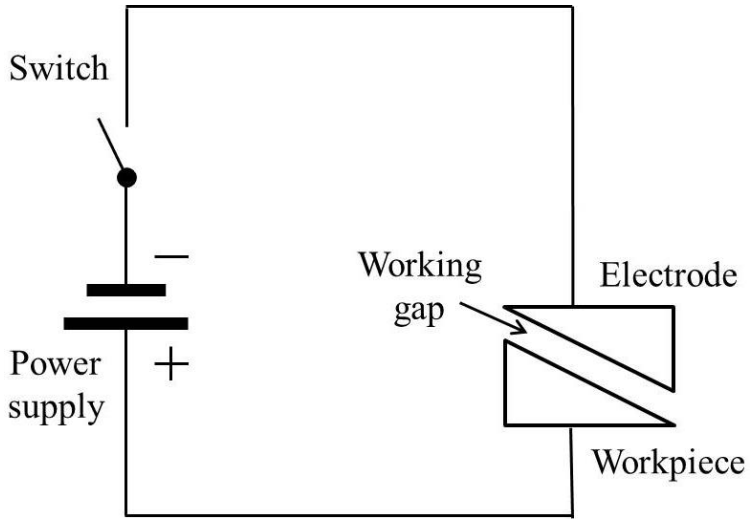

（b）ECM electrical circuit and workpiece after processed.

Figure 1.3 Schematic of electrochemical machining method.

When machining currents are flowing inside of the working gap, the workpiece is dissolved by the electrolysis during ECM. And the shape of the processed area of the workpiece is a negative mirror image of the electrode shape approximately.

1.2 ECM system

As shown in Figure 1.4, several necessary devices [15], including the power supply, the workpiece, electrolytes, the electrolyte supplying and cleaning devices, the electrode, and the process controlling and monitoring devices in ECM and the schematic of ECM equipment were presented.

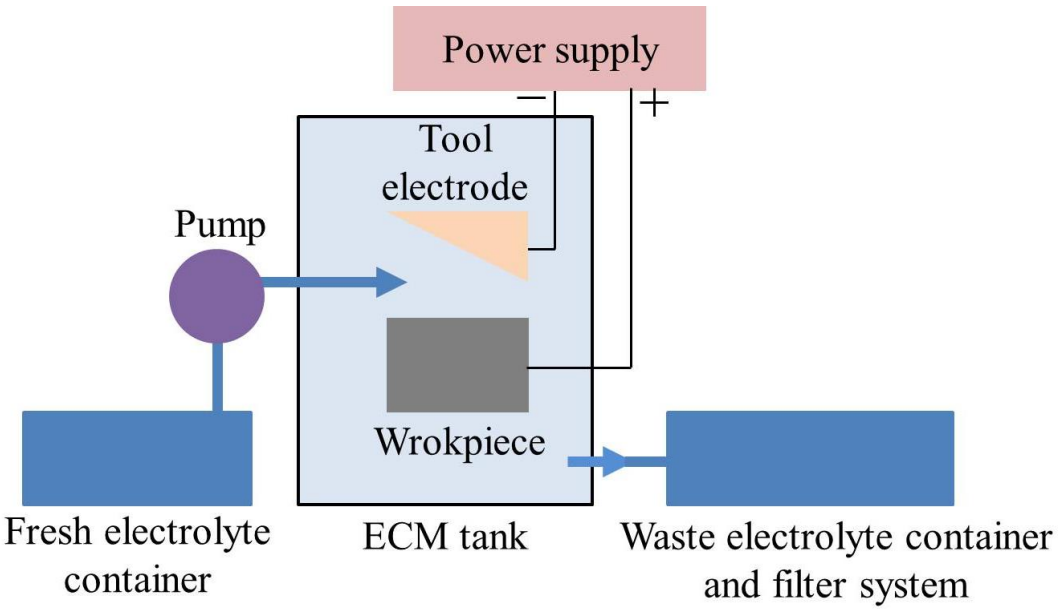

Figure 1.4 Schematic of ECM system.

1.2.1 Power supply

Used to supply the electric power to the whole ECM processing system, a direct current (DC) or an alternating current (AC) power supply is one of the basic devices for ECM processing. During ECM, a high value of direct current (may be as high as 40000 A) and a low value of electric potential (in the range of 5-25 V) across the working gap are desirable. The highest current density achieved so far is around 20,000 A/cm^2 [11].

1.2.2 Tool electrode

Usually pre-shaped before processing, the tool electrode is made of copper, brass, and graphite et al., because these materials are easy to be processed, well conductive, and preservative. Theoretically, the electrode does not participate in electrochemical reactions, it can be used continuously. However, because the electrode and its fixtures need to work in the corrosive environment of electrolytes, the anti-corrosion of the electrode is important.

Besides that, it is difficult to process the shaped electrode in advance, because there are strict requirements for the electrode to provide a suitable cathode dimension and a suitable electrolyte path providing an effective electrolyte flushing in the working gap. Hence, a metal rod or a metal nozzle, instead of a pre-shaped electrode is used as the electrode in ECM sometimes.

1.2.3 Electrolyte, electrolyte supply and filter system

The electrolyte is the primary component of the ECM method. Supplied by a pump from the fresh electrolyte container to the working gap, the flowing electrolyte plays three significant roles mainly in the ECM process, which include carrying the current between workpiece and tool, removing the ECM by-products of reactions from the working gap [16], and cooling down the processing area.

Electrolytes can be classified into four main categories depending upon their nature and physical form. Respectively, they are neutral aqueous salts, aqueous acids, aqueous alkalis, and nonaqueous electrolytes.

One of the most common electrolytes in the ECM process is sodium chloride (NaCl). It is suitable for machining stainless steel, because there is no passivation layer, which is produced usually on the stainless steel surface when using the sodium nitrate electrolyte, and the ECM process can be carried out conveniently.

Another electrolyte named sodium nitrate is normally used for machining the steel in case a

very close replication of the tool is required. Sodium nitrate prevents stray corrosion, which helps obtain a high precise replica of the tool electrode [17, 18]. The extent of current density also impacts the ECM process. For instance, in the case of sodium nitrate electrolyte, high current density leads to anodic dissolution, whereas the low current density increases the passivation on the workpiece surface [16].

1.2.4 Workpiece

As reported in the principle of ECM, electric currents start from the anodic workpiece and pass through the electrolyte to arrive on the workpiece surface. During ECM, the workpiece made of non-metallic materials cannot be corroded by the electrolysis.

It is thought that almost all of the metallic materials, no matter how hard they are, can be processed by ECM, because the material of the workpiece is removed by electrochemical reaction at the level of atoms. While, when processing with the conventional machining of cutting or drilling, and the EDM, the laser machining, etc., because they remove materials by chipping or melting, after processing, there are residual stress and micro-cracks in the processed area. These defects do not appear on the processed workpiece surface after ECM.

1.3 Advantages and disadvantages of ECM

1.3.1 Advantages of ECM

For the merits of the ECM method, as mentioned in section 1.1, since the workpiece materials are corroded by the electrolysis at the level of atoms, the ECM is non-contact and unstressed cutting between the workpiece and the electrode. The hardness of the workpiece is not a factor in the ECM process, and the ECM method can be used to process difficult-to-machined materials, which cannot be processed by conventional cutting techniques, such as grinding, turning, or milling. Because when using techniques dependent on such physical properties as shear strength, hardness, etc. to remove the unwanted materials of the workpiece, the tools have to be made of a material that is harder than the workpiece. Also, there is no residual stress on the workpiece surface after ECM processing.

Different from the other non-contact processing method, such as the electric discharge machining (EDM) method, or the laser beam machining method, there is no heat-affected zone, micro cracks, and burrs in the workpiece surface after ECM. When using processing methods, like the EDM or the laser beam machining method, both of them melt and remove materials with high thermal energy. After processing, not only heat-affected layers but also micro cracks are present in the workpiece surface, as shown in Figure 1.5.

In addition, during EDM processing, the discharge occurs at a single discharge location with an electric pulse, hence, the volume of the removal rate of EDM is small. However, during ECM processing, material removal occurs over the whole workpiece surface. And the potential difference between the workpiece and the electrode is being kept constant in processing, the current density is almost the same too, and the tool feed speed, which is independent of the processing area, is constant. Hence, when processing in a large area, the removal rate of ECM is much higher than that of EDM.

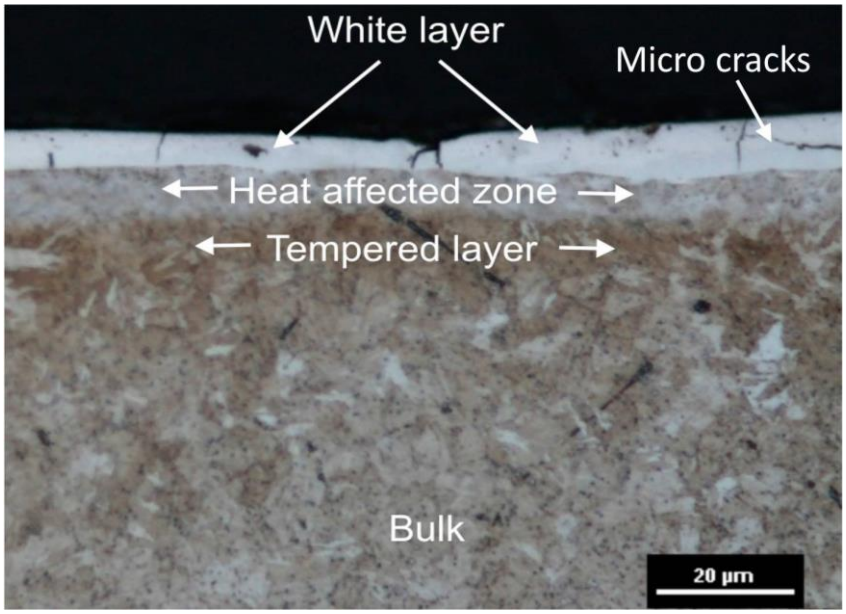

Figure 1.5 Micrograph of workpiece surface after EDM. [17]

Besides that, ECM has many other advantages such as no tool wear, smooth and bright surface, and production of components of complex geometry et al. These merits make it sure that the ECM method plays an important role in industrial production.

1.3.2 Disadvantages of ECM

However, there are some demerits existing in ECM processing. These demerits are listed as followings:

(1) Non-metallic material cannot be processed by ECM.

(2) It is time-consuming since the ECM process always needs to be repeated multiple times to obtain desired results.

(3) ECM is a high-cost process. Compared with other conventional cutting processes, special equipment and training for operators are necessary before ECM. And the ECM process requires large amounts of electricity which increases the cost much more.

(4) As a core part of ECM, the electrolyte is necessary, sometimes, the acidic electrolyte like

HNO_3 or alkaline solution, such as NaOH and KaOH are needed to be used. However, those electrolytes are harmful to operators and the environment. Besides that, as mentioned before, after ECM, by-products are precipitated in the form of sludge, which is also harmful due to lots of heavy metal elements inside of the sludge.

(5) To ensure that electrochemical reactions occur smoothly, there should be electrolytes flowing in the working gap between the workpiece and the electrode, as shown in Figure 1.4. Hence, usually the workpiece and the electrode have to be immersed in the electrolyte solution. Because of the fluidity of liquids, it is difficult to limit the distribution of the electrolyte. The difficulty in controlling the electrolyte distribution leads to an intractable problem, which is called stray-current corrosion [18, 19], in ECM processing.

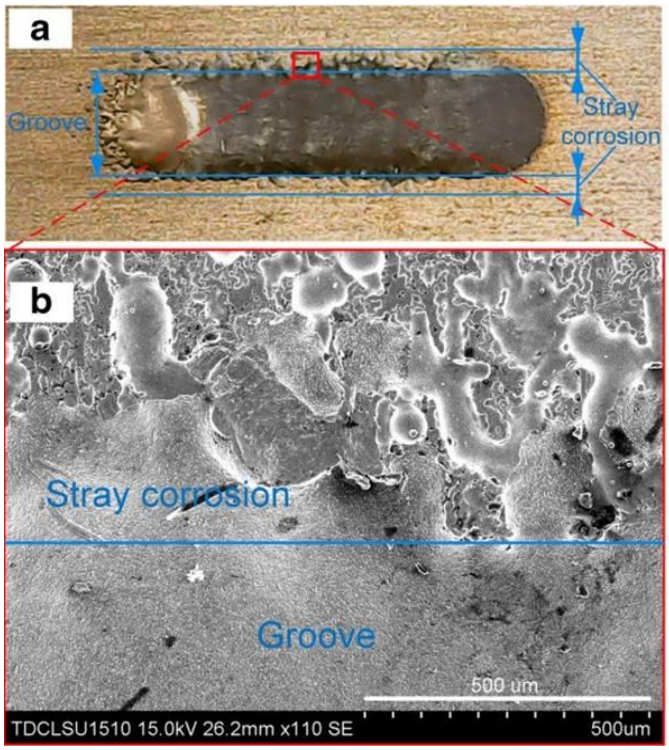

Figure 1.6 Stray-corrosion around processed groove and its micrograph. [18]

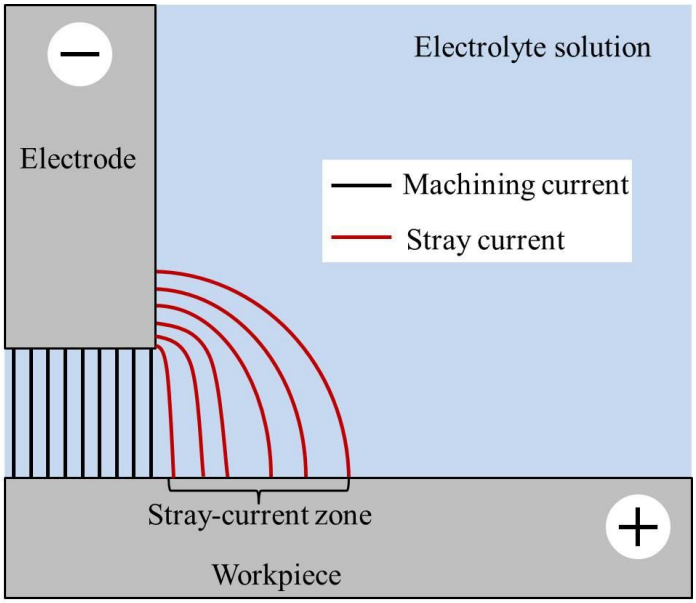

Figure 1.7 Schematic of stray-corrosion and distribution of currents lines in ECM.

Stray-current corrosion occurs in stray-current zones, where the workpiece is not intended to be processed. A groove processed by the Jet-ECM method and its stray-corrosion micrograph is shown in Figure 1.6. The stray-current corrosion and the distribution of current lines are shown in Figure 1.7. Stray-current corrosion leads to material removal in the part of the workpiece far from the tool electrode and decreases the processing accuracy of ECM. Hence, how to limit the distribution of the electrolyte is an effective way to restrict the electrolytic current distribution, which is helpful and necessary for ECM.

1.3.3 Solutions about reduce stray-corrosion

To solve the shortcoming of the stray-corrosion in ECM, many studies on controlling the machining area have been conducted. For example, lots of researches were carried out by supplying electrolytic currents through an electrolyte jet ejected from a nozzle in ECM, which is called the Jet-ECM method. The schematic of the Jet-ECM is shown in Figure 1.8. As reported by Kunieda and Natsu [20-22], the current density peak value at the center of the jet and decreases

rapidly, as shown in Figure 1.9. Therefore, only the workpiece material exposed to the electrolyte jet is corroded by electrochemical reactions because the current is restricted at the area limited by the electrolyte jet.

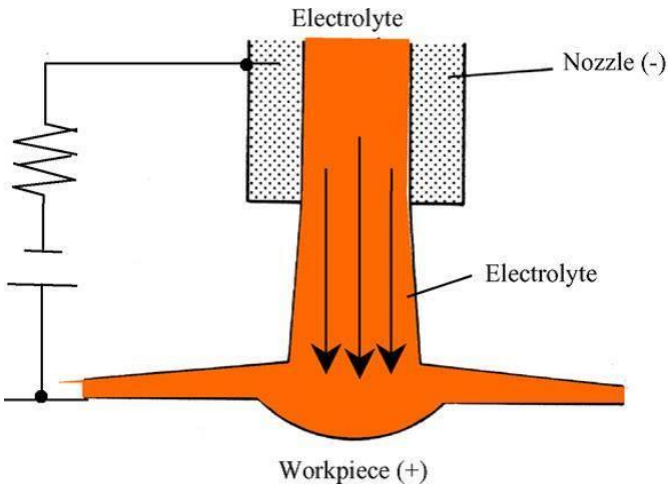

Figure 1.8 Schematic of Jet-ECM. [21]

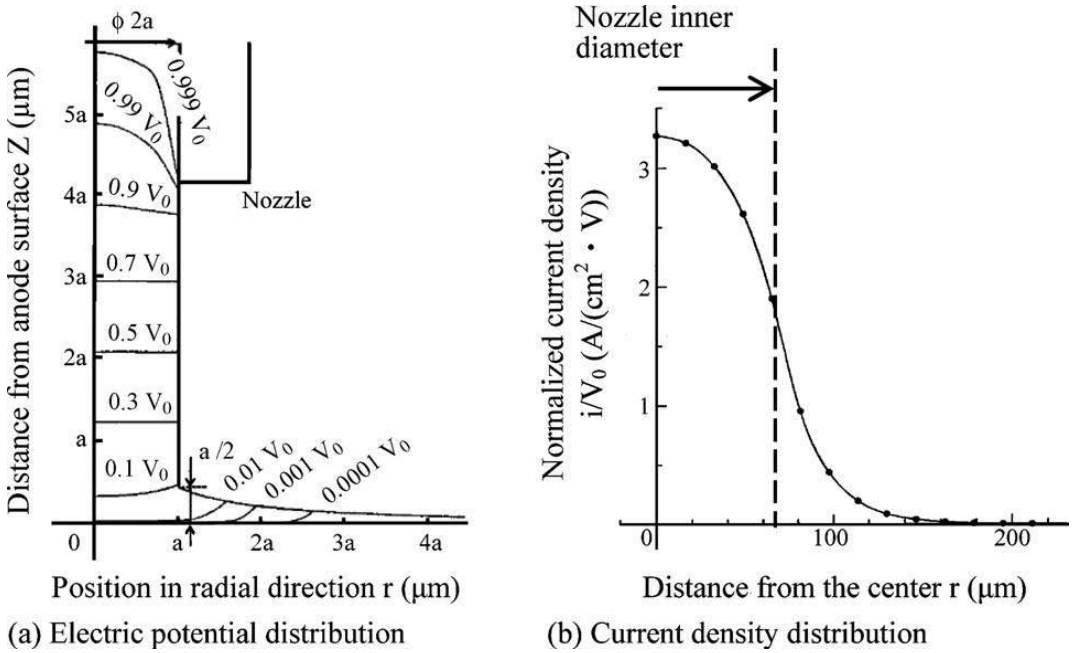

Figure 1.9 Electric potential distribution and current density distribution of Jet-ECM. [22]

Hackert et al. [23] used Jet-ECM with the assistance of air to protect an area from unintentional

machining as shown in Figure 1.10. In processing, Hacker et al. used a jet electrolyte spray on the workpiece surface, at the same time an additional jet of compressed air was used to remove the electrolyte film enclosing the nozzle caused by the surface tension of the liquid and reduce the working gap as much as possible. Finally, the stray-corrosion of the processing area was reduced obviously, and sharper edges were produced in grooved channels.

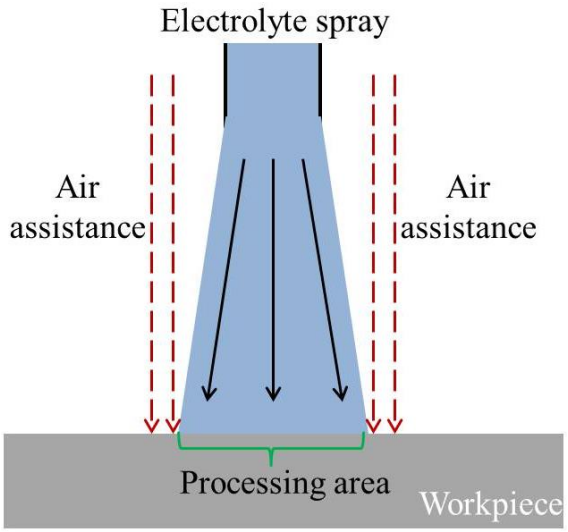

Figure 1.10 Schematic of Jet-ECM with the assistance of air.

Wang et al. [24] used Jet-ECM in groove processing and determined variations in the jet shape and their effect on the groove edge. In addition, they significantly reduced stray-current corrosion on the edge of the groove by adjusting the jet shape. A photo of the influence of the jet shape on the edge condition is shown in Figure 1.11.

Nonetheless, in Jet-ECM, it is inevitable for the electrolyte to splash onto the non-processing area of the workpiece and onto the machine tool, which will eventually lead to rust corrosion, which means that outside of the processing area of the workpiece is rusted by stray-corrosion due to contact with electrolytes. Hence, limiting the distribution of electrolytes within the

processing area is an effective strategy for eliminating stray-current corrosion and rust-corrosion in ECM.

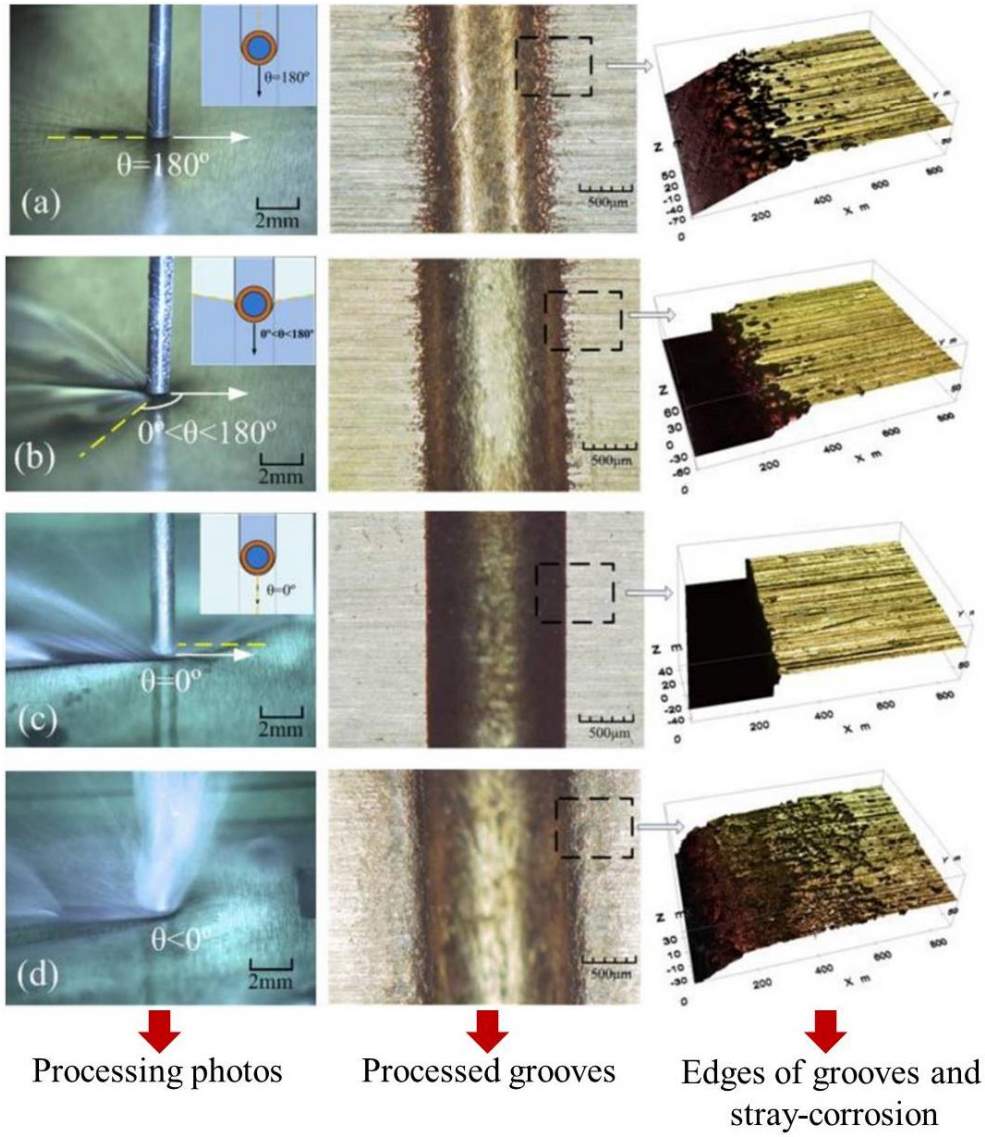

Figure 1.11 Influence of the jet shape on the edge condition: (a) all-scattered; (b) part-scattered; (c) all-reflected; (d) chaotic-reflection. [24]

To achieve this objective, an ECM method based on the use of an electrolyte suction tool [25, 26], as shown in Figure 1.12, has been proposed. During processing with this method, the

flowing electrolyte is sucked into the region between the tool tip and workpiece to limit the electrolyte distribution. However, the suction tool is too precise and complex to achieve miniaturization, and the manufacturing cost is expensive.

In addition, whether it is processing with the electrolyte jet or an electrolyte suction tool, ECM is performed by pumping the electrolytes onto the processing area of the workpiece, and by-products from the inter-electrode area are removed before supplying the processing area with fresh electrolytes. However, if the electrolyte leakage occurs during ECM, corrosion will appear in the unintended machining area, which may lead to the failure of the entire process. Hence, although it is difficult, restricting the electrolyte only flow over the processing area is necessary.

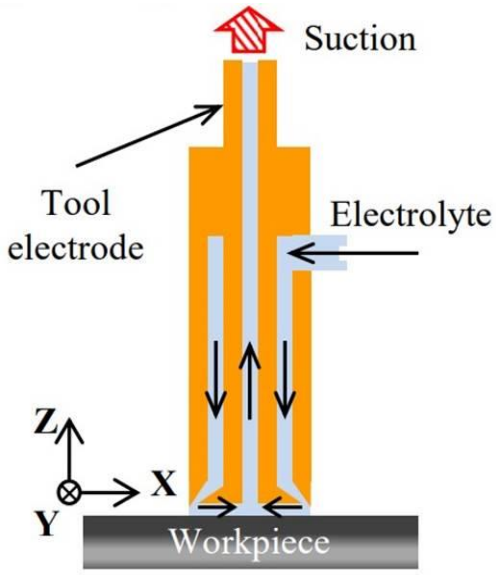

Figure 1.12 Schematic of processing with suction tool in ECM. [25]

Another well-known method used to control the machining area during ECM is Through-mask micro electrochemical machining (TMMECM) [27-30]. In this process, a through-mask with target patterns on its surface is directly attached to the anodic surface to selectively dissolve metallic materials in the unmasked areas. However, the dissolution of a

workpiece through a patterned through-mask always leads to undercutting, which is shown in Figure 1.13. At the same time, ECM by-products are blocked at the corner area and are difficult to be taken away. These occasions enlarge the target pattern shape and decrease the machining accuracy. As shown in Figure 1.14, Zhai et al. [28] tried to use the megasonic in TMMECM to improve the removal rate of ECM by-products.

Another drawback of TMECM is the need to mask each workpiece to be textured, which increases the cost and time of the process method [31].

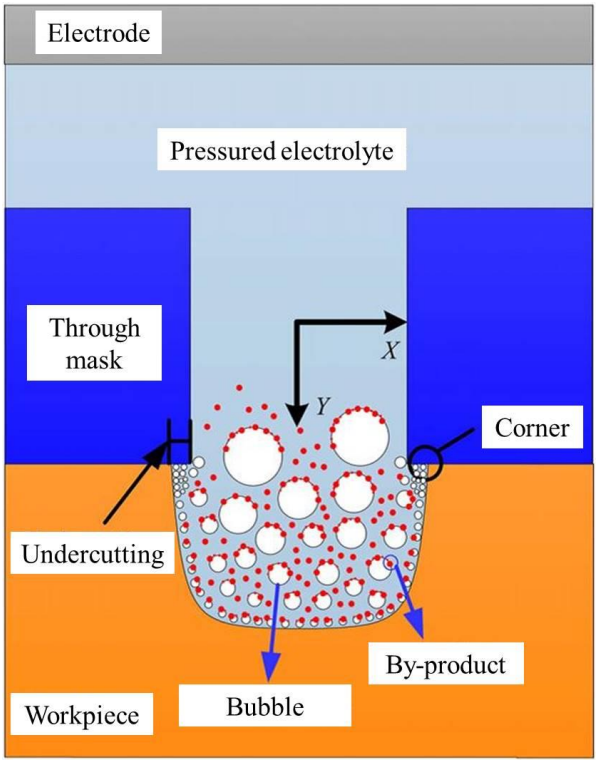

Figure 1.13 Schematic of through-mask micro electrochemical machining. [27]

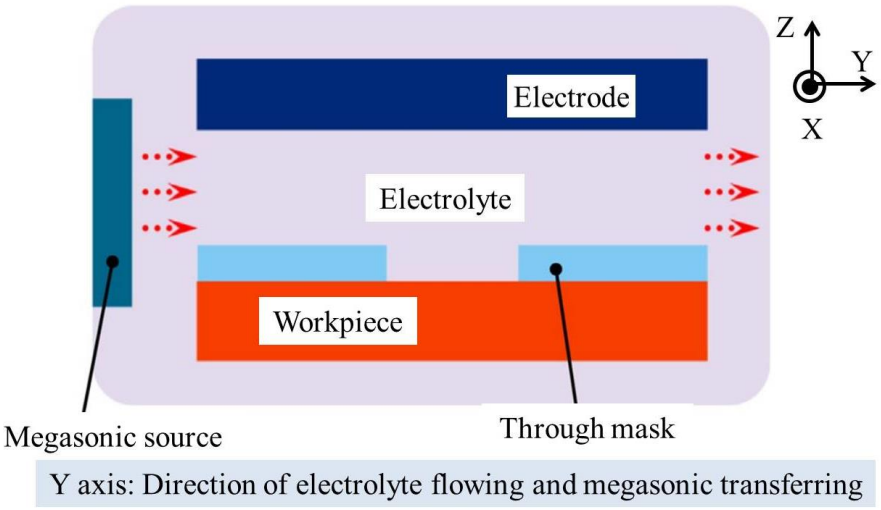

Figure 1.14 Schematic of TMMECM with megasonic assistance. [28]

Besides that, Natsu et al. [32] proposed the use of a type of non-metallic absorption material, known as woolen felt, in ECM to limit the electrolyte distribution and prevent electrolyte scattering. Schematics of this method are shown in Figure 1.15 and Figure 1.16. During processing, the electrolyte is absorbed by the absorption material, and does not flow over the workpiece surface. The absorption material is inserted in the working gap between the tool electrode and workpiece to let the electrolyte is limited to the area under the tool electrode. However, the machining mechanism of ECM involving the use of an electrolyte absorption material has not been verified. In addition, woolen felt is easily scorched by the heat generated during the machining.

1.4 Research purpose and significance

According to those shortcomings mentioned in chapter 1.2, in this research, the main purpose is focused on controlling the electrolyte distribution and limiting the electrolyte exiting only in the target area.

In daily life, it is normally known that when a piece of sponge that contains water is used to wipe a table, only the areas rubbed by the sponge are wetted by water, whereas the other areas of the table surface are not affected by water at all. If using a non-conductive porous solid in ECM to act as materials for electrolyte absorption, similar to household sponges for water absorption, it is easy to achieve the task of limiting the electrolyte to the desired processing area. In this case, the flowing electrolyte used in ECM processing usually is replaced with an electrolyte that is absorbed and confined in an absorption material. A schematic of ECM based on the use of an electrolyte absorption material is shown in Figure 1.15.

During machining, the absorption material is inserted between the electrode and the workpiece after absorbing the electrolyte. Due to the flowing electrolyte being replaced with the electrolyte, which is absorbed and confined inside of the absorption material, the electrolyte distribution and the limitation of the processing area of ECM come true. Because of the properties of the electrolyte absorption material, the electrolyte in ECM can form a thin electrolyte film on the processing area of the workpiece surface, there is no electrolyte existing on the other areas of the workpiece, and there will not be corroded at all.

Suppose some material like a sponge block is used to cover the processing area. Due to the electrolyte being consumed gradually, the by-products generated during ECM processing accumulate in the processing area. In that case, ECM processing cannot be carried out for a long time continuously. As shown in the schematic of continuous ECM in Figure 1.16, the felt is mounted on the outer periphery of the metal disk. During processing, part of the felt contacts the

workpiece surface, and part of it sinks in an ultrasonic vibration tank filled with electrolytes. The disk is connected to the negative pole of the power supply, and the workpiece is connected to the positive pole of the power supply. The dissolution of workpiece material and generation of ECM by-products occur in the contact area of the felt and the workpiece. Due to the rotation of the disk, by-products that adhere to the felt are cleaned by the electrolyte inside of the ultrasonic vibration tank, and the fresh electrolyte is absorbed into the felt at the same time. With this self-designed and fabricated setup, the continuous ECM is realized.

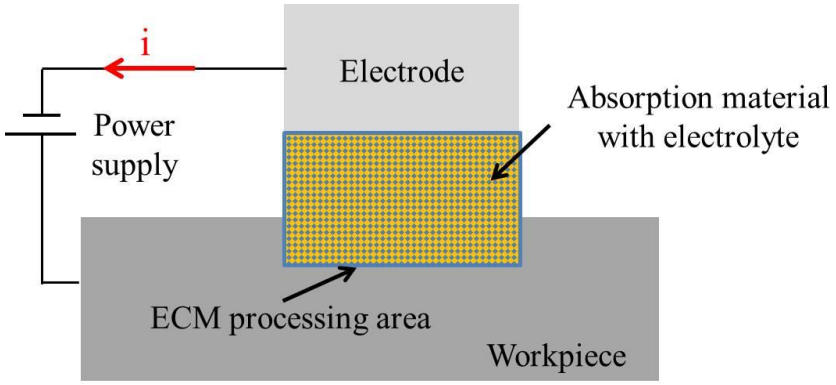

Figure 1.15 Schematic of ECM with electrolyte absorbed inside electrolyte absorption material.

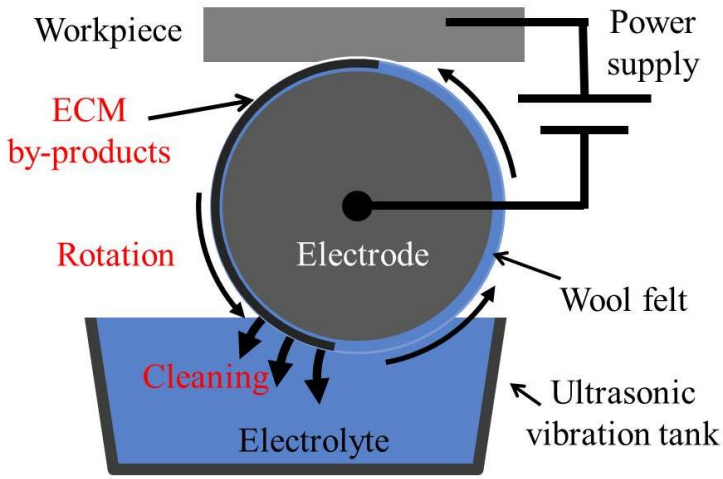

Figure 1.16 Schematic of experimental setup for continuous ECM. [31]

Hence, from the results before, we can conclude that in order to provide fresh electrolytes and take away ECM by-products, a rolling electrolyte absorption material should be used during processing.

The schematic and a photo of the ball-point pen nib are shown in Figure1.16. When writing with a ball-point pen, as the part of the ball contacts with the paper, the ink adhering to the ball surface is applied to the paper. At the same time, the other part of the ball re-attaches the ink inside of the pen tube to its surface. Hence, during writing with a ball-point pen, the rolling ball can apply the ink to the paper continuously. Inspired by that, we think that if some spherical absorption material may be used in ECM and work as the ball-point pen, ECM processing can be operated as writing with a ball-point pen.

Combining with the advantages of the sponge and the ball-point pen, in this research, a kind of porous solid ball is used as the electrolyte absorption material in ECM to limit the distribution of the electrolyte.

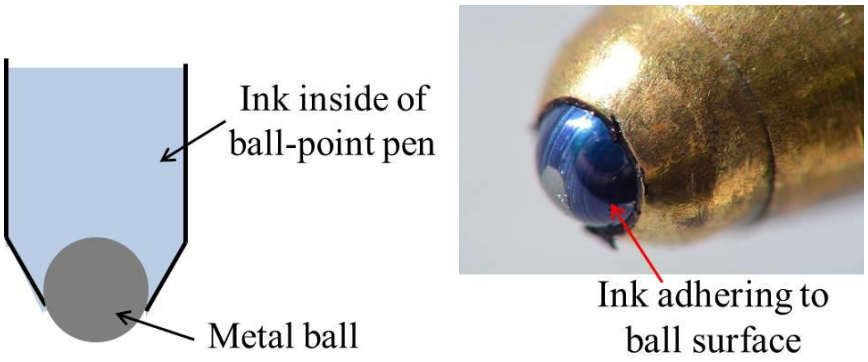

(a) Schematic of ball-point pen. (b) Photo of ball-point pen. [33]

Figure 1.17 Schematic and photo of ball-point pen.

1.5 Dissertation structure

This dissertation consists of six chapters.

Chapter 1

In chapter 1, we introduced the principle, background, processing method, and several key devices of electrochemical machining first. Then advantages and disadvantages of the ECM method were summarized. Among those disadvantages of ECM, we focused on introducing and explaining the stray-current corrosion and take how to eliminate stray-current corrosion as the research purpose of this study. Based on the research purpose, by referring to research results of predecessors, and being inspired by daily life phenomena, including water-absorbing the sponge and writing with a ball-point pen, we decide and plan to use spherical water-absorbing materials as the electrolyte absorption material in ECM to limit the electrolyte distribution.

Chapter 2

In chapter 2, experimental equipment and experimental materials were introduced in this research, which included a power supply, a waveform generator, the electrode, and the workpiece. In addition, the measurement equipment for experimental results was mentioned.

Then, several attempt experiments were carried out beforehand to select the suitable electrolyte absorption material for this study. During which, two kinds of porous solid materials, including the diatomaceous earth chip and the Maifan stone ball (hereinafter abbreviated as MFS-ball), were used. And by comparing the applicability and processed results, the MFS-ball was selected to be used as the electrolyte absorption material in ECM. Then, the features of the MFS-ball were introduced, and the absorption principle of capillary action of the MFS-ball and the reason for electrolyte distribution controlling at the workpiece surface were summarized respectively.

Finally, with the experimental devices mentioned above, the processing method and mechanism were listed in detail, and an attempted experiment was carried out. Based on the experiment result, current paths during ECM processing were explored and measured with actual experiments.

Chapter 3

In chapter 3, experimental materials and devices, processing principle and method, the processed groove, the electrolyte distribution, and values of machining currents flowing through each path were obtained. However, processing situations, such as the potential between the workpiece and the electrode, the current density distribution at the processing area, and the processed results during processing cannot be observed and measured. Besides that, the explanations for the depth difference that occurs at the cross-section of the processed trace were not obtained clearly until now. And it is thought that the machining current density and its distribution are difficult to be measured or calculated from experiment results.

Hence, in this chapter, a finite element analysis software COMSOL Multiphysics was used to try to calculate the machining current density and its distribution at the processing area by simulating ECM processing. At the same time, the potential between the workpiece and the electrode was obtained. Combining with the machining current density and its distribution, the processed results in simulating and the profile of the processed trace, and the depth difference of the processing area were confirmed and explained fully. In addition, by changing the conductivity of the MFS-ball, which is difficult to be accomplished in actual experiments, the relation between the MFS-ball and its surface electrolyte film and the roles the MFS-ball plays in ECM processing were obtained by simulation.

After that, experiments were carried out with this ECM method to verify the simulation results. And by comparing with processing results of the point processing and the groove processing of chapter 2, discussions and summaries were done.

Chapter 4

In chapter 4, during the ECM process, machining characteristics are usually influenced by experimental parameters. To explore the influence results and the reasons, in this section, the influences of the following main experimental parameters, including the pressure between the workpiece and the MFS-ball, the electrolyte flow rate, the time of pre-scanning, the machining constant current (CC) value, the machining time, and the moving speed of workpiece are ascertained. After that, the influence of the MFS-ball's size difference and its solution method were explored.

Chapter 5

In this chapter, according to the research results before, since the electrode where there is a V-shaped cross-section track is used in ECM processing, a strip-shaped groove is processed at the workpiece surface after processing. And because of the electrolyte distribution limitation of the porous MFS-ball, the stray-corrosion, and the rust corrosion are prevented effectively.

Explorations of expanding the application of this ECM method were listed as follows.

First of all, wide grooves with different cross-section profiles were processed by changing the interval between two grooves when processing with the ECM method. Before that, to predict the cross-section shape of processed grooves, we calculated the cross-section profile with the software of Microsoft Excel.

Then, to be used in the metal marking of this stray-corrosion-free ECM method, a new tool,

named the universal moving unit, was designed and manufactured. Combining with the universal moving unit during the ECM process of this research, several dimple English alphabets were etched on the workpiece surface.

Besides that, based on the research result before, we found that by using the ECM method of this research, the processed grooves with shallow depths are suitable to be used as oil pockets for sliding surfaces. Hence, with a relay module used as the switch of the power supply in experiments, shallow grooves with different lengths and different depths were processed.

Chapter 6

In this chapter, we summarize shortcomings, future issues of the ECM method of this research, and the main content of each chapter of this article.

Chapter 2: Processing method, mechanism, and experimental verification

2.1 Introduction

In this chapter, first of all, experimental equipment and experimental materials used, which includes a power supply, a waveform generator, the electrode, the workpiece, and measurement equipment used in this study were reported.

Then, to select the suitable electrolyte absorption material for this study, several attempting experiments were carried out. During which, two kinds of porous solid materials, including the diatomaceous earth chip and the Maifan stone ball (hereinafter abbreviated as MFS-ball), were used. And by comparing the applicability and processed results, the MFS-ball was selected to be used as the electrolyte absorption material in ECM. Then, the features of the MFS-ball were introduced, the absorption principle of capillary action of the MFS-ball and the reason of electrolyte distribution controlling at the workpiece surface were summarized respectively.

By using the experimental devices mentioned above, processing method and mechanism were listed in detail, and an attempt experiment was carried out. Basing on the experiment result, current paths during ECM processing were explored and measured with actual experiments.

2.2 Experimental equipment

Experimental equipment of this research is shown in Figure 2.1. Several main devices of this research are introduces as following:

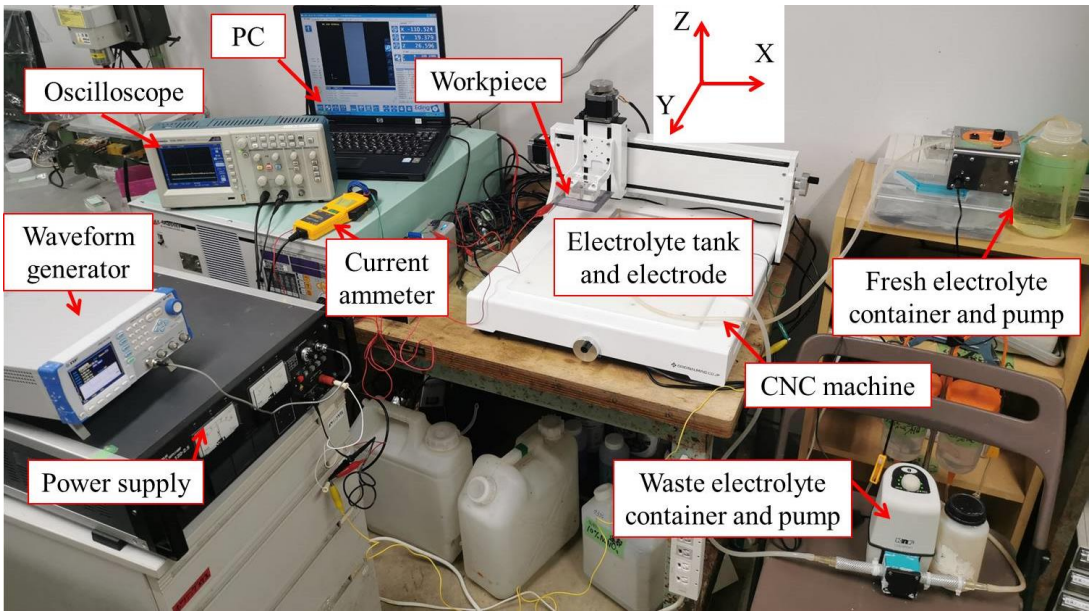

Figure 2.1 Experimental equipment.

2.2.1 Workpiece and electrolyte

In this research, the SAE 304 stainless steel, (hereinafter abbreviated as SUS304), was used as the workpiece. Because, first of all, SUS304 is the most common stainless steel in industrial applications, such as food handling, processing equipment, screws et al. Besides that, this study mainly focuses on the ECM method with the MFS-ball used as the electrolyte absorption material, the influence when processing with different materials of the workpiece was not considered. Hence the SUS304 was selected and used.

For the electrolyte, as mentioned in chapter 1, the NaCl solution is the most commonly used in ECM, especially when processing the stainless steel. And compared with processing with the $NaNO_3$ solution, NaCl is understood to be a kind of more aggressive electrolyte, because the

electrolyte conductivity of NaCl solution is greater than that of the $NaNO_3$ with the same concentration. However, the greater electrolyte conductivity of NaCl solution leads to the stray-corrosion occurring more seriously than the $NaNO_3$ solution in ECM processing.

Hence, in order to verify the limitation of the stray-corrosion by using the ECM method during which the MFS-ball is used as the electrolyte absorption material, the more aggressive electrolyte of the NaCl solution was used.

2.2.2 Power supply

In this research, as shown in Figure 2.2, a power supply（BWS 120-2.5, TAKASAGO LTD.）was used. The key parameters of the power supply are listed in Table 2.1.

Figure 2.2 Power supply.

Table 2.1 Key parameters of power supply.

Series of power supply	BWS 120-2.5
Output mode	Constant voltage mode
	Constant current mode
Maximum value of output voltage	± 120 V
Maximum value of output current	± 2.5 A
Frequency characteristic	0~120 kHz

2.2.3 Waveform generator

As shown in Figure 2.3, a function generator (WF1973, NF Corp.) was used to input waveform needed to the power supply, because some of the following experiments, the pulse current will be used. With the function generator, pulse waveform, such as sinusoidal, square, ramp, etc. can be generated and output to the power supply. The key parameters of the function generator are shown in in Table 2.2.

Figure 2.3 Function generator.

Table 2.2 Key parameters of function generator.

Waveform	Sine, Square, Pulse, Ramp, Noise, Sin(x)/x etc.
Frequency range of arbitrary waveform	0.01 μHz ~ 5 MHz
Variable duty ratio (Standard range)	0.01 % ~ 99.99 %
Time of rise / fall	⩽ 17 ns

2.2.4 CNC machine

During processing, the movement of the workpiece is controlled by using a CNC machine (KitMill CL420, ORIGINALMIND INC.), as shown in Figure 2.4. The key specifications are listed in Table 2.2.

Figure 2.4 CNC machine.

Table 2.3 Key specifications of CNC machine.

Series	KitMill CL420
Stoke along axis	X axis: 355.4 mm
	Y axis: 424.8 mm
	Z axis: 80.4 mm
Maximum feed rate (X, Y axis)	35 mm/s
Maximum feed rate (Z axis)	16.7 mm/s
Maximum rated speed of spindle	5600 r/min

2.3 Measurement equipment

2.3.1 3D measurement device

In order to measure the overall shape and depth of a processed result, a 3D measurement device, consist of a laser displacement sensor (KL-1300B, Anritsu Corp.) with a three-dimensional measuring instrument (KS-1100, KEYENCE Corp.), was used. The photo of the 3D measurement device is shown in Figure 2.5.

(a) Laser displacement sensor.

(b) High-precision shape measurement system.

Figure 2.5 Three-dimensional measuring devices.

2.3.2 Cross-section measurement device

Besides the 3D measurement result, aiming at measuring the cross-section of the processed area, a contour-measuring machine (CV-3100S4, Mitutoyo Corp.) was used. The photo of the contour-measuring machine is shown in Figure 2.6.

Figure 2.6 Contour-measuring machine.

2.4 Selection and trying of electrolyte absorption materials

It is generally known that many porous materials, such as sponges, have good abilities to absorb and retain water in their structures. As mentioned in chapter 1, in everyday life, when a piece of sponge that contains water is used to wipe a table, only the areas rubbed by the sponge are wetted by water, whereas the other areas of the table are not influenced by water. If using non-conductive porous solids as materials of electrolyte absorption in ECM, similar to household sponges for water absorption, the limitation of the electrolyte distribution can be realized easily. Hence, the flowing electrolyte is replaced with an electrolyte that is absorbed and confined in the absorption material.

2.4.1 Attempting with diatomaceous earth

Diatomaceous earth is a kind of effective water-absorbing material, and lots of absorbent products sold commercially are mainly made of the diatomaceous earth, for example, the dehumidifying stick and the bathroom mat as shown in Figure 2.7. It is because there are a lot of tiny holes inside of the diatomaceous earth, the micrograph of the inside of the diatomaceous earth is shown in Figure 2.8. Due to the capillary action, liquids can be absorbed by those tiny holes.

As an attempt, we bought some dehumidifying sticks made of the diatomaceous earth mainly and cut a piece to put into the electrolyte to absorb the electrolyte, as shown in Figure 2.3. The experiment conditions are shown in Table 2.4. The whole processing lasted about 30 s. After that, due to the electrolyte absorbed by the diatomaceous earth chip being used up, the ECM process was stopped.

As shown in Figure 2.9 after absorbing electrolytes, a diatomaceous earth chip is put on the workpiece surface, and on the other facet of the chip, it is connected with the electrode. When applied with a voltage between the workpiece and the electrode, electrochemical reactions occur

in the processing area. The processed result is shown in Figure 2.11(a). By using a three-dimensional measuring instrument, the 3D measurement result was obtained and is shown in Figure 2.11(b).

From Figure 2.11(b), it can be found that a shallow groove with a depth of about 10 μm was processed by the electrolysis, and the shape and size of the processed groove are the same as that of the diatomaceous earth chip. It is considered that the electrolyte was limited in the processed area by the diatomaceous earth, hence electrochemical reactions only occurred below the diatomaceous earth chip, and the other areas of the workpiece surface were not etched.

(a) Dehumidifying stick. (b) Bath mat.

Figure 2.7 Products made of diatomaceous earth.

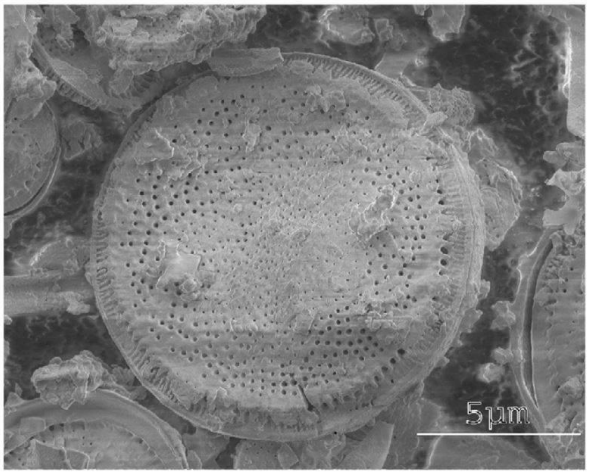

Figure 2.8 Scanning electron micrograph of diatomaceous earth. [34]

However, during the experiment, it is found that, due to the poor water resistance, lots of powdered diatomite dispersed in the electrolyte after soaking in the electrolyte solution, and the chip became fragile. Hence, it is thought that the diatomaceous earth is not suitable for being used as the electrolyte absorption material in ECM. Materials with better water resistance and greater hardness than the diatomaceous earth should be used.

Figure 2.9 Diatomaceous earth chip before absorbing electrolyte.

Table 2.4 Experimental conditions.

Item	Specification
Absorption material	diatomaceous earth
Size of diatomaceous earth chip	10 × 8 × 2 mm
Workpiece material	SUS304 plate
Electrode material	SUS304 plate
Electrolyte	10 wt.% NaCl solution
Constant current value	100 mA
Processing time	30 s

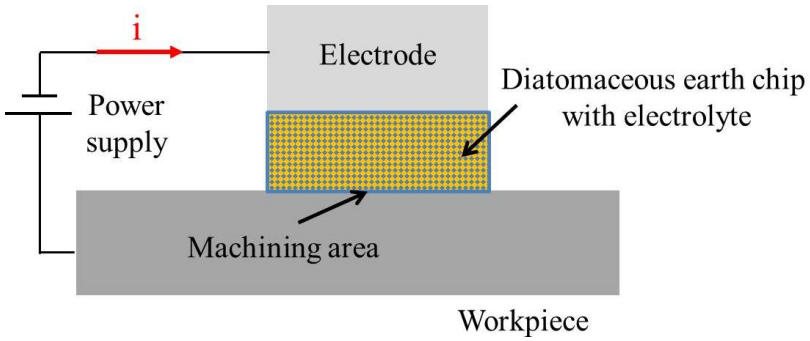

Figure 2.10 Schematic of ECM processing with a diatomaceous earth chip.

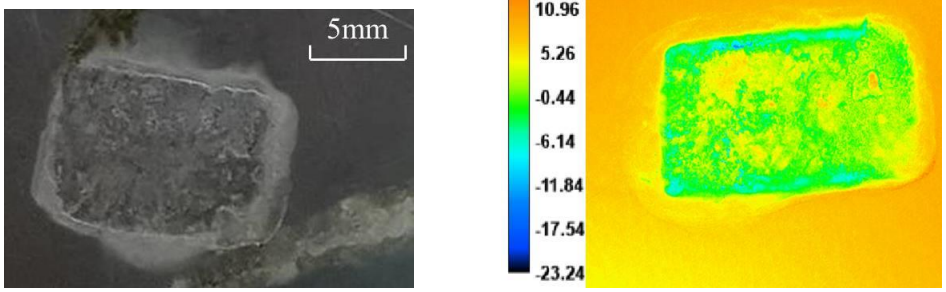

(a) Processed groove. (b) 3D measurement result of processed groove.

Figure 2.11 Processed groove and 3D measurement result by using diatomaceous earth chip.

2.4.2 Attempting with MFS-ball

After attempting with the diatomaceous earth, we tried to process by using another solid porous material, known as the Maifan Stone ball (hereinafter abbreviated as MFS-ball), as an electrolyte absorption material. The photo of the MFS-ball is shown in Figure 2.12. With the greater hardness and water resistance than the diatomaceous earth, though the MFS-ball is immersed in the electrolyte for a long time, its strength does not change totally. Hence, an attempting experiment was carried out by using the MFS-ball as the electrolyte material of this research.

The schematic of the attempting experiment is shown in Figure 2.13. During processing, the

MFS-ball was sandwiched between the workpiece and the electrode. The electrode was fixed, and the workpiece could move along the reciprocating moving direction of Figure 2.13. At the same time, driven by the friction of the workpiece, the MFS-ball rolled along the moving direction of the workpiece. To continuously provide fresh electrolytes and take away the ECM by-products adhering to the MFS-ball surface, an electrolyte nozzle was fixed on the other side of the electrode.

Figure 2.12 Photo of MFS-balls.

The experimental parameters used in this experiment are shown in Table 2.5. Due to the amount of the electrolyte absorbed inside of the MFS-ball is less than that of the diatomaceous earth, if a greater constant current is used, the ECM processed will be stopped soon. Hence, in this experiment, the constant current of 30 mA was used. At the same time, because there are fresh electrolytes providing incessantly, the ECM process can be carried out continuously.

The processed groove of the attempting experiment and movement traces of the MFS-ball are shown in Figure 2.14. Along the measuring line, the cross-section of the processed groove was obtained by using a contour-measuring machine, the measurement result is shown in Figure 2.14(c).

From the processed result and its measurement result of the cross-section, it can be found that

the workpiece surface was corroded to groove shallowly by electrochemical reactions. And due to the distribution of the electrolyte being limited, electrochemical reactions occur at the electrolyte distribution, and the stray-corrosion can be avoided obviously.

Hence, it is verified that the MFS-ball can be used as the electrolyte absorption material in ECM.

As shown in Figure 2.14(b), three pieces of the movement traces were marked by the red line, the orange line, and the black line. Though driven by the moving workpiece, the MFS-ball moves between A and B, in the direction perpendicular to the moving direction of the workpiece, due to there being no restriction, the movement traces shift, which leads to the three pieces of the movement traces are not overlapped well. Hence, to overcome this shortcoming, it is necessary to restrict the movement in the direction perpendicular to the moving direction of the workpiece.

Table 2.5 Common experimental conditions.

Item	Specification
Absorption material	MFS-ball
MFS-ball diameter	10 mm
Workpiece material	SUS304 plate
Electrode material	SUS304 plate
Electrolyte	10 wt.% NaCl solution
Length of reciprocating movement	50 mm
Constant current value	30 mA
Moving speed of workpiece	10 mm/s
Reciprocating processing time	150 s
Number of reciprocating processing	12

In brief, in this research, a solid porous ball referred to as an MFS-ball, can be used as the electrolyte absorption material during ECM.

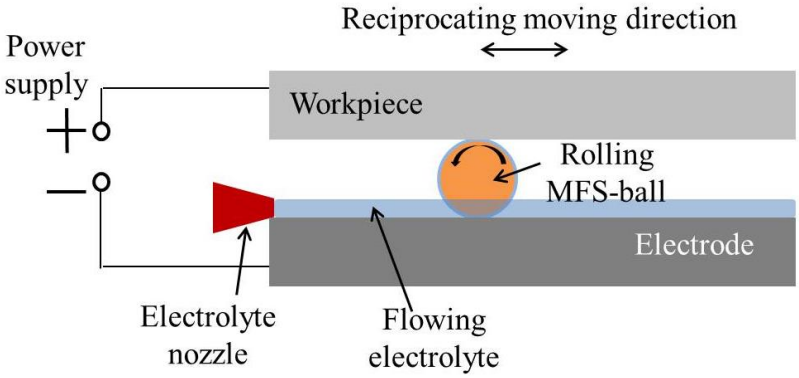

Figure 2.13 Schematic of ECM with MFS-ball.

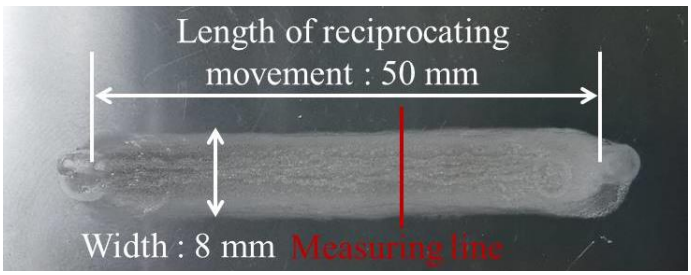

(a) Processed groove and its size.

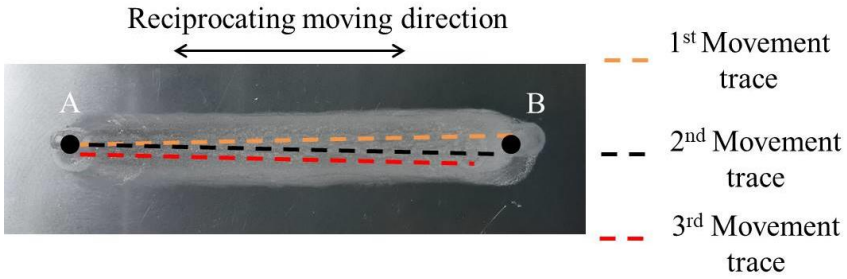

(b) Movement traces of MFS-ball.

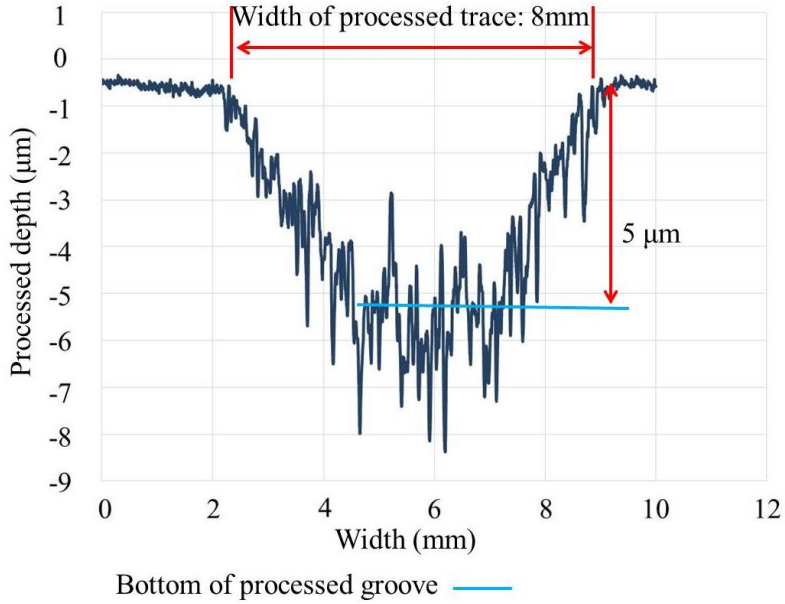

(c) Measurement result of processed groove's cross-section.

Figure 2.14 Processed groove, movement traces and measurement result of cross-section.

2.5 Introduction of MFS-ball

The MFS-ball is a common filter material typically used in water purifiers and filter showers. It is made of clay and Maifan Stone mainly, and all of these materials were heated to 800 °C, and the temperature in the burner was maintained for approximately 9-10 h to create the MFS-balls [35]. The Maifan Stone, which is the main material of the MFS-ball, is a kind of natural ore; its main components are SiO_2, Al_2O_3, CaO, MgO, etc., and it contains a variety of trace elements. Maifan Stone has the advantages of good adsorption performance, pH regulation, and bioactive dissolution [36].

An internal micrograph, taken by a digital microscope (VHX-8000, KEYENCE Corp.), of the MFS-ball is shown in Figure 2.15. It can be found from the internal micrograph that there are lots of micro holes inside of the MFS-ball, for easy observation, micro holes of porous structures are marked in blue. The average diameter of those tiny holes is approximately 16.6 μm, and the area covered by tiny holes occupies approximately 2.7 % of the total micrograph area.

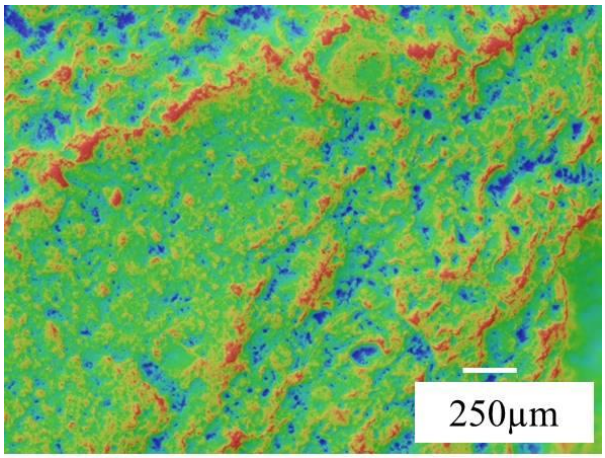

Figure 2.15 Micrograph of inside porous structures of MFS-ball.

MFS-balls used in this study were bought commercially as there were no strict requirements on their sizes and tolerances. The diameters of the commercial MFS-balls were specified as 10 ± 0.5 mm on the label. To verify the average diameter of the MFS-balls, we randomly selected five MFS-balls and measured the diameters at five different parts on each MFS-ball. The measured diameters were consistent with the values specified on the commercial label and are given in Table 2.6. Therefore, in this study, 10 mm was chosen as the average diameter of the MFS-balls.

Table 2.6 Diameter and tolerance of MFS-balls.

Measured part (mm) / MFS-ball	Part 1	Part 2	Part 3	Part 4	Part 5	Average	Tolerance
B1	9.35	9.57	9.48	9.51	9.63	9.51	+ 0.12 - 0.16
B2	9.87	9.92	9.69	9.71	9.93	9.82	+ 0.11 - 0.13
B3	10.09	10.14	10.01	10.18	10.11	10.11	+ 0.07 - 0.10

Furthermore, the tiny holes inside the MFS-ball were randomly distributed and separated from each other. In dry conditions, these porous structures contain a large amount of air. Therefore, to fill the inner cavity with electrolytes, it is necessary to first extrude the air from the MFS-ball. Hence, before the ECM experiments, the MFS-balls were placed in an electrolyte container with an ultrasonic cleaning function. The electrolyte absorption process is shown in

Figure 2.16. Figure 2.16 shows the relationship curve between the weights of ten MFS-balls that have absorbed the electrolyte and the electrolyte absorption time. The result shows that the change in weight of the ten MFS-balls after electrolyte absorption was 1.63 g, which indicates that each MFS-ball can absorb 0.163 g of the electrolyte.

The excellent water absorption ability of the MFS-ball was one of the main reasons that its use as an electrolyte absorption material was explored in this research. Another is MFS-ball's high hardness [35], which signifies that it will not be easily broken under pressures from the workpiece and tool electrode. Additionally, the MFS-ball has excellent durability, which ensures that stable experiments can be performed.

Besides that, the MFS-ball exhibits good solvent resistance. Even when it is soaked in water or an electrolyte solution, it will not disperse or dissolve. Hence, this electrolyte absorption material will not affect the electrolyte solution or hinder the ECM process.

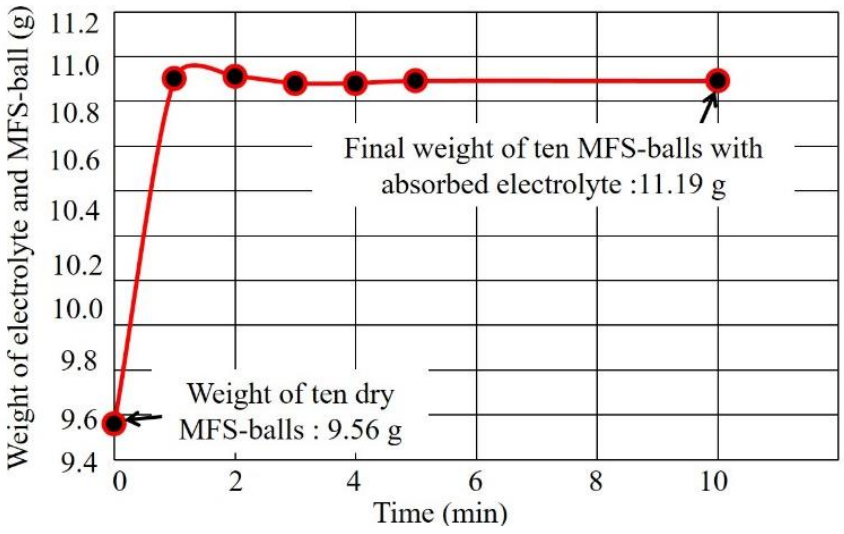

Figure 2.16 Combined weight of absorbed electrolyte and MFS-balls.

2.6 Electrolyte absorption principle of MFS-ball

For sponges and other porous solids, water absorption is caused by a liquid physical property known as capillary action [37]. Capillary action is very common in our daily life, for example, when part of a paper towel is dipped in water or other liquids, water or other liquids will spread to the other areas of the paper towel, appearing to ignore gravity.

Capillary action, which is called capillary filling or wicking, is the process of liquid flow or rise in narrow spaces without the assistance of external forces, such as gravity. It is like a force that can cause the liquid to be sucked into narrow tubes or tiny holes in some materials. The most common example of the capillary action is that when a piece of the thin glass tube is dipped into water, driven by the capillary force of capillary action, the liquid level of the water surface inside of the glass tube rises to a height which is higher than the level outside the tube. The schematic of capillary action is shown in Figure 2.17. And the liquid-level difference can be calculated using Jurin's law, expressed herein as equation (1) [37].

$$h = \frac{2\sigma \cos\theta}{\rho g r} \qquad (2\text{-}1)$$

where h is the liquid level difference, σ is the liquid–air surface tension, ρ is the density of the liquid, θ is the contact angle, g is the acceleration due to gravity, and r is the radius of the narrow tube.

Capillary action [38-41] is first recorded observation by Leonardo da Vinci during the 15th century. Although experimental studies continued during the 18th century, successful quantitative treatment of capillary action was not attained until 1805 by two investigators: Thomas Young and Pierre-Simon Laplace [42, 43]. They derived the Young–Laplace equation of capillary action. Albert Einstein's first paper, which was submitted to Annalen der Physik in

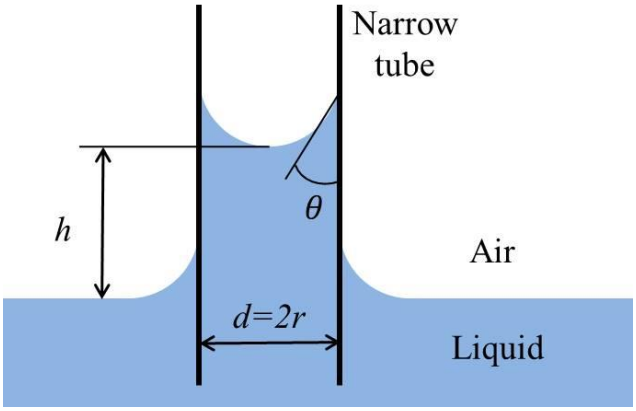

Figure 2.18 Schematic of capillary action.

1900, was on capillarity [44, 45].

Capillary action does not only exist in water, but also in oils and any other liquid. Though it seems simple and commonplace, capillary action has a major role in lots of natural, industries, and human lives. For example, because of capillary action, water can transport from the roots of trees to treetops and move into aquifers of the earth. In our daily life, the use of an absorbent kitchen sponge to clean liquid spills is based on the principle of capillary action.

In this research, capillary action works in MFS-balls to absorb electrolytes and limit the electrolyte distribution in ECM processing.

When a dry MFS-ball is immersed in an electrolyte solution, electrolyte absorption occurs similar to liquid rising inside a narrow tube. A schematic of the electrolyte absorption into the MFS-ball is shown in Figure 2.15. Because of capillary action, the electrolyte is absorbed and retained in the tiny holes of the MFS-ball. At the same time, also driven by capillary action, small amounts of electrolyte accumulate around the entrances of the tiny holes. Both the electrolyte absorbed by the MFS-ball and that accumulated around the entrances of its holes form an electrolyte film on the surface of the MFS-ball.

When the MFS-ball contacts the workpiece, the electrolyte is spread onto the surface of the

workpiece, covering a small area around the contact area, because of the surface tension of the liquid, as shown in Figure 2.19. In ECM, because the current flows from the anodic workpiece to the cathodic electrode through the electrolyte, electrochemical reactions occur in the area contacted by the electrolyte. As the MFS-ball rolls over the workpiece surface, the electrolyte absorbed by the MFS-ball is continuously delivered to the machining area.

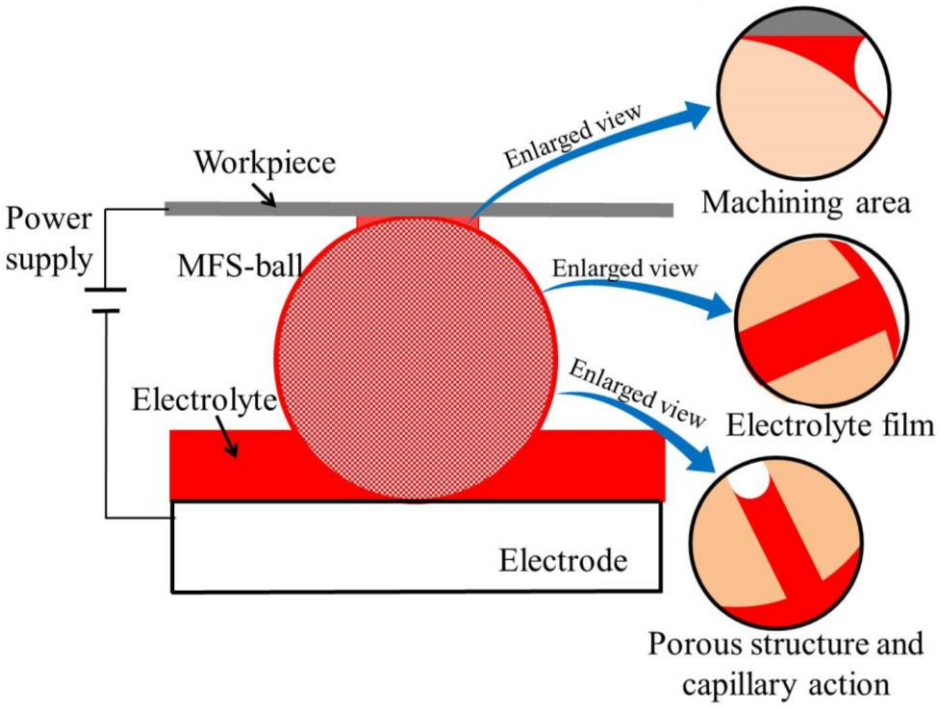

Figure 2.19 Schematic of electrolyte absorption.

2.7 Processing mechanism and Experimental method

2.7.1 Electrode with a V-shaped cross-section track

According to the experience in section 2.4, to restrict the movement of the MFS-ball in the direction perpendicular to the moving direction of the workpiece, an electrode with a V-shaped cross-section trace on its surface was used, as shown in Figure 2.20. From that, it can be observed that there is a V-shaped cross-section paralleling the reciprocating moving direction of the workpiece on the electrode surface. During processing, because of this V-shaped cross-sectional track, the movement of the MFS-ball on the Y-axis can be restricted. At the same time, the movement in the Z-axis was limited by the workpiece and the electrode. Finally, the ball could only roll in the X-axis direction.

In addition, in order to make sure that the starting point of the movement of the MFS-ball can be determined and remained in the same area, as shown in Figure 2.20, a short tube is fixed on the left end of the V-shaped cross-section track. Before processing, the MFS-ball is placed next to the short tube. After that, to provide fresh electrolytes to the MFS-ball constantly, an electrolyte nozzle is inserted into the short tube, and then the electrolyte flows along the V-shaped cross-section track.

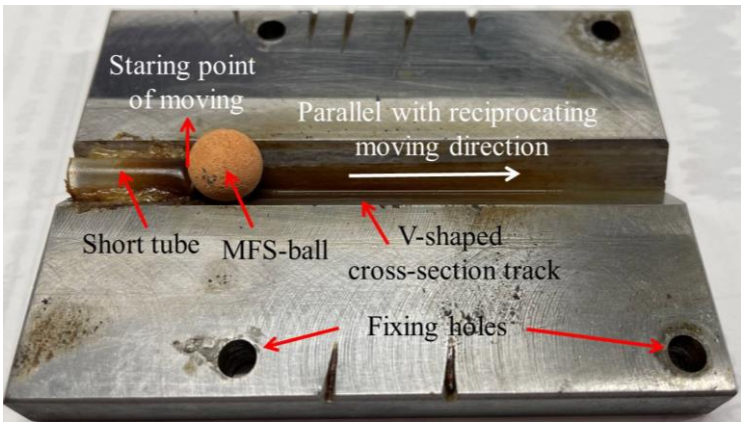

Figure 2.20 Electrode with V-shaped cross-section track.

2.7.2 Processing method

The photo of the electrode and the schematic of the proposed ECM method are shown in Figures 2.21(a) and Figure 2.21(b). After absorbing the electrolyte, the MFS-ball is inserted between the electrode and the workpiece. The electrode, which has the flowing electrolyte on its surface, is placed beneath the workpiece and the MFS-ball. In contrast to the conventional ECM, the workpiece is placed above the electrode and MFS-ball, instead of being immersed in an electrolyte tank.

During the entire ECM process, the distance between the electrode and workpiece is maintained constant, and the workpiece driven by the CNC machine scans linearly and reciprocates along the X-axis direction. At the same time, the MFS-ball rolls along the scanning direction of the workpiece because of the friction between them. In addition, in the areas where the MFS-ball contacts the flowing electrolyte on the electrode surface, the ECM by-products that adhere to the MFS-ball are cleaned off by the flowing electrolyte, and the MFS-ball re-absorbs fresh electrolyte and delivers it to the machining area.

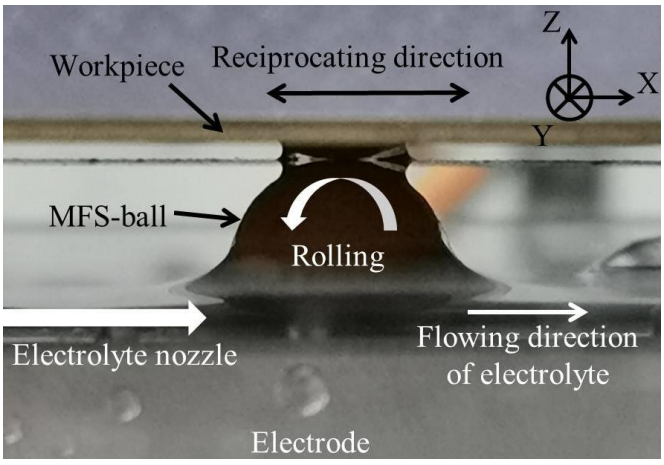

(a) Process photographic view parallel to moving direction.

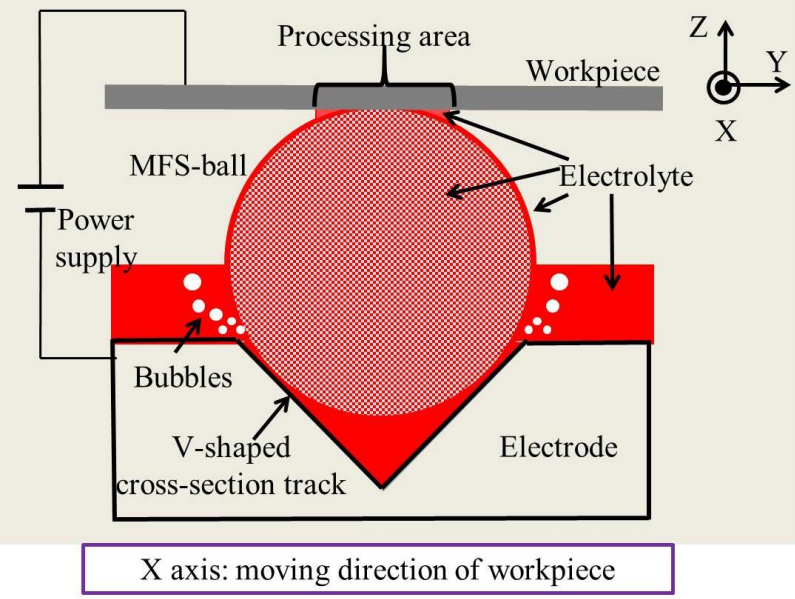

(b) Schematic cross-sectional view of the ECM process perpendicular to the moving direction.

Figure 2.21 Photo and schematic of ECM process.

2.7.3 Experimental procedure

The experimental procedure is as follows:

(1) Workpiece positioning and contact detection test:

During the power-off period, the workpiece was moved toward the MFS-ball in the Z-axis direction, which was placed on the V-shaped track of the electrode. Because the workpiece and electrode were connected separately to the probes of a digital multimeter (CUSTOM DM-01, CUSTOM Corp.), closing the circuit via contact between the workpiece and MFS-ball caused the multi-tester to beep. To ensure that the workpiece was in contact fully with the MFS-ball along the entire movement track, the workpiece was moved 0.1 mm further after the contact, defined as the extra movement distance. At the same time, the maximum pressure between the MFS-ball and workpiece was measured to be approximately 15 N.

As obtained in section 2.5, the MFS-ball is not of an ideal spherical shape, and the diameter of the MFS-ball as measured from its different parts was not exactly the same. If the extra

movement distance were to be less than 0.1 mm, the MFS-ball would be unable to contact the workpiece. It would signify that the MFS-ball would not be rolling upon the workpiece during that duration of the ECM process, stopping the electrolyte circulation in that machining area. On the other hand, if the extra movement distance were to be greater than 0.1 mm, the maximum pressure between the MFS-ball and workpiece would be higher than 15 N. Because of the excessive pressure, the MFS-ball would be easily broken, which would result in the failure of the ECM process.

(2) Pre-scanning:

Two electrolyte pumps (GPU-1, AS ONE Corp.) were switched on, one of them is used to pump the electrolyte into the V-shaped track on the surface of the electrode, and another is used to pump waste electrolytes from the electrolyte tank to filter devices. Subsequently, the workpiece reciprocated along the X-axis direction under the drive of the CNC machine. At the same time, the MFS-ball rolled along the V-shaped track with the reciprocating movement of the workpiece. This step in the experiment, without the participation of the power supply, is referred to as pre-scanning. The purpose of the pre-scanning is to form an electrolyte film on the MFS-ball surface and accumulate electrolytes at the processing area. Otherwise, the whole ECM cannot be performed stably. The influence of the processed result and the necessity of the pre-scanning will be reported in chapter 4.

(3) ECM processing:

After the pre-scanning period, the power supply was switched on, and the workpiece and the MFS-ball were moved repetitively. With the machining current flowing in the circuit, electrochemical reactions occurred on the workpiece surface where the electrolyte was present.

(4) Ending:

After the ECM, the power supply and electrolyte pump were turned off, and the workpiece was moved in the positive Z-axis direction, then the CNC machine was switched off.

This study applied common experimental conditions, given in Table 2.7, to verify the feasibility of this experimental method.

Table 2.7 Common experimental conditions.

Item	Specification
Absorption material	MFS-ball
MFS-ball diameter	10 mm
Workpiece material	SUS304 plate
Electrode material	SUS304 plate
Electrolyte	10 wt.% NaCl solution
Number of reciprocating pre-scanning	8

2.8 Experimental result

By using the experimental equipment and the processing method, and experimental procedures reported before, the ECM processing was started, and the experimental parameters shown in Table 2.8 and Table 2.9 were used.

Table 2.8 Experimental parameters.

Parameter	Value
Movement distance of workpiece	50 mm
Movement speed of workpiece	8 mm/s
Constant current	40 mA
Pre-scanning time	100 s
Machining time	400 s
Number of machining reciprocating cycles	32

2.8.1 Mechanical grinding effect of MFS-ball

As reported in section 2.5, the MFS-ball is a kind of hard porous solid, hence the mechanical grinding process could grind some of the workpiece material when the MFS-ball is moved over the workpiece. To examine the effect of mechanical grinding caused by the MFS-ball, an experiment was conducted before the ECM process without a power supply, the other machining conditions remained unchanged.

After this experiment, the processing area was measured by using the contour-measuring machine, and the results are shown in Figure 2.23(b) using a yellow line. By comparing with the measurement result of the green line, it can be found that there is no difference between them. The results indicate that no shallow groove was produced without a power supply, which verified that the grinding of the MFS-ball would not affect the ECM process.

2.8.2 Experimental result and measurement result

At the end of the ECM, a photograph was captured parallel to the scanning direction, as shown in Figure 2.22(a). The diameter of the MFS-ball was approximately 10 mm, whereas the width of the electrolyte distribution area was measured to be 5.6 mm approximately.

A photo of the processed trace is shown in Figure 2.22(b). At any moment in the procedure, a circular area, where the electrolyte was present, was etched by electrochemical reactions. The entire processed groove can be regarded as an overlap of countless circular machining areas. Because the circular areas were equal to each other, the current density and machining rate were maintained nearly constant under a constant current mode.

In addition, as shown in Figure 2.22(b), the length of the processed groove, measured between the centers of the two end circles, was approximately 50 mm, which was equal to the distance moved by the workpiece. Therefore, it verifies that during the ECM process, the MFS-ball spins along the moving direction of the workpiece instead of slipping.

The three-dimensional machined shape in the red frame of Figure 2.22(b) was measured using the 3D measurement device. The measurement results are shown in Figure 2.22(a). In addition, the cross-sectional shape of the processed groove was measured along the measuring line using the contour-measuring machine, as shown in Figure 2.22(b). To facilitate comparison, a cross-section of the same area was measured before machining.

To evaluate the processed groove from the cross-sectional measurement results, the groove width and the depth, which is defined as the distance between the deepest point of the groove and the raw surface of the workpiece, are shown in Figure 2.22(b).

According to Figure 2.22, the width of the cross-section of the processed groove was approximately 5.6 mm, the depth was approximately 17 μm, and there was no electrochemical corrosion on the workpiece surface other than on the processed groove. In addition, the width of

the cross-section of the processed groove was equal to the width of the electrolyte covering area. This result proves that the MFS-ball can limit the electrolyte distribution and the scope of the electrochemical reactions.

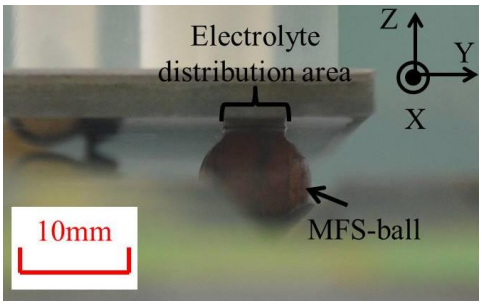

(a) Process photographic view parallel to scanning direction.

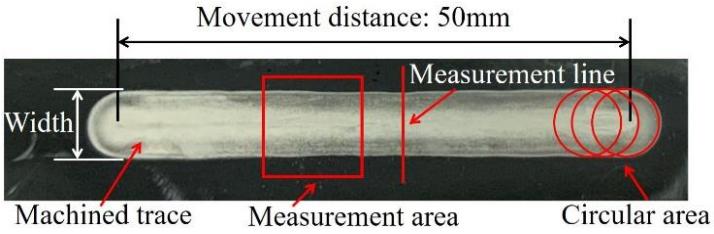

(b) Machined trace on workpiece surface.

Figure 2.22 Process photograph and machined trace.

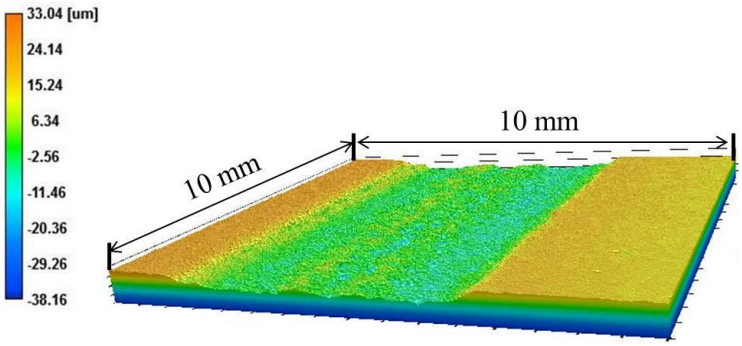

(a) Three-dimensional values in the measurement area.

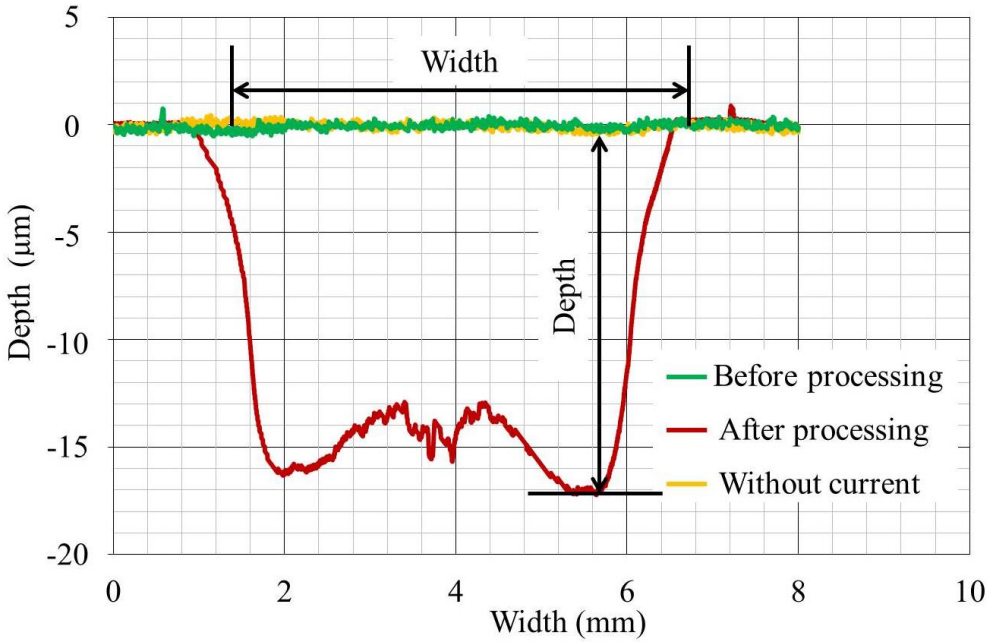

(b) Cross section of the machined trace.

Figure 2.23 Measurement results for the machined trace.

2.9 Discussion about processed result

From the aforementioned machined results, it was determined that the depth of the edge area of the processed groove is greater than that of the processed groove's center area. It is thought that the depth difference is caused by the distribution of the electrolyte and the machining current. At the edge area of the processed groove, the amount of electrolytes is more than that at the center area. At the same time, the value of the machining current flowing through the electrolyte film is greater than the machining current flowing through the inside electrolyte of the MFS-ball.

To verify the two hypotheses above, the following research was carried out.

2.9.1 Discussion about electrolyte distribution

In ECM, because of the restrictions induced by the MFS-ball, the electrolyte and machining current can exist only in the machining area, as shown in Figure 2.24(a). Based on this observation, combined with the measurement results shown in Figure 2.24(b), the machining area can be divided into two parts: Zone A and Zone B. The center area where around the contact point of the MFS-ball and workpiece, is defined as Zone B and the other area of the processing area is defined as Zone A.

For Zone B, the electrolyte required for ECM is mainly from the electrolyte absorbed inside the MFS-ball. Here, less of the machining current, which also flows through the inside of the MFS-ball, is accumulated. After the processing, some of the ECM by-products, which are distributed in the electrolyte solution, remain in the machining area, as shown in Figure 2.25(a). The others are adsorbed onto the surface or absorbed inside the MFS-ball because of capillary action. Therefore, the specific penetration of ECM by-products into the MFS-ball needs to be investigated in follow-up experiments.

For Zone A, the electrolyte film can directly provide electrolytes for electrochemical

reactions, and thus, much more of the machining current is accumulated here. Because there are more electrolytes and machining currents in Zone A than in Zone B, the speed of the ECM process is increased. Moreover, the depth of Zone A is greater than that of Zone B.

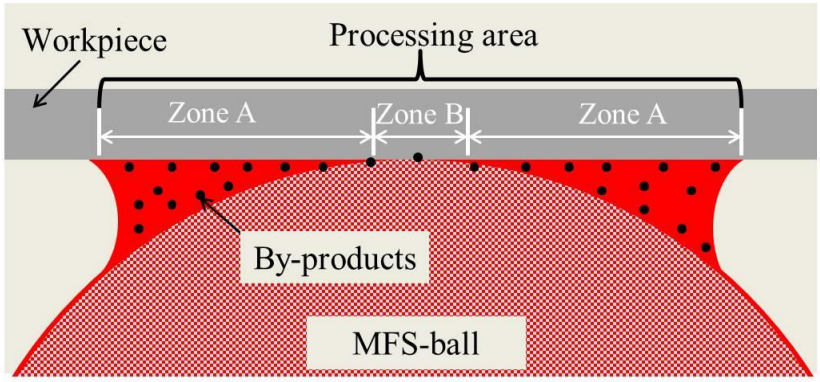

(a) Partition of the machining area.

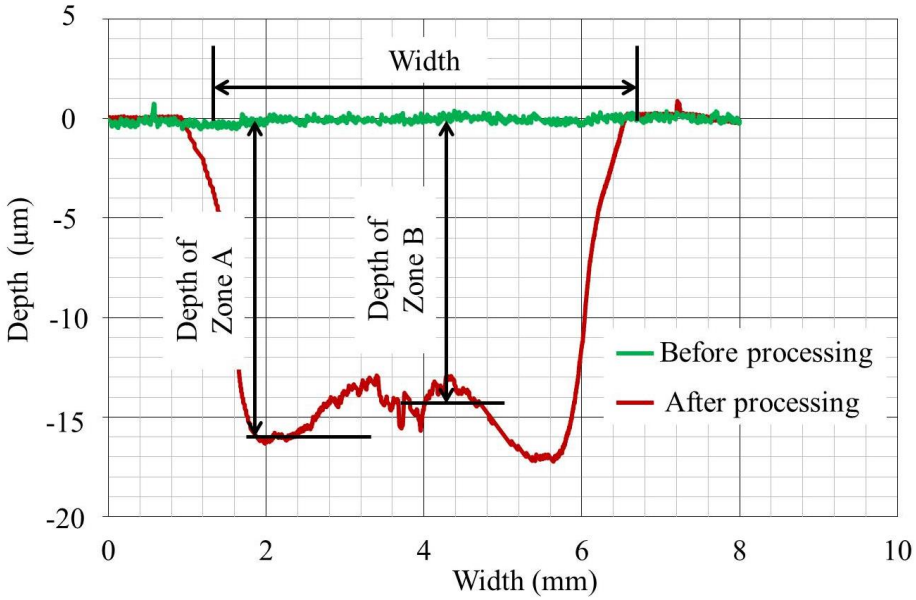

(b) Cross section of the processed groove.

Figure 2.24 Partition of machining area and cross section of machined trace.

As the MFS-ball rolls, the adhering by-products are moved to the area near the electrode, where there is a flowing electrolyte. Most of the by-products are washed away by the flowing electrolyte and flow into the waste electrolyte pool along the V-shaped cross-sectional track on the electrode, as shown in Figure 2.25(b).

In addition, to thoroughly clean off the ECM by-products that adhere to or are absorbed by the MFS-ball, it is necessary to use the ultrasonic cleaning machine on the MFS-ball after every experiment.

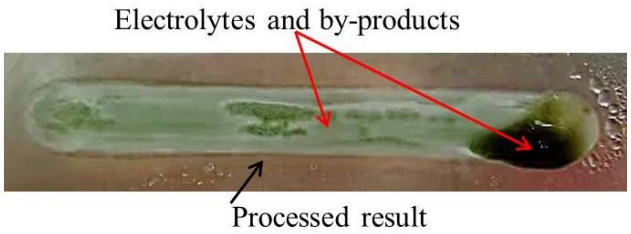

(a) Processed result, electrolytes and by-products at workpiece surface.

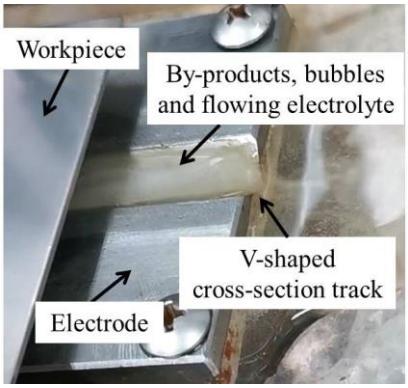

(b) Photograph of exit of the electrode with V-shaped cross-section track.

Figure 2.25 Photograph of Processed result and exit of the electrode.

2.9.2 Discussion about machining current paths

As described in section 2.6, the MFS-ball carries the electrolyte not only inside its porous structure but also as a film covering its surface. Hence, during ECM, the machining currents

flow through paths that include both the electrolyte inside the MFS-ball and the electrolyte film on its surface. The diagram of these current paths is shown in Figure 2.27(a). The equivalent circuit for machining using the MFS-ball is shown in Figure 2.27(b). For obtaining the machining currents flowing through the electrolyte film and inside the MFS-ball separately, the current flowing paths are regarded as two branches of the electric circuit. The relationship between the electrical currents can be obtained with equation (2-2).

The following experiments were performed to verify the inferred machining current flowing paths and to measure the value of the machining current flowing through each current path.

2.9.2.1 Total machining current of ECM

In the first experiment, the total machining current value of the normal ECM process was measured. This experiment was performed using the procedure described in section 2.7, the parameters given in Table 2.8, and a machining time of 100 s. And a constant voltage of 4 V, which is smaller than the voltage in ECM when the MFS-ball was covered by the electrolyte film, was used. Therefore, in the subsequent experiments, where the MFS-ball is used without an electrolyte film, the electrolyte inside the MFS-ball will not be consumed quickly, and the ECM can proceed for a longer period.

The waveforms of the machining current and voltage, shown in Figure 2.27, were measured using a current probe (i30s/i30 AC/DC Current Clamps, FLUKE Corp.) and a voltage probe with an oscilloscope (TDS 2001C, Tektronix Inc.). The average total machining current I was 33.1 mA. With the equation (2-3) and (2-4), the electrical resistance between the workpiece and the electrode R is about 71 Ω.

$$I = I_f + I_i \quad (2\text{-}2)$$

$$R = \frac{U}{I} \quad (2\text{-}3)$$

$$\frac{1}{R} = \frac{1}{R_f} + \frac{1}{R_i} \quad (2\text{-}4)$$

where I is the total machining current, I_f is the machining current flowing through the electrolyte film, and I_i is the machining current flowing through the inside of the MFS-ball. R is the total electrical resistance, U is the potential between the workpiece and the electrode, R_f is the electrical resistance of the electrolyte film, R_i is the electrical resistance of the inside of the MFS-ball absorbed with electrolytes.

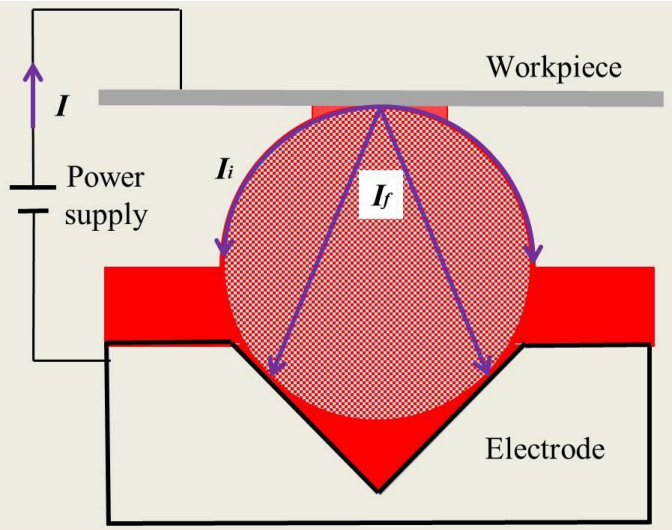

(a) Current paths of ECM.

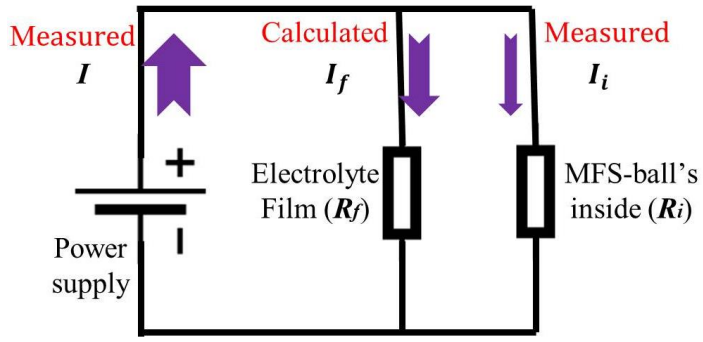

(b) Diagram of electric circuit.

Figure 2.26 Diagram of current paths and electric circuit.

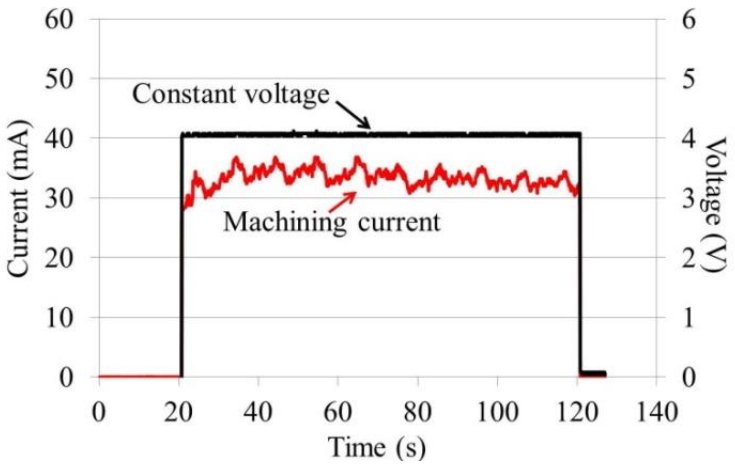

Figure 2.27 Current and voltage waveforms for MFS-ball with an electrolyte film.

2.9.2.2 Machining current flowing through every path

In the second experiment, the machining current that flows through the inside of the MFS-ball was measured. As shown in Figure 2.28, the electrolyte film on the MFS-ball surface was cleaned after the electrolyte absorption process. During the entire ECM process, there is no electrolyte suppling, whereas the other experimental parameters and procedures were the same as those in the first experiment. The machining results are shown in Figure 2.29. Because there was no electrolyte supply, the experiment lasted for approximately 65 s. Finally, once the electrolyte inside the MFS-ball was consumed completely, only the insulated dry MFS-ball was

present between the workpiece and the electrode, rapidly decreasing the machining current to 0 mA. Hence, the entire experiment had to be stopped.

The machining results show that the workpiece surface was corroded by electrochemical reactions, and an average machining current I_i of 11.8 mA was detected between the electrode and the workpiece. From these two experiments, it was determined that the machining current I_i flowing through the inside of the MFS-ball accounted for 35.6% of the total machining current I of the circuit. The electrical resistance of the inside of the MFS-ball absorbed with electrolytes R_i is about 289 Ω.

Using equations (2-2), (2-3), and (2-4), we calculated that the machining current flowing through the electrolyte film was 21.3 mA, which accounted for 64.4% of the total machining current I, the electrical resistance of the electrolyte film R_f is about 94 Ω.

From these results, we inferred that, during an ECM process using an MFS-ball, the machining current starts from the workpiece and flows not only through the electrolyte film on the surface of the MFS-ball but also through the inside of the MFS-ball to the electrode. Moreover, affected by the electrical resistance of every through path, the machining current flowing through the electrolyte film is greater than that flowing through the inside of the MFS-ball.

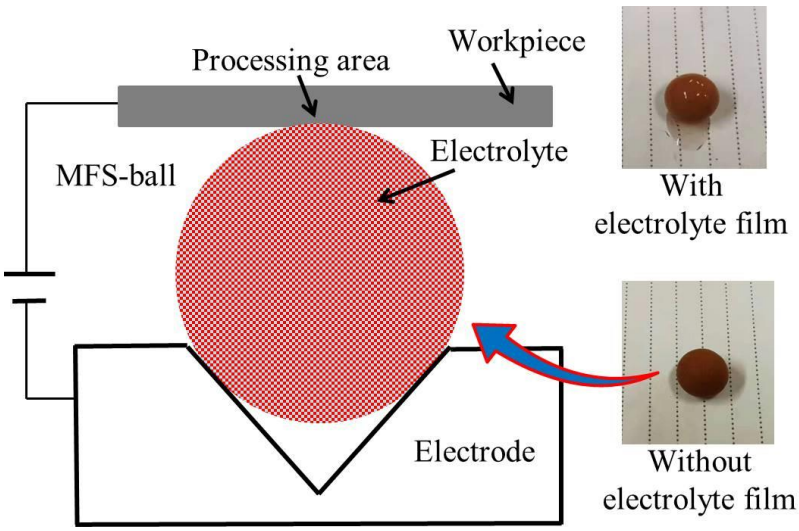

Figure 2.28 Process without electrolyte film on surface of the MFS-ball.

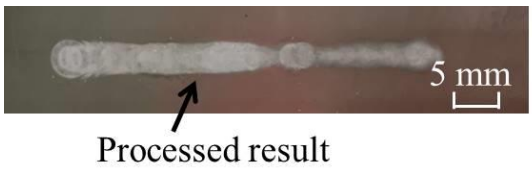

(a) Processed result on the workpiece surface.

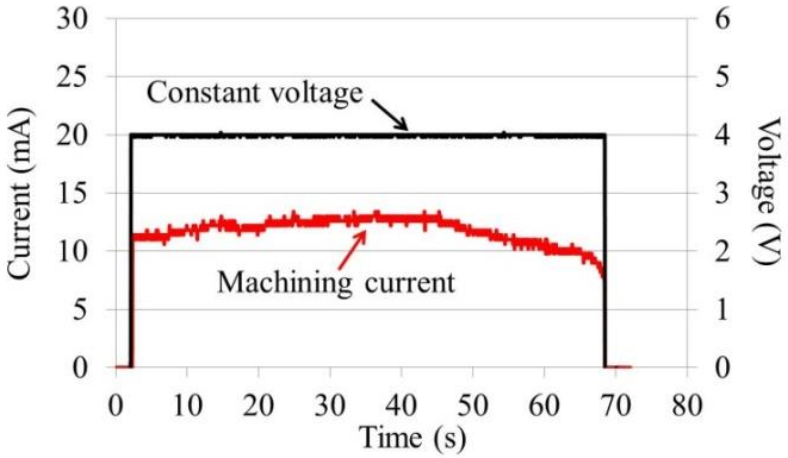

(b) Current and voltage waveforms for MFS-ball without electrolyte film.

Figure 2.29 Processing results and current and voltage waveforms for MFS-ball without electrolyte film.

2.10 Conclusion

In this chapter, first of all, by using two kinds of water absorption materials, the diatomaceous earth chip, and the MFS-ball, ECM experiments were carried out tentatively. According to experiment results, it is found that though the diatomaceous earth chip has superior electrolyte absorption, due to its poor water resistance and soft texture, the diatomaceous earth chip is easily dispersed in electrolytes and broken during ECM.

Compared with the diatomaceous earth chip, when it is used in experiments, the MFS-ball has good water resistance and absorption, and the strength of the MFS-ball is good enough to be used for a long time. In ECM processing, the distribution of the electrolyte is controlled well too. Hence, the MFS-ball is selected as the electrolyte absorption material in ECM for the following research.

After that, we introduced the MFS-ball and its electrolyte-absorbed principle of capillary action in detail. Thanks to the MFS-ball's porous structures consisting of abundant micro holes, the electrolyte is absorbed into the MFS-ball and forms an electrolyte film on the MFS-ball surface driven by a physical phenomenon of capillary action. During ECM, the MFS-ball can take the electrolyte to the ECM processing area, and due to the limitation of the MFS-ball, electrolytes cannot flow at the workpiece surface, which eliminates the effects of the stray-current corrosion.

Before processing with the MFS-ball, several main devices the experimental equipment, and the electrode were introduced. Then, experimental procedures of using the experimental equipment in ECM were listed.

And through the photo of ECM and the processing schematic, we summarized that, due to capillary action, the MFS-ball can absorb electrolytes to its inside and form an electrolyte film on its

surface. As rolls of the MFS-ball in ECM, the MFS-ball provides fresh electrolytes to the processing area and takes away ECM by-products continuously. At the processing area, limited by the MFS-ball, the electrolyte distributes to a small area around the contact point between the workpiece and the MFS-ball.

Besides that, from the experimental results, it is verified that the stray-current corrosion can be eliminated due to the distribution of the electrolyte being limited by the MFS-ball, and only the area where there are electrolytes existing dissolved to become a shallow groove. And the depth of the groove's edge area is deeper than that of the groove's center area.

It is clear that during ECM processing of this research, machining currents flow through both the inside electrolyte and the electrolyte film of the MFS-ball, and the value of the machining current flowing through the electrolyte film is greater than the current flowing through the MFS-ball's inside electrolyte.

Chapter 3 Simulation and verification of processed result of ECM

3.1 Introduction

From the results of chapter 2, experimental materials and devices, processing principle and method, the processed groove, the electrolyte distribution, and values of machining currents flowing through each path were obtained. However, during the processing of this ECM method, situations including the potential between the workpiece and the electrode, the current density distribution at the processing area cannot be observed and measured. Besides that, the explanations for the depth difference that exists at the cross-section of the processed trace were not solved well. And it is thought that the machining current density and the current distribution are difficult to be measured and calculated from experiment results.

Hence, in this chapter, a finite element analysis software COMSOL Multiphysics was used to try to calculate the machining current density and its distribution at the processing area by simulating ECM processing. At the same time, the potential between the workpiece and the electrode was obtained. Combining with the machining current density and its distribution, the processed results in simulating and the profile of the processed trace, and the depth difference of the processing area were confirmed and explained fully. In addition, by changing the conductivity of the MFS-ball, which is difficult to be accomplished in actual experiments, in simulating, the relation between the MFS-ball and its surface electrolyte film and the roles they play in ECM processing were obtained.

After that, actual experiments were carried out with this ECM method to verify the simulation results. And by comparing with processing results of the point processing and the groove processing of chapter 2, discussions and summaries were done.

3.2 Concept and geometry model for simulation

In order to build the simulation model, it is necessary to know the thickness of the electrolyte film covering the surface of the MFS-ball first.

Under the conditions as shown in Figure 4.1(a), the diameter of the MFS-ball without the electrolyte film on is surface is measured at about 10 mm. In the case that the MFS-ball is being covered by the electrolyte film, as shown in Figure 4.1(b), the outer diameter of the film becomes 10.23 mm. Hence, the thickness of the electrolyte film can be calculated to be about 0.115 mm. In order to facilitate subsequent simulations and calculations, the electrolyte film thickness in simulating was set as 0.2 mm roughly.

When model building, in order to highlight the processing area of ECM, the part of the green frame in Figure 4.1(b) was selected and used. The 2D model is shown in Figure 4.2. As measured from experiments of chapter 3, the width of the whole electrolyte distribution area during ECM is about 5.6 mm. Since half of the electrolyte distribution area was used in the 2D model, its width was set as 2.7 mm. And to reduce the complexity of the model while preserving the important and relevant conditions, the following assumptions were made to the 2D model:

· During simulating, the workpiece contacted with the MFS-ball and the electrolyte film of the MFS-ball surface, hence, currents could flow through the MFS-ball's inside and the electrolyte film at the same time.

· During the simulation, the capillary action of the MFS-ball and the surface tension of the electrolyte were not taken into consideration.

· The material of electrolyte film was liquid, whose electrical conductivity was set to be 12 S/m, which is the same as the electrical conductivity of 10 wt.% NaCl solution.

· The material of the MFS-ball was set as a stone material. In order to ensure that currents could flow through the MFS-ball inside during simulating, in section 4.3, the electrical conductivity of the MFS-ball was set to be 6 S/m hypothetically. In simulations of section 4.4, the influence of the electrical conductivity of the MFS-ball was considered.

· Electrochemical polarization and concentration polarization were ignored.

· Both the cathode of the 2D model's bottom and anode of the workpiece were considered distinct equipotential surfaces. And only the potential, the current distribution, and the processed result of the processing area were simulated.

· The change in conductivity, temperature, concentration and film thickness of the electrolyte during ECM processing was ignored.

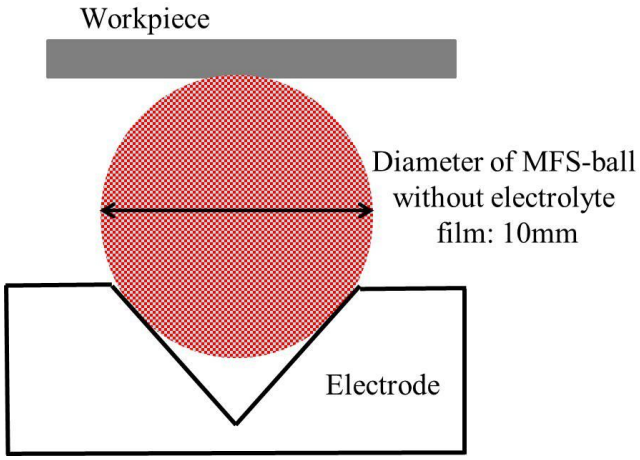

(a) Diameter measuring of MFS-ball without electrolytefilm.

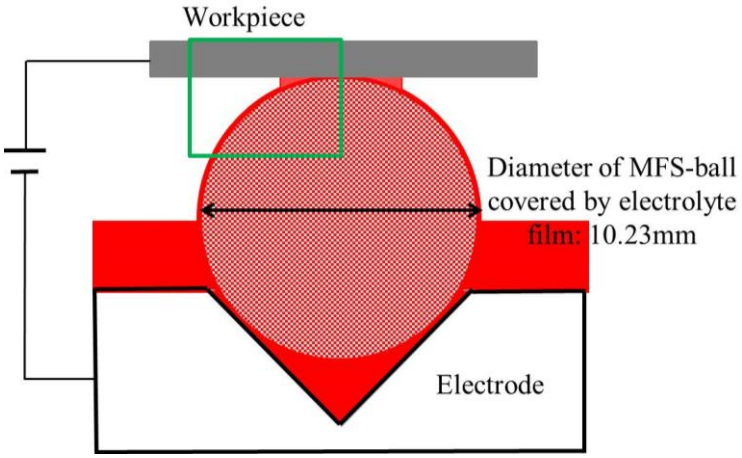

(b) Diameter measuring of MFS-ball with electrolytefilm.

Figure 3.1 Schematic of diameter measuring of MFS-ball without /with electrolyhte film.

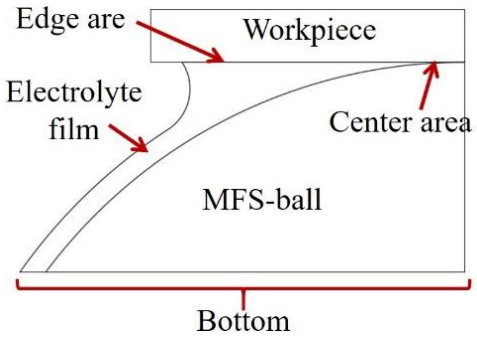

Figure 3.2 2D geometry model of ECM.

3.3 Multiphysics formulations

According to the electric field theory, the Laplace equation is capable of obtaining potential at any point in the electrolyte domain, given by:

$$\nabla^2 \nu = 0 \qquad (3\text{-}1)$$

where ∇ is the Laplace operator and ν is the potential field. Similarly, Ohm's law is used to obtain a normal current density (J_n) across the electrolytic domain.

$$J_n = -\sigma \cdot \nabla \nu \qquad (3\text{-}2)$$

where σ is the electrical conductivity of the electrolyte.

Faraday's equation is used to govern the material dissolution rate of the ECM process, given by:

$$V_n = \frac{\eta \cdot A \cdot J_n}{z \cdot F \cdot \rho_w} \qquad (3\text{-}3)$$

where η is the current efficiency, which is set to 100 % in this research since a NaCl aqueous solution is used. V_n is the material dissolution rate, A is the atomic weight, z is the valence of the workpiece material, and ρ_w is the density of the workpiece material. Those parameters depend on the workpiece material in simulations and experiments. F is the Faraday's Constant which is equal to 96,500 C/mol, J_n is the current density obtained from Equation. (3-2).

3.4 Simulation results

3.4.1 Simulation results of potential, current density distribution, and processed result

By using the 2D model of ECM, Multiphysics formulations of section 3.2, and simulation conditions of Table 3.1, simulations were carried out, and simulation results are obtained and shown in Figure 3.3. With Equation (3-3), simulation results of the location and the profile at the processed area are obtained and shown in Figure 3.4. For ease of the description and the understanding of the following, the area whose processed depth is less than 2 μm is called the center area, and the other area whose processed depth is more than 2 μm is called the edge area.

It can be found clearly from Figure 3.3 that the edge area has a greater current density. In

Table 3.1 Simulation conditions.

Item	Specification
Material of workpiece	SUS304
Thickness of electrolyte film	0.2 mm
Width of processing area	2.7 mm
Potential of workpiece	13 V
Potential of 2D model's bottom	0 V
Electrical conductivity of electrolyte film	12 S/m
Electrical conductivity of MFS-ball	6 S/m
Temperature	293.15 K
Simulation time	0.8 s

the center area close to the contact point of the MFS-ball and the workpiece, the current density gradually decreases.

The current density distribution curve is shown in Figure 3.3(c). The current density increases to the maximum value, which is about 11 A/m^2, along the horizontal axis first, and then decreases gradually to the minimum value, which is about 3.5 A/m^2.

To facilitate the following comparison and discussion, we took the line of X=0 in the 2D model as the symmetry axis and symmetrized the processed result of Figure 3.4(a) to get the whole cross-section profile of the processed area, shown in Figure 3.4(b). From Figure 3.4, we found that the electrolyte distribution area is dissolved by electrochemical reactions, and the greater the current density, the deeper the depth of corrosion.

In summary, from the simulation results above, the machining current density and its distribution were obtained and affected by the machining current density distribution at the processing area, the depth difference exists in the simulation result of the processed area.

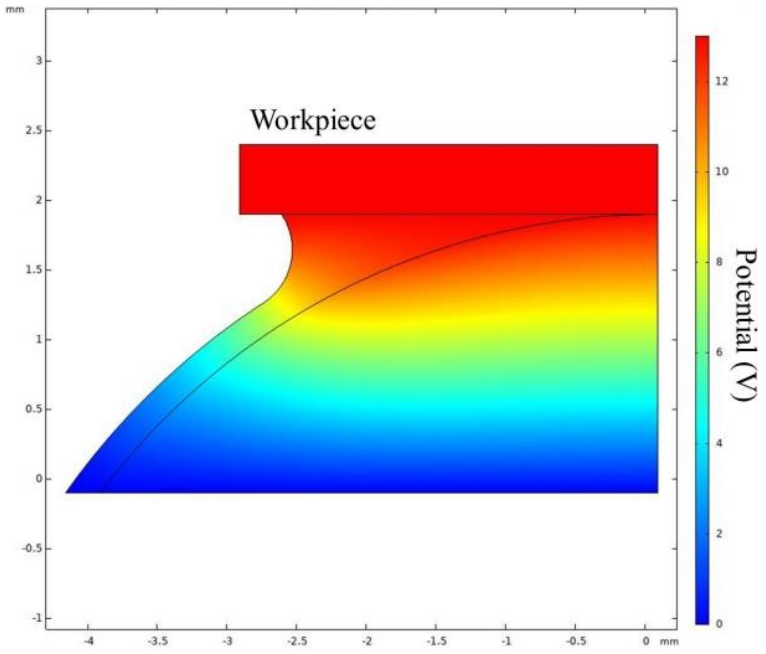

(a) Simulation result about potential.

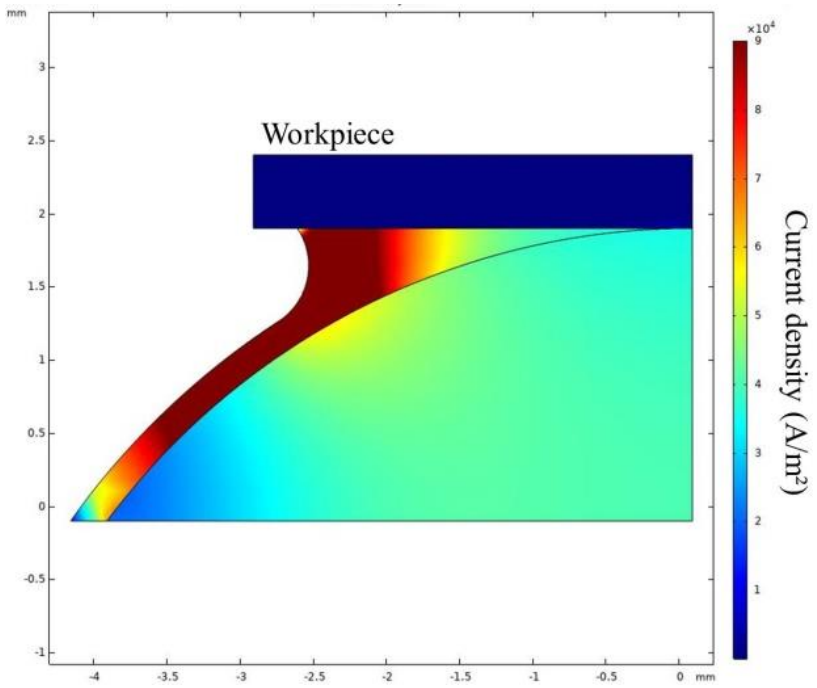

(b) Simulation result about current density distribution.

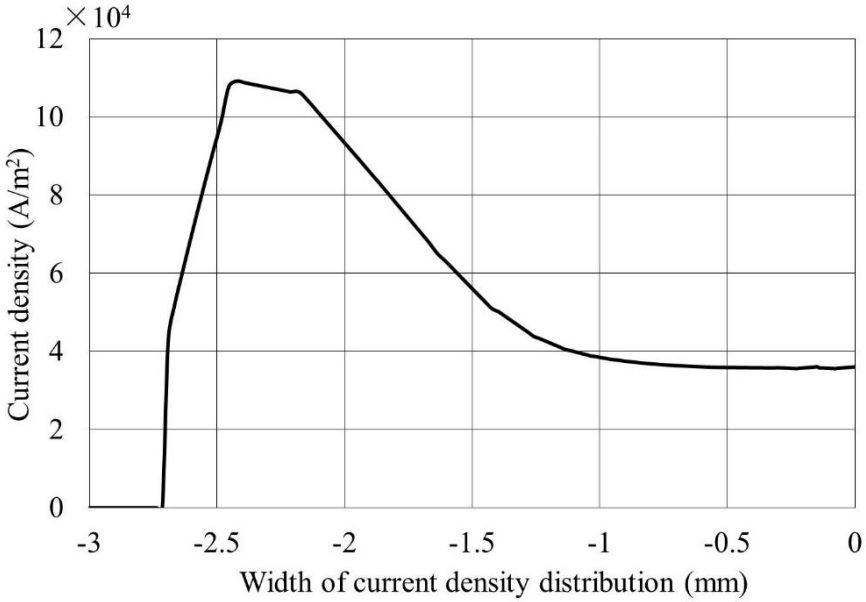

(c) Simulation result about current density distribution curve along processing area.

Figure 3.3 Simulation result about potential, current density distribution, and current density distribution curve along processing area of 2D model.

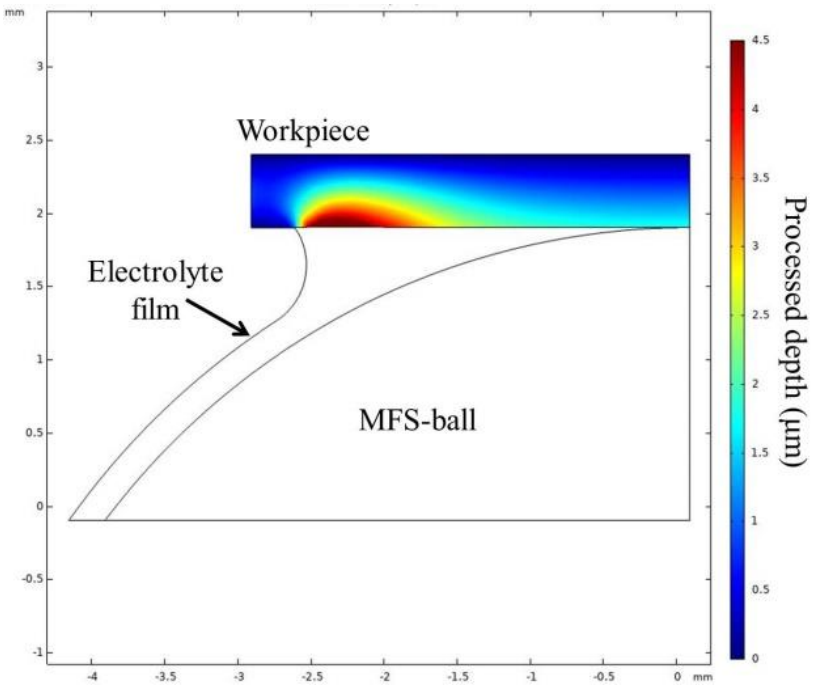

(a) Simulation results about processed location and depth.

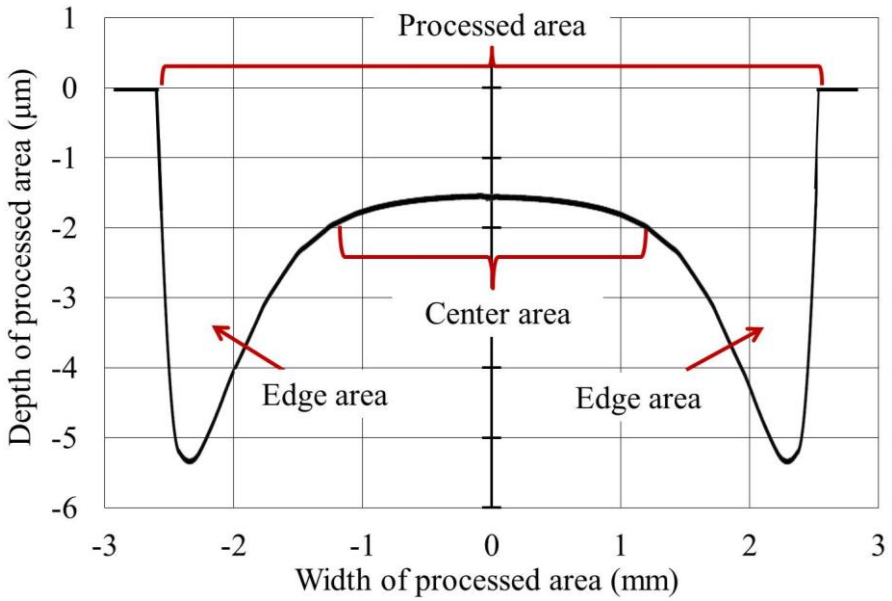

(b) Simulation results about profile of processed area.

Figure 3.4 Simulation results about processed location and depth, and profile of processed area.

3.4.2 Simulation by changing electrical conductivities of MFS-ball

After absorbing electrolytes, there are currents following through the inside electrolyte of the MFS-ball, which was measured in section 2.9 and simulated in section 3.4.1. However, the electrical conductivity of the MFS-ball is unknown and not measurable. Hence, in section 3.4.1, we tentatively set it as 6 S/m. But, when the MFS-ball's electrical conductivity is changed, if and how the processed result of ECM is affected and how the processed result is affected are not investigated until now.

In this section, to explore whether the processing result will be affected when the conductivity of the MFS-ball is changed, simulations by changing the electrical conductivity of the MFS-ball were carried out. During simulating, the MFS-ball electrical conductivity was increased from 0 S/m, which means no electrolyte exists inside of the insulation MFS-ball, to 12 S/m, which is equal to the electrical conductivities of the 10 wt.% NaCl solution. And we used the simulation conditions listed in Table 3.1 except for the electrical conductivity of the MFS-ball.

Simulation results are shown in Figure 3.5. When changing the electrical conductivity of the MFS-ball, the distribution of the machining current density and the shape of the profile of the processed result are not affected roughly. Similar to the simulation result of section 3.4.1, the current density and the processed depth of the edge area are greater than that of the center area.

However, as the electrical conductivity of the MFS-ball increasing, both the current density value and the processed depth at the processing area increase. The reason is that because the potential between the workpiece and the electrode is kept constant, as the electrical conductivity of the MFS-ball is increased, the resistance between them decreases. Finally, at the processed area, the value of the current density and the processed depth increase at the same time.

Besides that, it can be found that when the electrical conductivity of the MFS-ball is equal to

0, there are still machining currents existing at the edge area of the electrolyte distribution. The reason is thought that although the machining current cannot follow through the inside of the ball, due to there is the electrolyte film on the MFS-ball surface, it can flow through the electrolyte film to arrive at the processed area. In addition, the workpiece surface was corroded slightly by ECM in Figure 3.5(b). Hence, we can speculate that if an insulating ball, which can form an electrolyte film as the MFS-ball does, is used in ECM to control the electrolyte distribution, a shallow groove can be obtained by electrochemical corrosion.

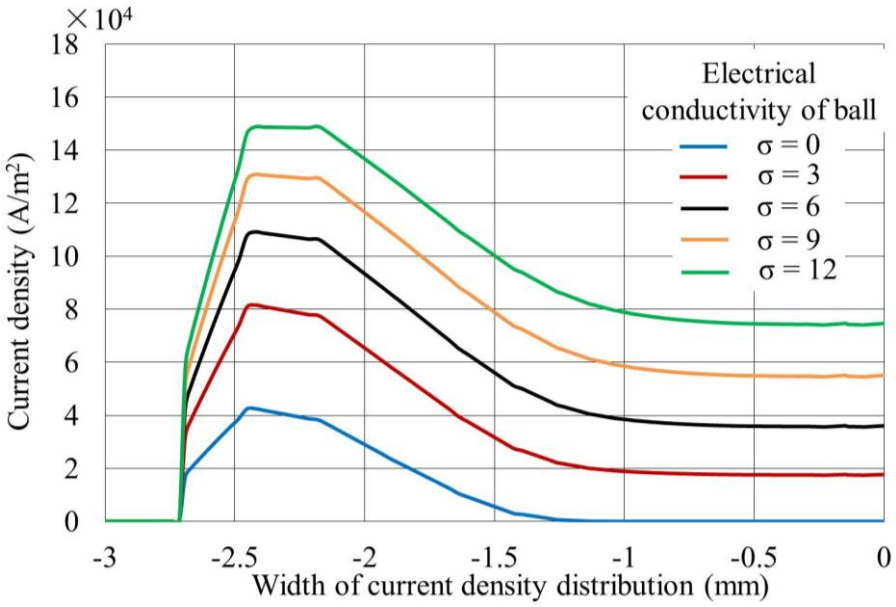

(a) Simulation results about current density distributions.

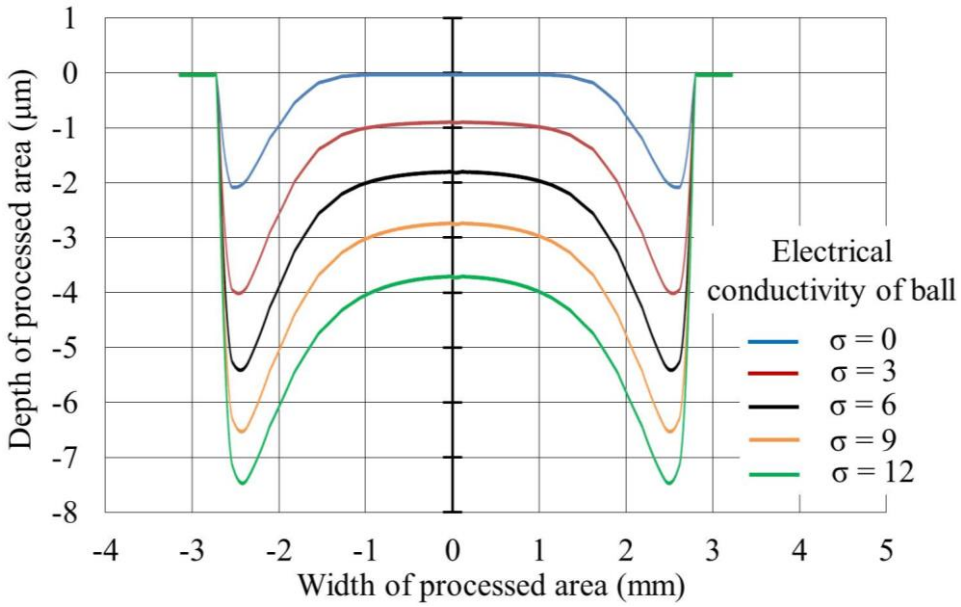

(b) Simulation results about profile of processed area.

Figure 3.5 Simulation results about current density distributions and profile of processed area by changing electrical conductivities of MFS-ball.

In brief, based on the simulation results above, the simulating results about the machining current density distribution and the cross-section profile of the processed area are reliable for the ECM method of this research.

Moreover, the reason for the depth difference of the processed trace existing in chapter 2 can also be explained initially through the simulation results of the machining current density distribution and the cross-section profile of the processed result in this chapter.

3.5 Discussion of experimental results with simulation results

3.5.1 Point processing method and result

During the simulations above, the ECM processing time was 0.8 s, and the voltage between the workpiece and the electrode was set as 13 V. Hence, we used the same conditions in the experiment on point processing. The detailed experimental conditions are listed in Table 3.2. The schematic of the point processing is shown in Figure 3.6. For easy presenting and understanding, we take the workpiece as the reference, which means that the rolling MFS-ball moves between A and B, while the workpiece is regarded as stationary.

Table 3.2 Experimental parameters.

Item	Specification
Pulse current value	200 mA
Frequency of pulse current	1 Hz
Duty ratio of pulse current	10 %
Pulse on time of current	0.1 s
Number of ECM processing	8
ECM processing times	0.8 s

The whole point processing was divided into 8 times, each ECM processing was carried out in 0.1 s. The purpose of this operation is explained as follows. Due to a stronger machining current being used, electrolytes accumulated at the processing area, and the MFS-ball is not enough to be used during the whole ECM process of 0.8 s, the MFS-ball has to supply fresh electrolytes for the next ECM during moving.

As shown in the schematic of the point processing, the MFS-ball moved between A and B, and the location of the point processing is set as the point C. When the MFS-ball arrived at C during the movement from A to B, it was stopped for 2 s. During the stopping period, the power supply provided one pulse current to let electrochemical reactions occur in the processing area. After that, the MFS-ball continued to move to B, and then it turned back to A for the next process. The operation of the reciprocating movement between A and B was repeated 8 times. And the point processing at C was repeated 8 times too, the whole ECM processing time is 0.8 s.

The photo of the point processing result is shown in Figure 3.7(a). As shown in Figure 3.7(b) and Figure 3.7(c), the 3D measurement result was measured by the 3D measuring instrument and the cross-section measurement result was measured by using the contour-measuring.

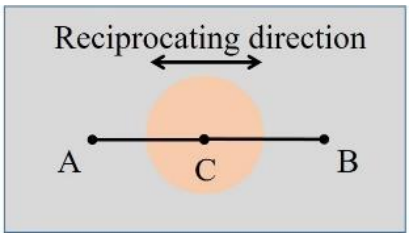

Figure 3.6 Schematic of point processing and moving trace.

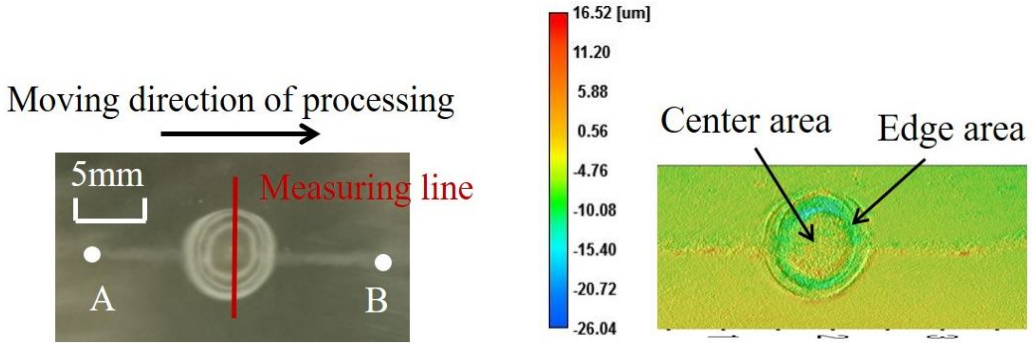

(a) Point processing result. (b) 3D measurement results.

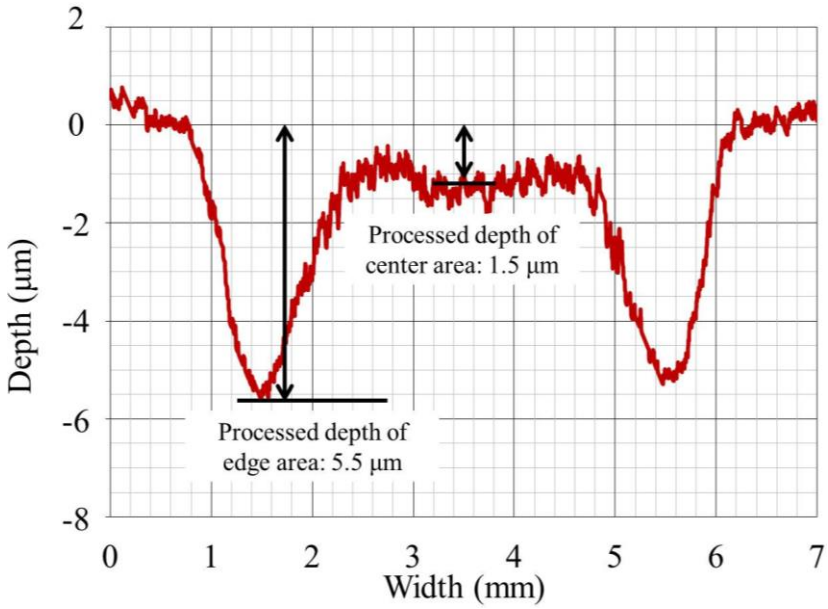

(c) Cross-section measurement result.

Figure 3.7 Point processing result, 3D measurement results, and cross-section measurement result of processed area.

3.5.2 Discussion and comparison between point processing result and simulation result

From measurement results in Figure 3.7(c), we can find that the cross-section shape of the point processing result is similar to the cross-section of the simulation result in Figure 3.4(b), because in both of them, the processed depth of the edge area is deeper than that of the center area, and maximum depths of them are about 5.5 μm, the processed depths of center areas are about 1.5 μm. The comparison of the simulation result and the experiment result of actual point processing is shown in Figure 3.8. Hence, it is considered that, because the processing method of ECM both in the point processing and simulating are similar to each other, the point processing result follows and verifies the simulation results of section 3.4.

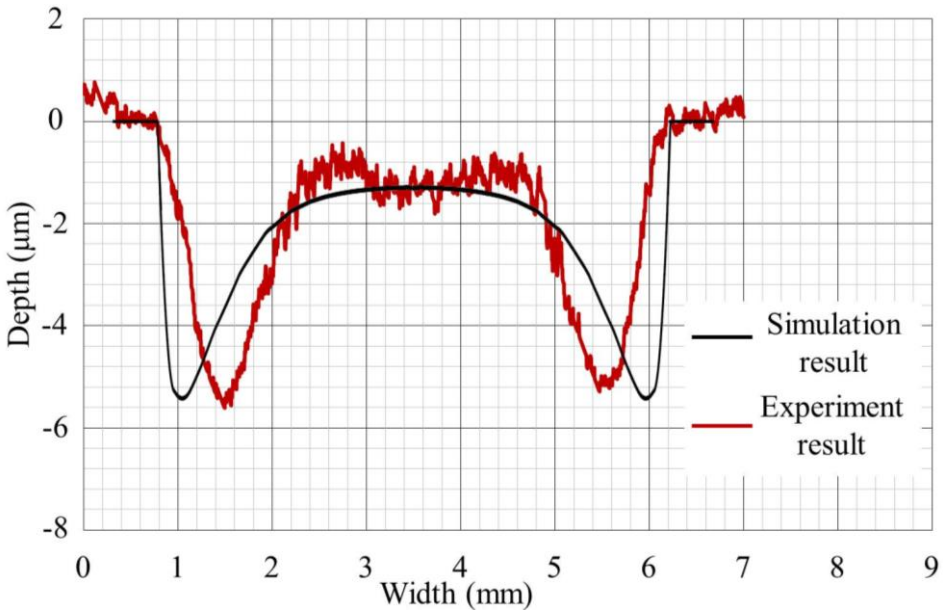

Figure 3.8 Comparison between the simulation result and the experiment result.

However, some differences exist between the simulation result and the experiment result, especially the position of the maximum depth. It is thought that the electrolyte film thickness is ignored during simulating. However, in contrast to simulation, during the actual processing, due to the MFS-ball being kept still without fresh electrolytes supplying, as the electrolyte is consumed by electrochemical reactions, the thickness of the electrolyte film and the area being covered by the electrolyte of the workpiece surface are decreased gradually. Hence, in the experiment result, the position of the maximum depth occurs closer to the center area than in the simulation result.

In conclusion, from the comparison result above, it is considered that the cross-section profile of the simulation result can be verified by the profile of the actual processing result, and the simulation results, which include the potential, the machining current density distribution, are reliable, which can well reflect the situation of the processing area in ECM.

3.6 Discussion of groove processing and point processing in ECM

From the discussion results of section 3.5, it is thought that the simulation results of section 3.4 were verified. However, by comparing the processing result of the point processing in section 3.5 with the groove processing result in Figure 3.9, it can be found that the value of depth difference of the groove processing result is smaller than the point processing result. Experimental parameters of the groove processing are listed in Table 3.3. And the consistency between the cross-section shape of the simulation result and the cross-section shape of the processed groove is less than between the simulation result and the point processing result. The reasons for those conditions above are unknown until now.

Hence, in this part of the research, we will discuss and verify the point processing and the groove processing to try to solve those problems.

Table 3.3 Experimental parameters.

Parameter	Value
Movement distance of workpiece	50 mm
Movement speed of workpiece	8 mm/s
Constant current	40 mA
Pre-scanning time	100 s
Machining time	100 s
Number of machining reciprocating cycles	8

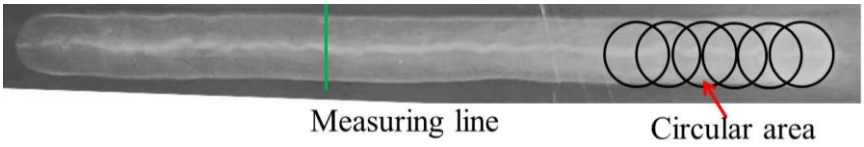

(a) Photo of processed groove.

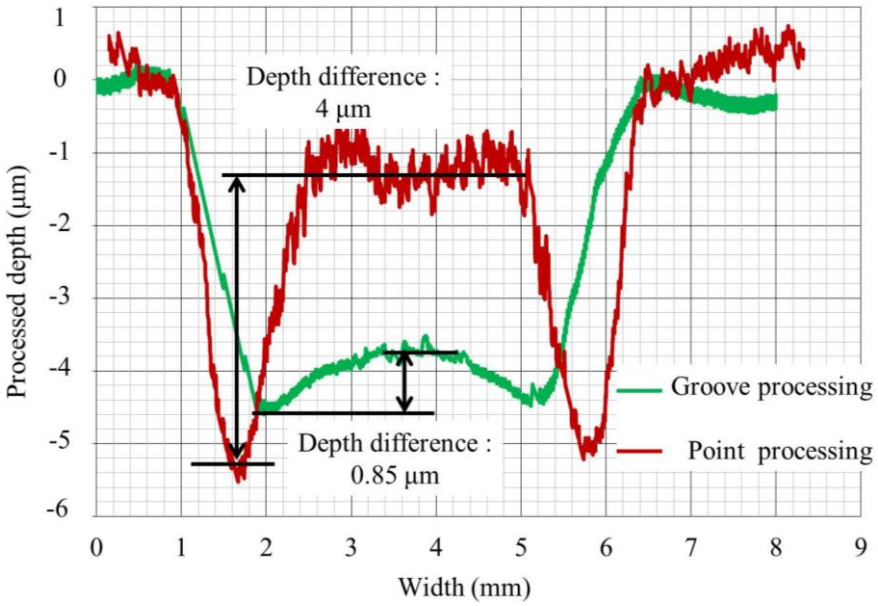

(b) Cross-section measurement result of processed groove.

Figure 3.9 Photo of processed groove and its cross-section measurement result.

3.6.1 Discussion between point processing and groove processing

In section 2.8.2, it was mentioned that the whole processed groove can be seen as an overlap of lots of point processing areas. Based on this assumption, the schematic of groove processing is shown in Figure 3.10.

Part (1) is the schematic of the processed result after the once point processing, it is the same as the point processing results in Figure 3.9(a). The processed depth of the center area, which is marked orange, is shallower than the processed depth of the edge area, which is marked blue. The right side of the part (1) and part (2) of Figure 3.10 is the schematic of the cross-section profile measured along the line crossing A, B, and C.

The part (2) is the schematic of the processed result after twice point processing, the distance between the first point processing and the second point processing is 1 mm, which is less than the diameter of the point processed area.

As shown in the schematic of part (2), part of the center area of the first point processing is overlapped by the edge area of the second point processing. As a result of this, the depth of the center area around A is increased by the second point processing, while the depths of edge areas around B and C are not changed. Hence, the depth difference decreases after the second point processing, as shown in the cross-section profile's schematic on the right side of the part (2).

With the increase of overlapping point processing, a groove as shown in the part (3) is processed.

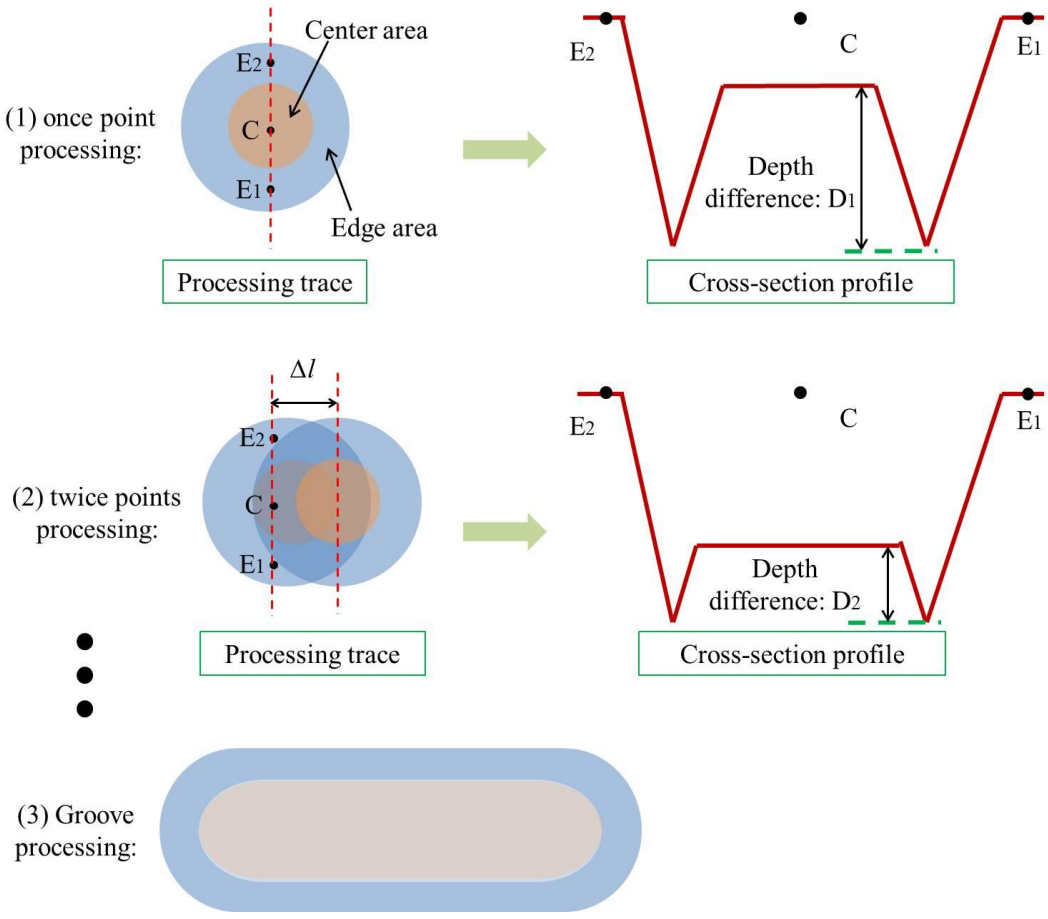

Figure 3.10 Schematic from point processing to groove processing and cross-section profile.

As demonstrated in Figure 3.10, although there is a large depth difference between the center area and the edge area of each point processing, due to the center area will be overlapped by the flowing point processing, and its depth will be deepened. Hence, the depth difference of the groove processing is reduced significantly to be smaller than that of the point processing and the simulation results.

3.6.2 Verification of point processing and groove processing

To verify the discussion in section 3.6.1, a groove was processed by using the method of the schematic of groove processing in Figure 3.10. The number of point processing times is 5, and the interval between them is 1 mm. The photo of the processed groove is shown in Figure 3.11(a), and the measurement result of the cross-section is shown in Figure 3.12(b).

By comparing the cross-sections of the processed groove of this section and the point processing result of Figure 3.7, the maximum depth of the two cross-sections is equal to each other roughly, but the depth of the center area of Figure 3.11 is larger than that of Figure 3.7. It means that after groove processing, the depth of the center area is deepened as discussed in section 3.6.1. And from the comparison result, the assumption above can be verified.

Besides that, it can be concluded that the simulation results obtained in section 3.4 can be used to explain the experimental results both the point processing and the groove processing.

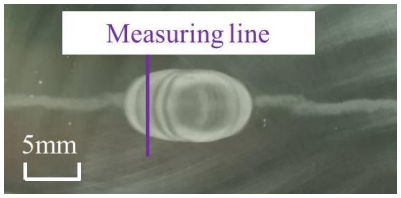

(a) Processed groove consist of point processing.

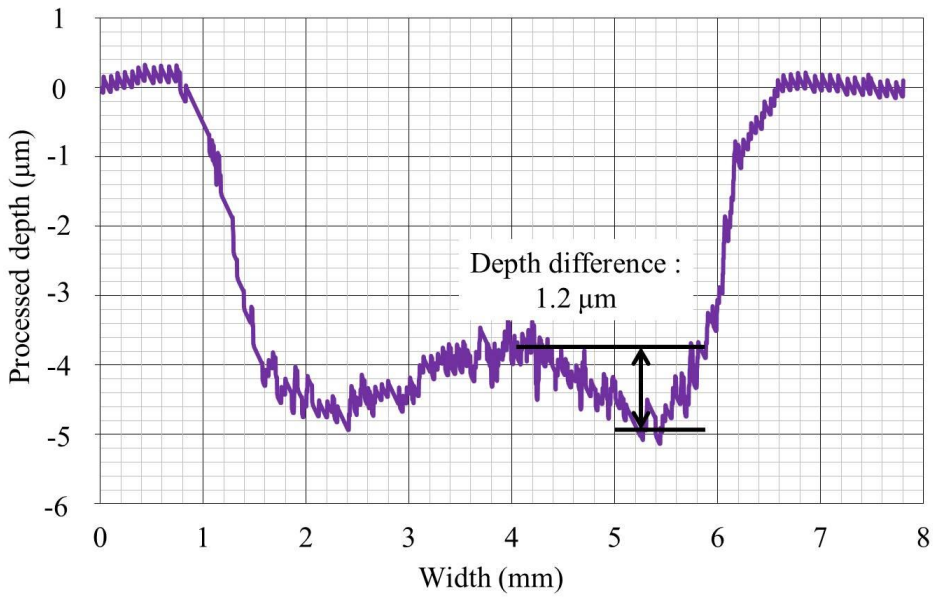

(b) Cross-section measurement of processed groove.

Figure 3.11 Processed groove consist of point processing and cross-section measurement result.

3.7 Conclusion

In this chapter, according to the actual experiment, we have 2D modeled for the processing area. And by using the software of COMSOL Multiphysics, the potential between the workpiece and the electrode, the current density distribution at the processing area, and the cross-section profile of the processed area were simulated.

Through the simulation, the discussion and the verification of this chapter, and combined with the groove processing result of chapter 2 and the simulation results of section 3.4, conclusions about the reasons for the occurrence of the depth difference of cross-sections can be summarized as follows:

(1) Due to the limitation of the electrolyte distribution by the MFS-ball, the amount of the electrolyte at the edge area of the electrolyte distribution is more than that in the center area of the electrolyte distribution, and the value of the machining current flowing through the electrolyte film is greater than that of flowing through the inside electrolyte of the MFS-ball. Differences in the electrolyte distribution and the value of the machining current lead to the depth difference occurring in the processed area.

(2) During ECM processing, the machining current density distribution at the edge area of the electrolyte distribution is greater than that of the center area, the greater the machining current density, the more materials are corroded from the workpiece surface. Finally, the processed depth of the edge area is deeper than that of the center area.

(3) Since the groove processing can be regarded as the process in which countless point processing is carried out and overlapped with a tiny interval, and the simulation results of section 3.4 are suitable for the point processing, the simulation results of chapter 4 also can be used to explain the experimental results of groove processing.

Chapter 4 Influence of processing parameters and optimal parameters selection

4.1 Introduction

During the ECM process, machining characteristics are usually influenced by experimental parameters. To explore the influence results and the reasons, in this section, the influences of the following main experimental parameters, including the pressure between the workpiece and the MFS-ball, the electrolyte flow rate, the time of pre-scanning, the machining constant current (CC) value, the machining time, and the moving speed of workpiece are ascertained. After that, the influence of the MFS-ball's size difference and its solution method were explored.

4.2 Influence of pressure between workpiece and MFS-ball

As mentioned in section 2.7.3, to ensure that the workpiece was in contact fully with the MFS-ball along the entire movement track, the workpiece was moved 0.1 mm further toward the MFS-ball after the contact, the maximum pressure between them was measured about 15 N. And from the attempts before, it is found that if the pressure between the workpiece and the MFS-ball is smaller than 10 N, the MFS-ball would be unable to contact the workpiece, it would signify that the MFS-ball would not be rolling upon the workpiece during that duration of the ECM process, stopping the electrolyte circulation in that machining area. On the other hand, if the pressure is bigger than 25 N, due to being pressed by the excessive pressure, the MFS-ball would be easily broken, which would fail in the ECM process.

To explore whether and how the pressure between the workpiece and the MFS-ball will influence the ECM results, we carried out experiments with the experimental parameter of Table 4.1, and the pressure between the workpiece and the MFS-ball is 10 N, 15 N, and 20 N respectively. The change of the pressure was realized by changing the extra movement distance.

Processing results of using different pressures and cross-section measurement results are shown in Figure 4.1. From the cross-section measurement results, we can find that though the different pressure between the workpiece and the MFS-ball were used in experiments, the three cross-section profiles almost overlap with each other, and they have equal widths and depths.

Hence, we can conclude that the pressure between the workpiece and the MFS-ball will not influence the ECM results of this study. And due to the MFS-ball used in experiments being made of hard and brittle materials, once the pressure is greater than the maximum pressure that the MFS-ball can bear, the MFS-ball will be crushed directly instead of being elastic deformation. Finally, to make the following experiments proceed stably, the pressure of 15 N is chosen and used.

Table 4.1 Common experimental conditions.

Item	Specification
Absorption material	MFS-ball
MFS-ball diameter	10 mm
Workpiece material	SUS304 plate
Electrode material	SUS304 plate
Electrolyte	10 wt.% NaCl solution
Movement distance of workpiece	50 mm
Movement speed of workpiece	8 mm/s
Constant current	40 mA
Machining time	100 s

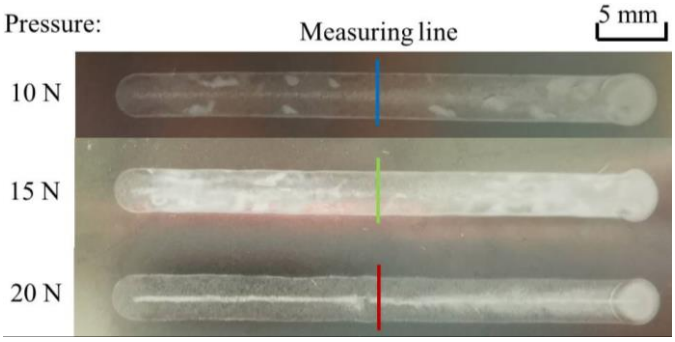

(1) Processing results.

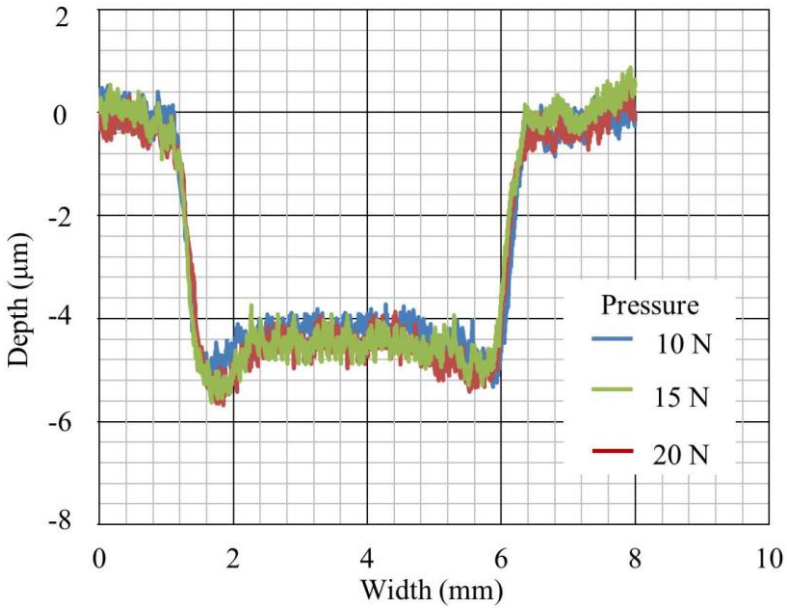

(b) Cross-section measuring results.

Figure 4.1 Processing results and cross-section measuring results of using different pressures.

4.3 Influence of electrolyte flow rate

In the conventional ECM process, the flowing electrolyte is needed to remove by-products of bobbles, metallic hydroxides, and Joule heat of the working gap. While, in this research, the following electrolyte is not in contact with the processing area of the workpiece surface, but is used to supply the fresh electrolyte to the MFS-ball and take away the ECM by-products.

As an attempt, we tried to do some experiments to explore the influence of the electrolyte flow. As shown in Figure 4.2(a), first of all, instead of providing flowing electrolytes, some electrolyte was added to the V-shaped cross-section track before the experiment. And exits at the two ends of the electrode were blocked. The other experimental parameters and method were same as reported before.

During ECM processing, though the MFS-ball absorbed electrolytes as rolling, the ECM by-products cannot be taken away, and they adhered to the MFS-ball surface and accumulate at the electrolyte of the V-shaped cross-section track yet. The photo is shown in Figure 4.2(b). This situation prevents electrochemical reactions from occurring and destroys the limitation of the electrolyte distribution. Hence, the flowing electrolyte is necessary for this research.

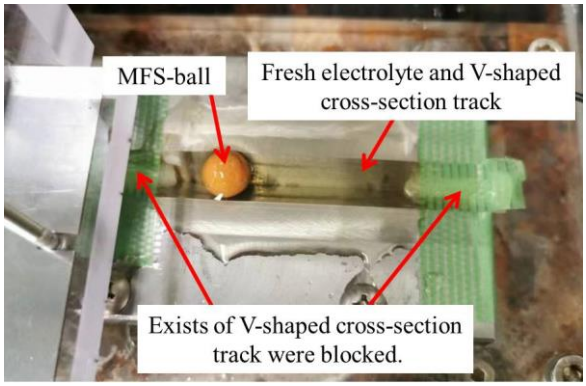

(a) Before ECM processing

(b) After ECM processing

Figure 4.2 Photo of ECM processing with non-flowing electrolyte.

After that, as increasing the flow rate of the electrolyte, it is found that there is no influence on ECM processing results. But, when the flow rate of the electrolyte flowing out of the electrolyte nozzle is greater than 4 ml/s, the flowing electrolyte may rush to the workpiece surface as the MFS-ball rolling, as shown in Figure 4.3(a), and then the distribution of the electrolyte at the workpiece surface becomes uncontrollable. The processed trace is shown in Figure 4.3(b), due to the electrolyte distributing without limitation around the contact point between the workpiece and the MFS-ball, the shape and the size of the processed trace are irregular and cannot be controlled. Hence, during ECM processing of this research, the flow rate of the electrolyte should be smaller than 4 ml/s.

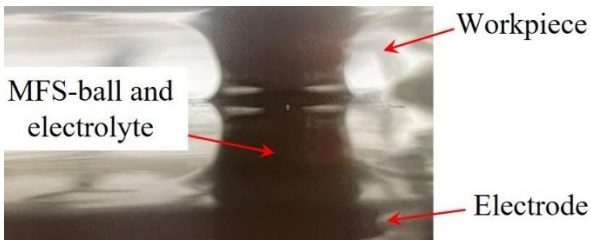

(a) Photo of ECM processing with electrolyte flow rate of 4 ml/s

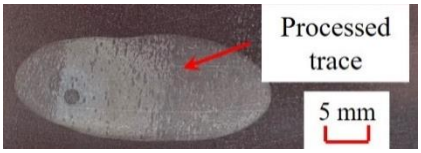

(b) Photo of processed trace

Figure 4.3 Photo of ECM processing with electrolyte flow rate of 4 ml/s and processed trace.

When the electrolyte rate is less than 3 ml/s, as an example, the electrolyte flow rate of 2 ml/s was used tentatively, the photo of the processed trace is shown in Figure 4.4. It is found that, though the ECM can be carried out successfully, because the amount of the provided electrolyte at the ECM processing area, the width of the processed trace is only about 3 mm, which is narrower than when using the electrolyte flow rate of 3 ml/s. At the same time, the edges of the processed trace are curved instead of straight, which leads to that the size of the processed groove cannot be controlled by the MFS-ball effectively.

Hence, according to attempts of this research, 3 ml/s is selected as the most suitable flow rate of the electrolyte. Because of processing with a flow rate of 3 ml/s, ECM by-products can be removed away immediately, and the flowing electrolyte will not affect the electrolyte distribution controlled by the MFS-ball on the workpiece surface.

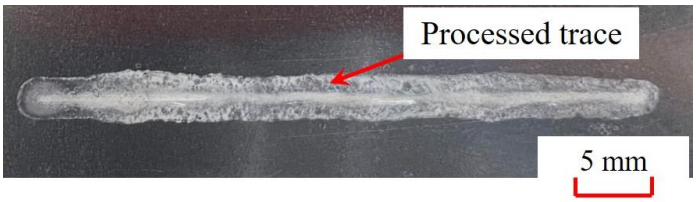

Figure 4.4 Photo of processed trace with electrolyte flow rate of 2 ml/s.

4.4 Influence and necessity of pre-scanning

As mentioned in chapter 2, before ECM processing, the procedure called the pre-scanning is necessary, and the purpose of pre-scanning was introduced briefly. In this section, the influence of the pre-scanning is explored first, and the necessity of the pre-scanning is discussed then.

4.4.1 Influence of pre-scanning

To investigate the influence of the pre-scanning time, the experimental parameters in Table 4.1, pre-scanning times ranging from 0 s to 350 s at intervals of 50 s, and the number of pre-scanning reciprocating cycles increase from 0 times to 28 times at the interval of 4 times. At the same time, the machining time of ECM is 100 s.

The cross-section measurement results when the pre-scanning time is less than 200 s are shown in Figure 4.5(a), and the measurement results for the width and maximum depth of the processed grooves are shown in Figure 4.5(b).

When the pre-scanning times were 0 s and 50 s, ECM was not conducted stably because the electrolyte accumulated in the machining area was insufficient. In this case, electrical discharge occurred in the processing area, and the voltage between the electrode and workpiece increased sharply to the overvoltage. Finally, the ECM process was stopped, and the processed groove is shown in Figure 4.5(b) was not obtained. Therefore, the machining results for these two cases are not shown in Figure 4.5.

From the machining results, it was determined that the groove width increased gradually concerning the pre-scanning time. However, because the volume removal rates of the ECM processes were approximately the same because of the same machining current being used, the

groove depth decreased as the width was increased. Furthermore, when the pre-scanning times were longer than 250 s, the groove width and depth did not change significantly.

This result indicates that the width of the groove gradually increases concerning pre-scanning times of up to 250 s, after which the electrolyte distribution at the machining area becomes stable.

While, to improve the processing efficiency of this ECM method, when using the same pre-scanning time, the influence of the pre-scanning becomes the same for each process, which leads to the influence of the pre-scanning can be ignored. Hence, the same pro-scanning time of 100 s was used in the following experiments.

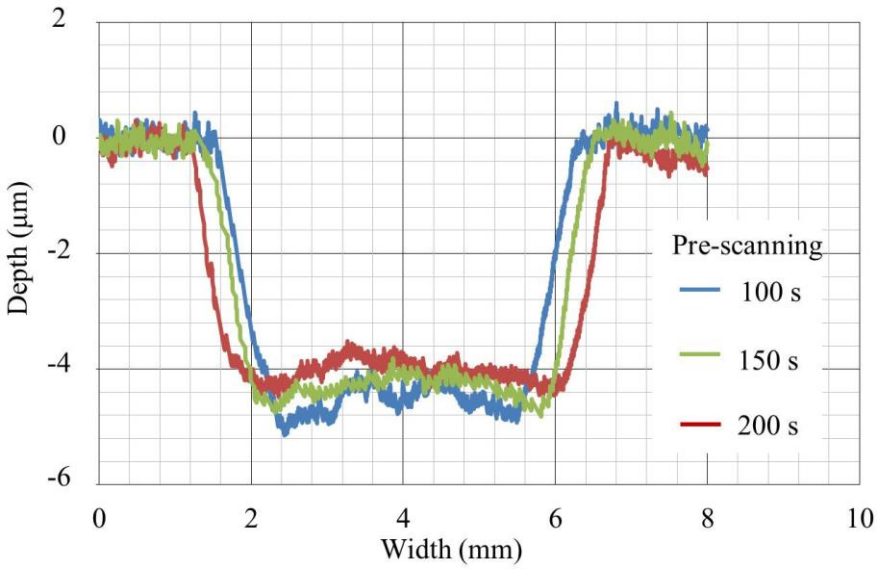

(a) Cross-section of pre-scanning time less than 200 s.

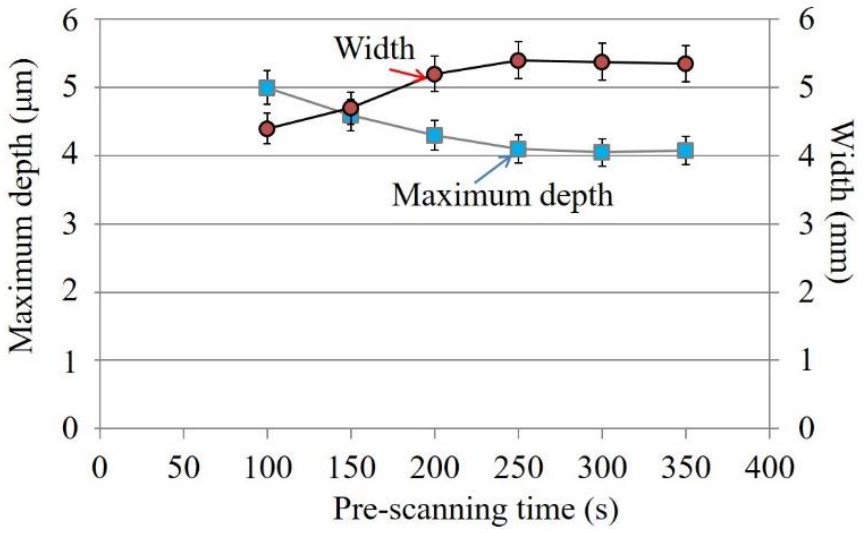

(b) Width and maximum depth of processed grooves.

Figure 4.5 Cross-section measurement results, width and maximum depth for different pre-scanning times.

4.4.2 Necessity of pre-scanning

Preliminary experiments revealed that pre-scanning is an important step for the entire ECM process of this research. However, the necessity of pre-scanning and the effects of eliminating the pre-scanning step on the ECM process are not clearly understood. Therefore, to explore the aforementioned questions, experiments were conducted without pre-scanning. Subsequently, two reasons for the necessity of pre-scanning were obtained as described below.

The first reason is to store electrolytes before the ECM process. Comparison diagrams of the process with and without pre-scanning are shown in Figure 4.6. Without the pre-scanning operation, the electrolyte accumulated in the machining area is not sufficient for use in ECM. Particularly, when the constant machining current is higher than 30 mA, the electrolyte accumulated in the machining area is consumed soon, subsequently, discharge occurs around the machining area, which

prevents the ECM from progressing smoothly.

A schematic of the occurrence of discharge is shown in Figure 4.7. During the ECM process without pre-scanning, the electrolyte around the machining area is easily consumed because of its relatively small quantity. However, as electrolytes are not consumed in other parts of the MFS-ball, the electrical resistance between the workpiece and the electrode rapidly increases. As a constant current (CC) mode was employed, the voltage increased to approximately 120 V, which is the maximum output voltage of the power supply. Because of this high voltage between the workpiece surface and the electrolyte boundary of the MFS-ball as shown in Figure 4.7, the insulation of air is broken down and discharge occurs.

The next and most important reason is to stabilize the electrolyte distribution in the machining area. Otherwise, it is impossible for the ECM process and the processing results are maintained stability. Even though the same experimental parameters are used in ECM processing, the sizes of the processing results are different from each other, indicating that these processing results have to be given up in subsequent studies.

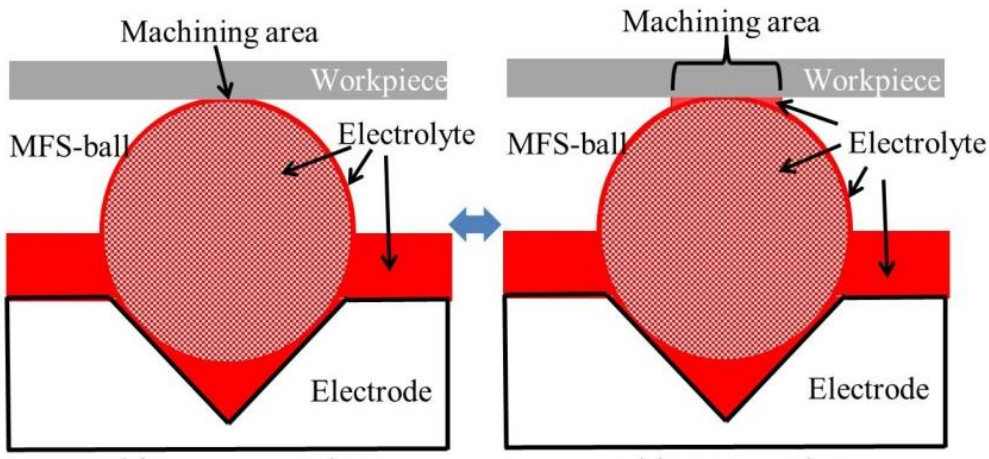

(a) Without pre-scanning. (b) With pre-scanning.

Figure 4.6 Comparison of electrolyte and machining areas with and without pre-scanning.

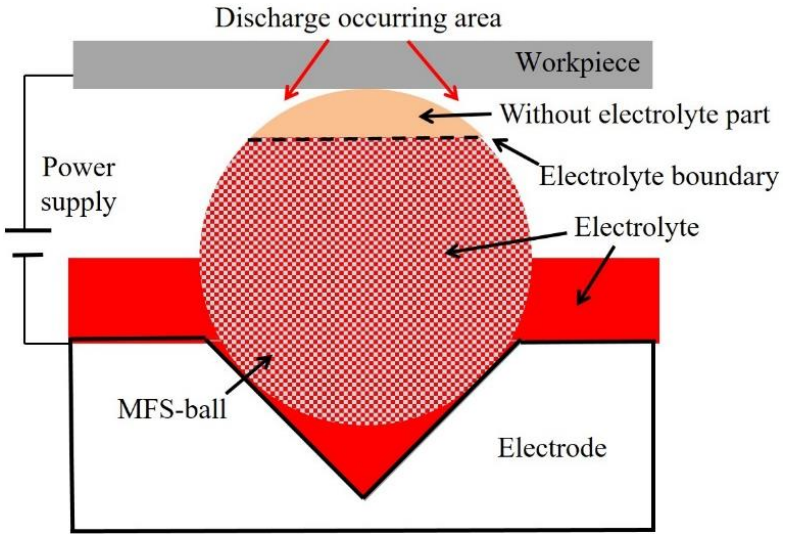

Figure 4.7 Schematic of discharge occurring area and electrolyte boundary.

Concerning its degree of influence, although pre-scanning has only a slight influence on the depths and widths of processed grooves, it is one of the decisive factors that ensure that the ECM process can be performed stably. Hence, a pre-scanning operation is necessary for this ECM method.

4.5 Influence of machining current and selection of optimal machining current value

As known, the greater machining current is promotional for ECM processing in some cases. In this section, to verify whether or how the increasing machining current influence the processing result of ECM, and provide references about the selection of the machining current for the subsequent experiments and processes, the following experiments were carried out.

4.5.1 Influence of different machining current value

In these experiments, wherein the effect of the machining current value was investigated, the CC value was varied between 10 mA and 50 mA and used in conjunction with the experimental parameters given in Table 4.1. The results are shown in Figure 4.8.

According to Figure 4.8, as the CC value was increased, the depth and width of the cross-section also increased. One of the reasons for this result is that the larger the machining current value, the more electricity is used for ECM during the same period, and the greater the amount of dissolved materials. In addition, because of the isotropy of the material dissolution, which signifies that, during ECM, the material dissolves in all directions of the workpiece. Machining currents not only work toward the depth but also laterally. Therefore, both the sidewall and bottom of the processed groove were dissolved by electrochemical action.

Additionally, during ECM, some by-products adhered to and accumulated in the machining area of the workpiece. For the same experimental parameters, excluding the CC value, the formation rates and amounts of these by-products increased as the CC value was increased. A photograph of the electrolytes and by-products accumulated on the processed groove is shown in Figure 4.9. In contrast to the by-products that adhere to the surface of the MFS-ball, these by-products cannot be cleaned by the flowing electrolyte. When the MFS-ball contacts the

workpiece, the by-products and electrolytes of the machining area are squeezed and spread, increasing the area covered by the electrolyte. This explains why the width of the processed groove widens as the CC value increases.

Finally, both the depth and width of the cross-section of the processed groove increased as the CC value was increased.

4.5.2 Selection of optimal machining current value

In the experiments above, ECM processing went on smoothly at the moving speed of 8 mm/s, when the maximum machining current value of 50 mA was used. While, when the moving speed is decreased to smaller than 8 mm/s because the speed of the fresh electrolyte supplying to the processing area of the workpiece surface decreases, the electrolyte accumulating at the processing area is not enough to be used in ECM processing. Hence, similar to Figure 4.5, discharge occurs, and the whole ECM has to be stopped.

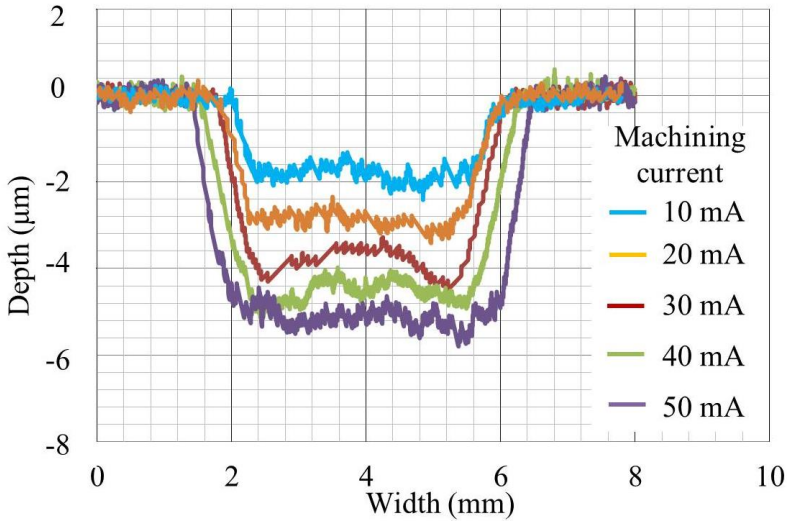

(a) Cross-section of processed grooves.

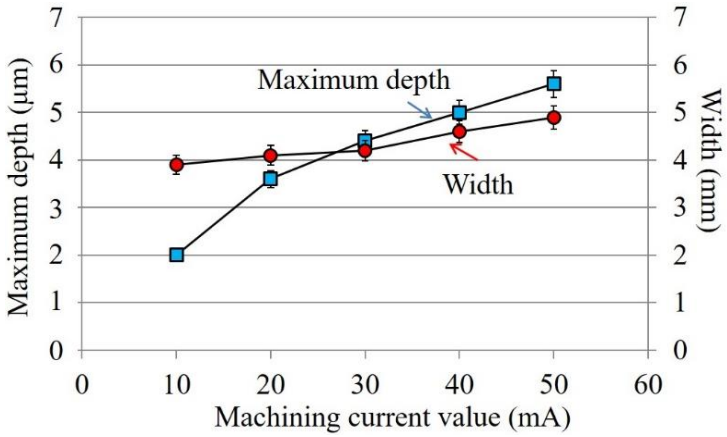

(b) Width and maximum depth of processed grooves.

Figure 4.8 Machining results for processed grooves for different CC values.

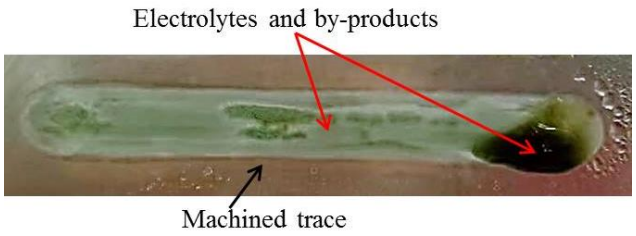

Figure 4.9 Photo showing the electrolytes and by-products accumulated on the processed groove.

In brief, when the moving speed of the workpiece is greater than or equal to 8 mm/s, to improve the processing efficiency of ECM, the machining current of 50 mA can be used. When processing with a moving speed less than 8 mm/s, the machining current of 40 mA should be used.

4.6 Influence of machining time

In these experiments, wherein the effect of the influence of machining time was investigated, machining times of 50 s, 100 s, 150 s, and 200 s, were used in conjunction with the experimental parameters given in Table 4.1. The corresponding numbers of reciprocating processing cycles were 4, 8, 12, and 16.

According to the measurement results shown in Figure 4.10, as the machining time was increased, the depth and width of the processed groove simultaneously increased. The reason for this result is inferred to be the increase in electricity quantity with the machining time, where the increasing electricity quantity led to an increase in the amount of corroded material in the machining area of the workpiece. Because of the isotropy of the metal dissolution, by-products, and electrolytes in the machining area, as explained in section 4.4, both the depth and width of the cross-section increased as the machining time increased.

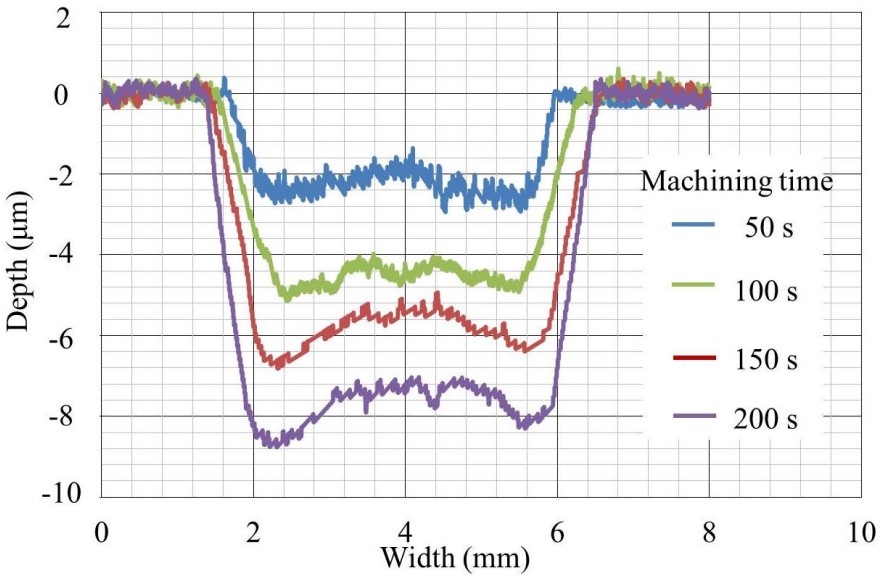

(a) Cross-section of processed grooves.

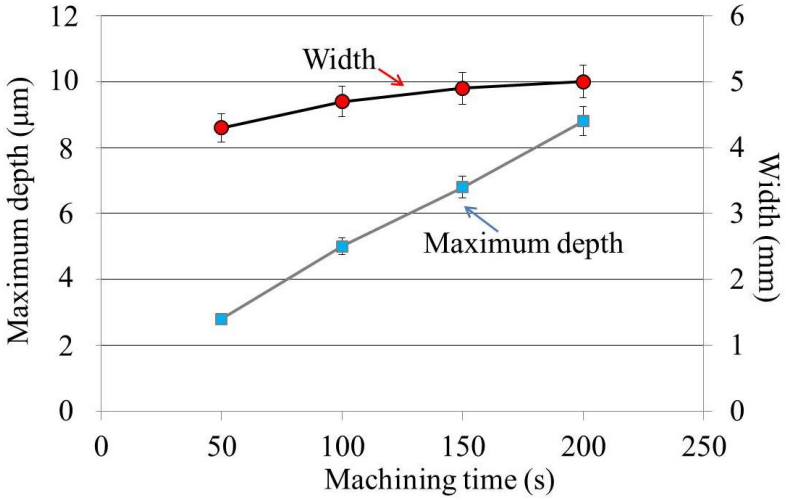

(b) Width and maximum depth of processed grooves.

Figure 4.10 Machining results under different machining time.

In deep grooves processing, it is more suitable to increase the machining time than it is to increase the CC value. It is because the amount of electrolyte accumulated in the machining area is small. When the CC value, especially when it is larger than 50 mA, is used, the electrolyte is consumed instantly, which leads to the occurrence of discharge in the machining area. Thus, the entire ECM process cannot be conducted continuously. On the other hand, as shown in Figure 4.10, the depth of the processed groove was almost proportional to the machining time and continued to deepen as the machining time was increased. Hence, increasing the machining time is beneficial for deep-groove machining.

4.7 Influence of workpiece moving speed

As reported in the processing method of chapter 2, driven by the friction from the workpiece surface, the MFS-ball rotates while moving along with the workpiece. Hence, the workpiece moving speed directly affects the moving speed and the rolling speed of the MFS-ball and affects the processing result of ECM indirectly. Aiming at exploring the influence of workpiece moving speed on the ECM processing result, the following experiments were carried out by changing the moving speed of the workpiece.

Based on variations in the workpiece movement speed of 4 mm/s, 6 mm/s, and 8 mm/s, in conjunction with the experimental parameters outlined given in Table 4.1, experiments were conducted to investigate the influence of the movement speed of the workpiece. If the moving speed of the workpiece is less than 4 mm/s, the electrolyte provided to the processing area is not enough consumed by ECM because the same machining current value of 40 mA was used in this part of the research. Hence, the minimum value of the workpiece moving speed was set to 4 mm/s.

To ensure that the amount of electricity supplied to each part of the processed groove remained constant, the number of reciprocating processing cycles was increased with the increase in the movement speed of the workpiece. For movement speeds of 4 mm/s, 6 mm/s, and 8 mm/s, the numbers of reciprocating processing cycles were 4, 6, and 8, respectively.

The measurement results of cross-sections are shown in Figure 4.11. According to these results, as the workpiece movement speed increased, the depth and width of the cross-section were slightly increased simultaneously.

Based on these observations, it is inferred that a faster workpiece movement speed results in a faster MFS-ball rolling speed. At the same time, because the speed of electrolyte supply in the

machining area is improved, ECM is accelerated. Hence, for the same machining current value and the same machining time, the amount of corroded material increases as the movement speed of the workpiece is increased.

However, compared with the conclusions of section 4.2, section 4.3, and section 4.4, the effect of using a faster workpiece movement speed is not as evident as those of using a greater CC value or a longer machining time.

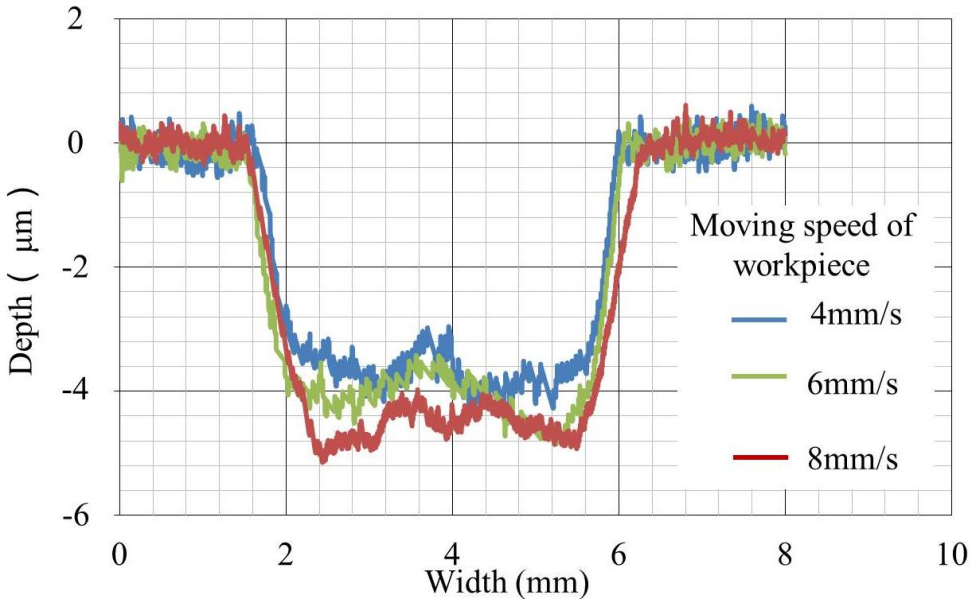

(a) Cross-section of processed grooves.

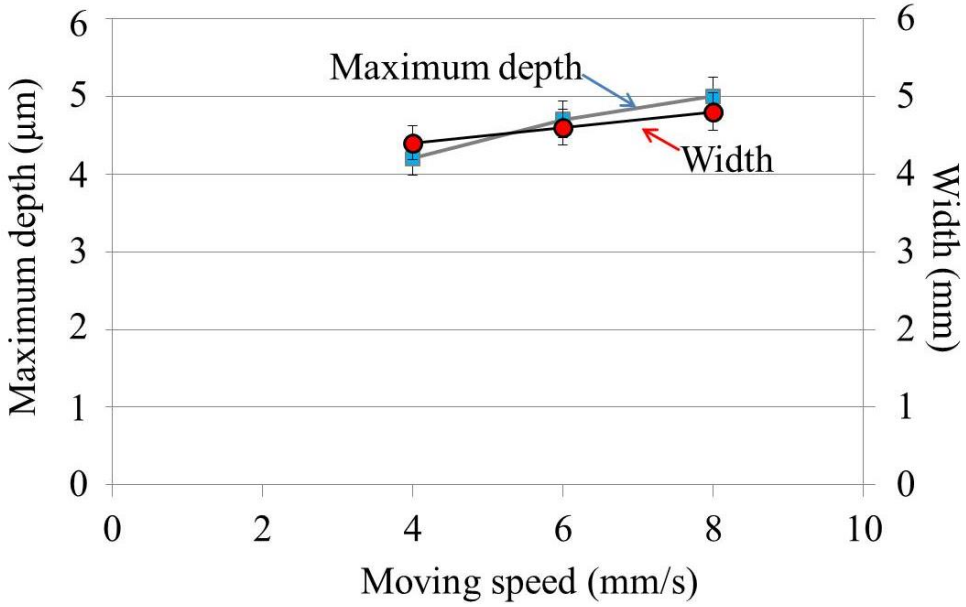

(b) Width and maximum depth of processed grooves.

Figure 4.11 Machining results under different moving speed.

4.8 Influence of MFS-ball's size difference and solution

MFS-balls used in this research are bought from the market, and without the restriction of the tolerance. These MFS-balls are used as water filters in daily life. Hence, as mentioned in section 2.5, there are size differences in MFS-balls. To find out the value of the MFS-ball's size difference and the influence on the size of processed results, the following experiments were done.

4.8.1 Influence of MFS-ball's size difference

First of all, we took out 3 pieces of MFS-ball randomly, as shown in Figure 4.12. And then diameters of 10 different parts for each MFS-ball were measured, where the largest diameter is defined as d_{max}, and the smallest diameter is defined as d_{min}. The difference between d_{max} and d_{min} is defined as the maximum of the MFS-ball's size difference (T_d).

After that, by using the formula (4-1) and (4-2), the average diameter ($\bar{d}$) and the dimensional difference percentage (P_d) of the MFS-ball can be calculated.

As we know, the smaller the difference between the maximum and minimum diameters, the closer the ball is to an ideal sphere and the smaller the value of dimensional difference percentage. Hence, in this paper, the dimensional difference percentage of the MFS-ball is used as the criterion for judging the MFS-ball's shape. The calculation result is shown in Table 4.2.

$$\bar{d} = \frac{1}{n}\sum_{i=1}^{n} d_i \quad (4\text{-}1)$$

$$P_d = 100\% \cdot \frac{T_d}{\bar{d}} \quad (4\text{-}2)$$

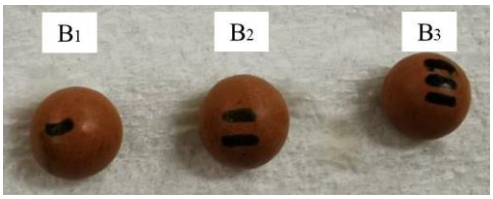

Figure 4.12 MFS-balls.

Table 4.2 Size difference and dimensional difference percentage of MFS-ball.

MFS-ball	T_d (mm)	$\bar{d}$ (mm)	P_d (%)
B_1	0.18	9.52	1.89
B_2	0.38	9.87	3.85
B_3	0.21	9.58	2.08

To find the influence of the MFS-ball's size difference on the width of the processed groove, combined with the experimental parameters of Table 4.1, MFS-balls: B_1, B_2, B_3 were used in ECM processing, the processing time is 50 s. After that, the widths of the processed groove's 10 different parts were measured randomly, where the largest width is defined as D_{max}, and the smallest width is defined as D_{min}. The difference between D_{max} and D_{min} is defined as the maximum size difference of the processed groove's width (T_D). One of the measurement results of the processed groove's cross-section is shown in Figure 4.13.

With the formula (4-3) and (4-4), the average width ($\overline{D}$) and the dimensional difference percentage (P_D) are obtained. The calculation results are shown in Table 4.3. The dimensional difference percentage of MFS-balls and processed grooves is shown in Figure 4.14.

Combining with Table 4.2, Table 4.3, and Figure 4.14, it can be found that the size difference of the MFS-ball affects the processed groove directly, the larger the size difference of the MFS-ball, the greater the size difference of the processed groove.

$$\overline{D} = \frac{1}{n}\sum_{i=1}^{n} D_i \quad (4\text{-}3)$$

$$P_D = 100\% \cdot \frac{T_D}{\overline{D}} \quad (4\text{-}4)$$

Table 4.3 Size difference and dimensional difference percentage of processed groove.

Processed groove	T_D (mm)	$\overline{D}$ (mm)	P_D (%)
Machined by B_1	0.10	4.83	2.07
Machined by B_2	0.30	5.43	5.52
Machined by B_3	0.10	4.90	2.04

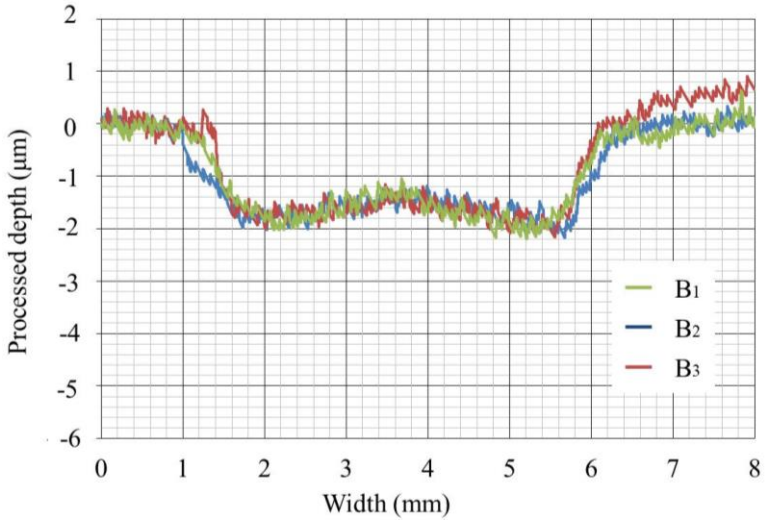

Figure 4.13 Cross-section measurement results of grooves processed by using un-machined MFS-balls.

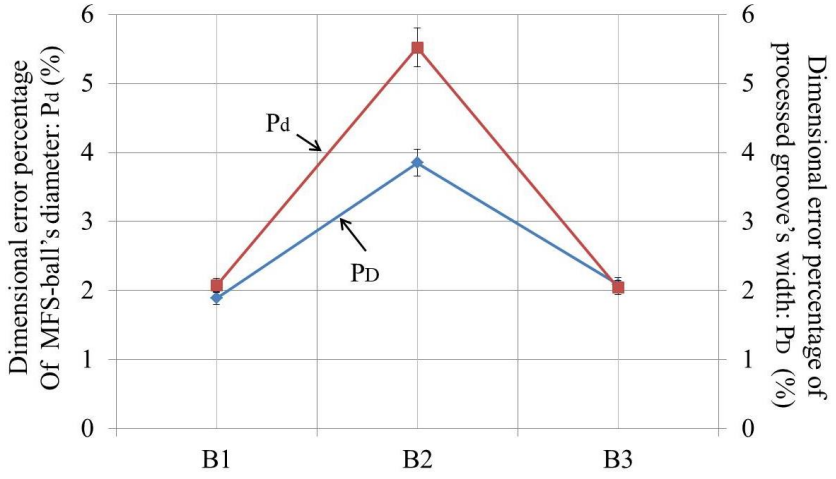

Figure 4.14 Dimensional difference percentage of MFS-balls and processed grooves.

4.8.2 Solution of MFS-ball's size difference

According to experiments before, the size difference of the MFS-ball's diameter leads to that there are size differences exist in the width and the depth of the processed grooves. To eliminate the size difference of the MFS-ball and its influence on the processed groove, the hemispherical

grinding tool was used. A photo of the hemispherical grinding tool is shown in Figure 4.15(a). The hemispherical grinding tool is used commonly in the processing of balls made of jewelry or jade. In this research, during the size regularize process, as shown in Figure 4.15(b), two hemispherical grinding tools were used to grind the MFS-ball to regularize its size. After the regularization process, the diameter of the MFS-ball is processed to 9.4 mm with a tolerance of less than 0.05 mm, which is reduced greatly than the tolerance of the un-regularized MFS-ball's diameter.

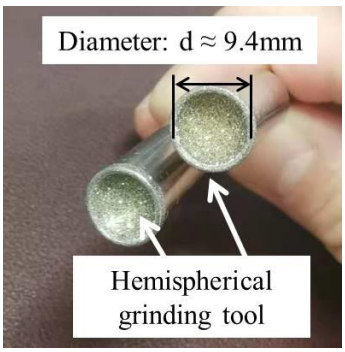

(a) Photo hemispherical grinding tool.

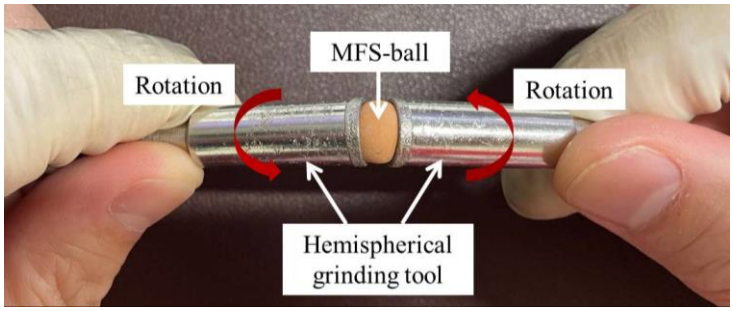

(b) Regularization process method.

Figure 4.15 Photo of hemispherical grinding tools and regularization process method.

By using the formula (4-1) and (4-2), the size difference and dimensional difference percentage of MFS-ball after regularization were obtained as listed in Table 4.4.

After that, ECM processing was carried out by using the regularized MFS-ball, and the experimental parameters. The cross-section measurement results of grooves are shown in Figure 4.16.

Table 4.4 Size difference and dimensional difference percentage of regularized MFS-ball.

MFS-ball	T_d (mm)	$\bar{d}$ (mm)	P_d (%)
A_1	0.04	9.43	0.42
A_2	0.05	9.42	0.53
A_3	0.04	9.42	0.42

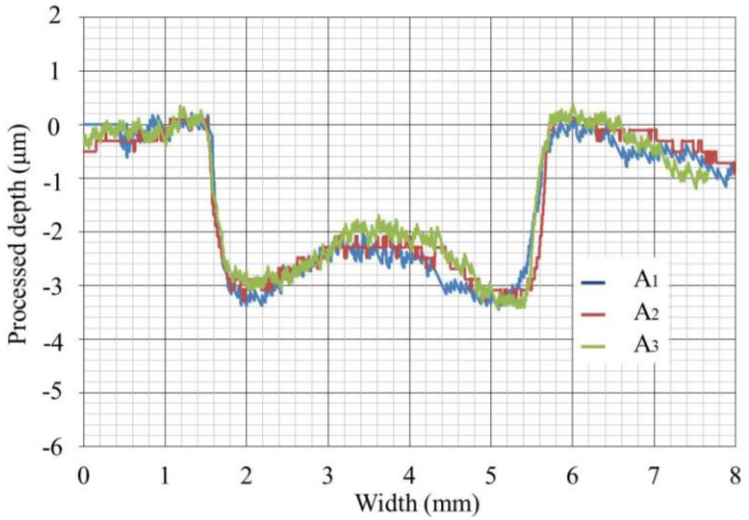

Figure 4.16 Cross-section measurement results of grooves processed by using regularized MFS-balls.

With the formula (4-3) and (4-4), the size difference and dimensional difference percentage of the processed groove were calculated, as shown in Table 4.5. The dimensional difference percentage of MFS-balls and processed grooves is shown in Figure 4.17.

According to the results of Table 4.4, Table 4.5, and Figure 4.17, it is found that the size difference of the processed groove is reduced when using the regularized MFS-ball. And this confirms that the smaller the size difference of the MFS-ball's diameter, the smaller the size difference of the processed groove.

Table 4.5 Size difference and dimensional difference percentage of processed groove of using regularized MFS-ball.

Processed groove	T_D (mm)	$\bar{D}$ (mm)	P_D (%)
Machined by A_1	0.03	4.26	0.7
Machined by A_2	0.03	4.16	0.72
Machined by A_3	0.03	4.13	0.73

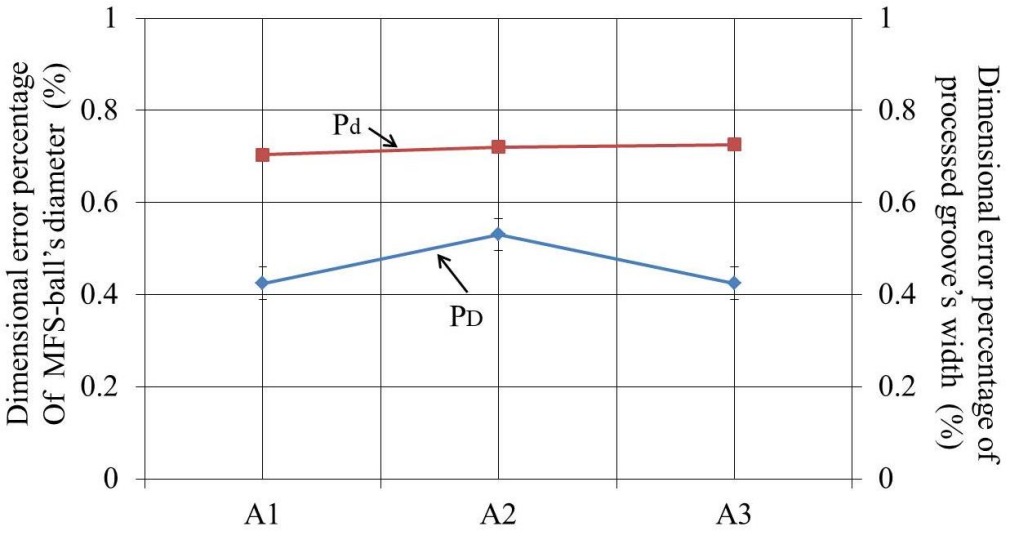

Figure 4.17 Dimensional difference percentage of MFS-balls and processed grooves.

4.9 Conclusion

This chapter summarized the influences of several main experimental parameters in this ECM method.

Although the pressure between the workpiece and the MFS-ball does not affect the processing results during ECM processing, to ensure that the workpiece and the MFS-ball contact with each other for the whole process and make the ECM process being carried out stably, the pressure value is selected as 15 N.

Due to the flowing electrolyte not working directly on the processing area of the workpiece surface, it is used to take away ECM by-products of the MFS-ball surface and the V-shaped cross-section track. Hence, a suitable electrolyte flow rate of 3 ml/s was selected for the following experiments.

According to experiments of this method, a necessary operation called the pre-scanning was summarized. The pre-scanning operation can accumulate electrolytes at the processing area in advance, and ensure the smooth progress of ECM. In addition, we found that when the pre-scanning time is less than 250 s, the width of the electrolyte distribution at the processing area increases as the time of the pre-scanning increases when the pre-scanning time is more than 250 s, the width of the electrolyte distribution will not be affected by the pre-scanning.

During the ECM processing of this method, the machining current value influences the processed groove directly. When using the same experimental parameters, the depth and the width of the processed groove increase as the machining current value increases. While, when the value of the machining current is larger than 50 mA, because the electrolyte supplied by the MFS-ball is not enough to be used in processing, the ECM cannot be carried out.

When using the same experimental parameters, except for the machining time, the depth and the width of the processed groove increase as the machining time.

Besides that, the depth of the processed groove increases, and the width of the processed groove decreases as the moving speed of the workpiece increases. It is considered that a faster moving speed of the workpiece promotes the rotation and the movement of the MFS-ball, hence the refresh rate of the electrolyte at the processing increases. This is helpful for ECM processing.

Finally, we find that there are size differences exiting of MFS-balls' diameters, and it is turn out be that the size differences of processed grooves are caused by the size differences of MFS-balls. The larger the MFS-ball's size difference, the greater the size difference in the processed groove. After being eliminated by the hemispherical grinding tool, size differences of the MFS-ball's diameter and the processed groove's width were decreased obviously.

Chapter 5 Applications of this ECM method

5.1 Introduction

According to the research results before, it is found that since the electrode where there is a V-shaped cross-section track is used in ECM processing, a strip-shaped groove is processed at the workpiece surface after processing. And because of the electrolyte distribution limitation of the porous MFS-ball, the stray-corrosion and the rust corrosion are prevented effectively.

In this chapter, we tried to explore the actual applications of this ECM method.

First of all, wide grooves with different cross-section profiles were processed by changing the interval between two grooves. Before that, to predict the cross-section shape of processed grooves, calculations for the cross-section profile were done with the software of Microsoft Excel.

Then, to be used in the mental marking of this stray-corrosion-free ECM method, a new tool, named the universal moving unit, was designed and fabricated. Combining with the universal moving unit during the ECM process of this research, several dimple English alphabets were etched on the workpiece surface.

Besides that, based on the research result until now, we found that by using the ECM method of this research, grooves with shallow depths were processed. And it is thought that these shallow grooves are suitable to be used as oil pockets for sliding surfaces. Hence, with a relay module used as the switch of the power supply in experiments, shallow grooves with different lengths and different depths were processed.

5.2 Processing of wide groove

5.2.1 Processing method

First of all, by using the processing method introduced in chapter 2, and the experimental parameters listed in Table 5.1, a single groove was processed at the workpiece surface. Along the measuring line, the cross-section profile of the processed groove was measured with the contour-measuring machine. And the photo and the schematic of ECM processing are shown in Figure 5.1, the single processed result is shown in Figure 5.2, and the measurement result is shown in Figure 5.3.

Table 5.1 Experimental parameters.

Parameter	Description
Absorption material	MFS-ball
MFS-ball diameter	Φ10 mm
Constant current value	40 mA
Material of workpiece and electrode	SUS304 plate
Electrolyte	10wt.% NaCl solution
Moving speed of workpiece	8 mm/s
Moving length of workpiece	50 mm
Time of pre-scanning	100 s
Time of single processing	100 s

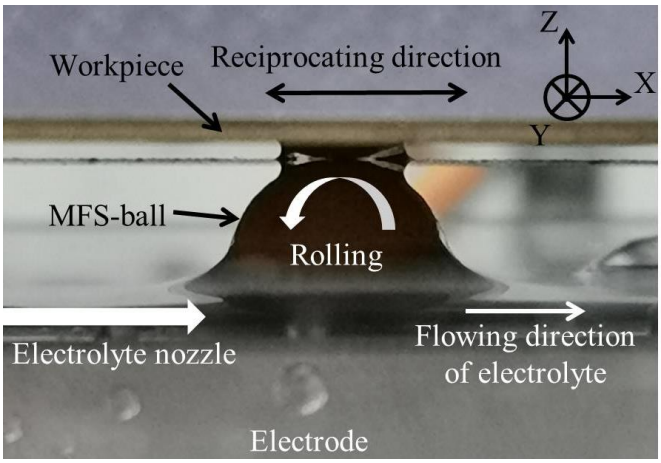

(b) Process photo view parallel to moving direction.

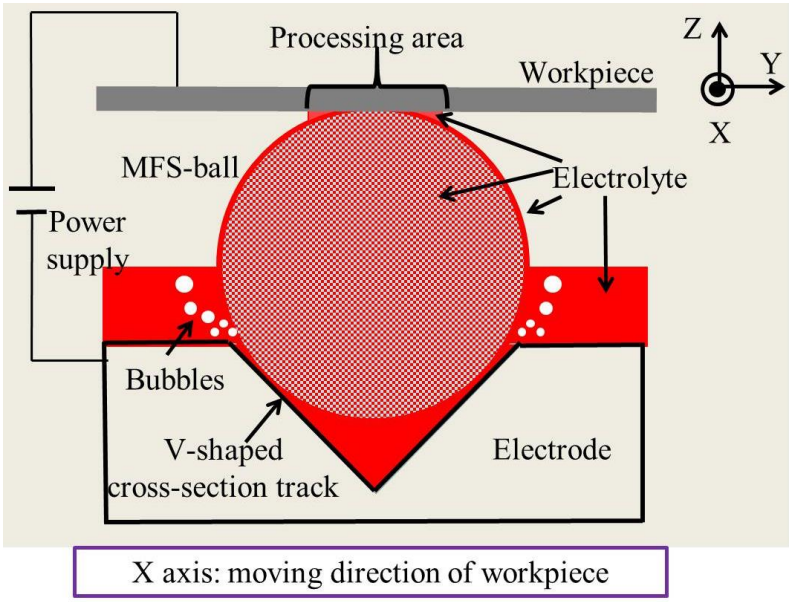

(c) Schematic cross-sectional view of the ECM process perpendicular to the moving direction.

Figure 5.1 Photographs and schematic of ECM process.

Based on the shape of the single processing groove and its cross-section profile in Figure 5.2 and Figure 5.3, the schematic of the wide groove processing method is shown in Figure 5.4.

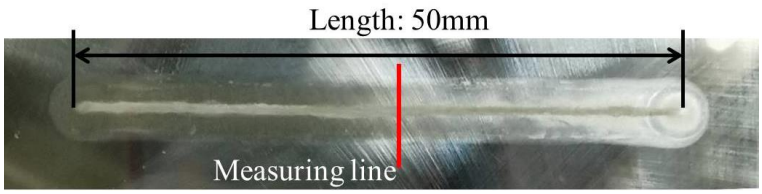

Figure 5.2 Photo of the groove after single processing.

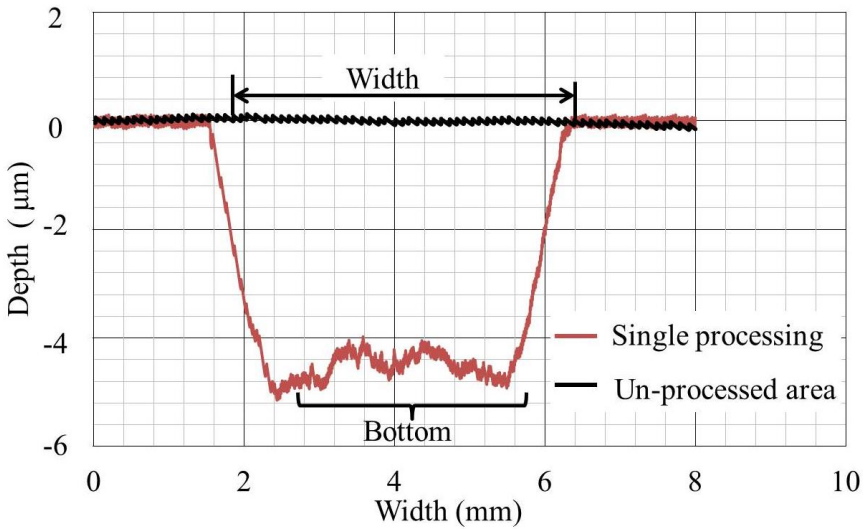

Figure 5.3 Cross-section of single processing groove.

After completing the ECM process of the single groove, the MFS-ball returns the initial position on the V-shaped cross-section track, then the workpiece moves up 10mm along the Z-axis of Figure 5.1 to separate from the MFS-ball. After that, the electrode and the MFS-ball move along the Y-axis to the target distance. And the workpiece moves down by 10mm along the Z-axis to contact with the MFS-ball, and then continues ECM processing. For the following groove processing, the above operation will be repeated to achieve the multiple processing trace. Since a little electrolyte will remain in the machining area, to prevent the remained electrolyte

from affecting the final results, the electrolyte that remained in the original position was cleaned out after every single groove processing.

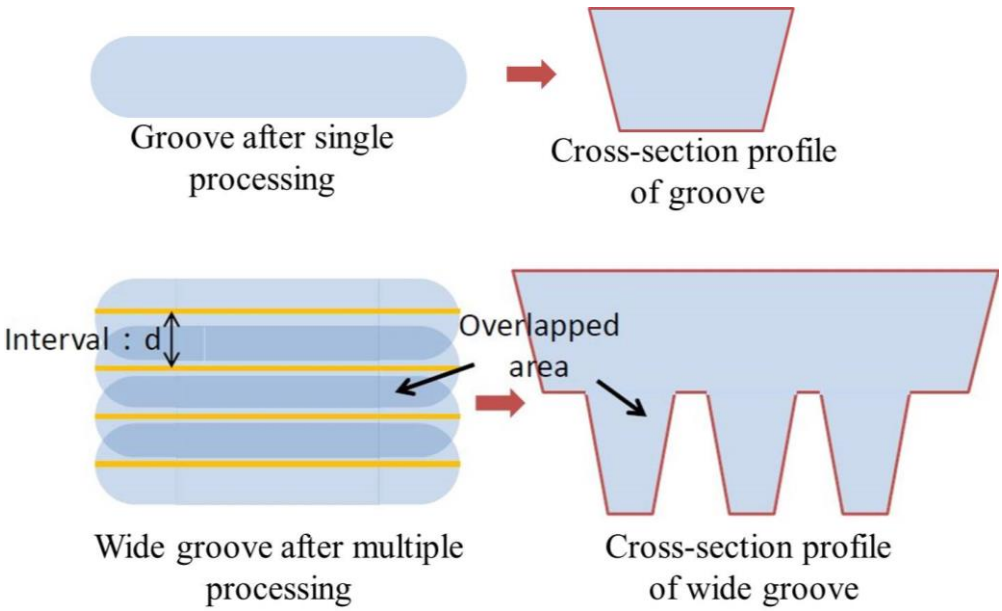

Figure 5.4 Schematic of wide groove processing.

5.2.2 Processing result of wide groove

By using the processing method of section 5.2.1, the wide groove processing was carried out at intervals from 0 mm to 3.5 mm, and the number of the wide groove processing is 4 times. Photo of the wide groove is shown in Figure 5.5, and measurement results of cross-section profiles are shown in Figure 5.7. From that, we can find that, although the same experimental parameters were used during processing, due to the interval between two single grooves being changed, cross-section profiles of wide groove are different from each other.

Before ECM processing, to foresee the cross-section profile of the wide groove, calculations about the cross-section profile were done by using the software of Microsoft Excel. During

calculating, the data of the latter single groove is accumulated on the former one. And the data of the single groove's cross-section shown in Figure 5.3 was used, the interval increases from 0 mm to 3.5 mm. The schematic of the cross-section calculation is shown in Figure 5.6, the calculation results are shown as black contour lines in Figure 5.7.

From Figure 5.7(b), when the interval is 0.5 mm, it is found that the cross-sectional profile of the wide groove is similar to a "V" shape, and the depth difference, which occurs in the former research results, in the cross-section, between the center area and the edge area was eliminated effectively.

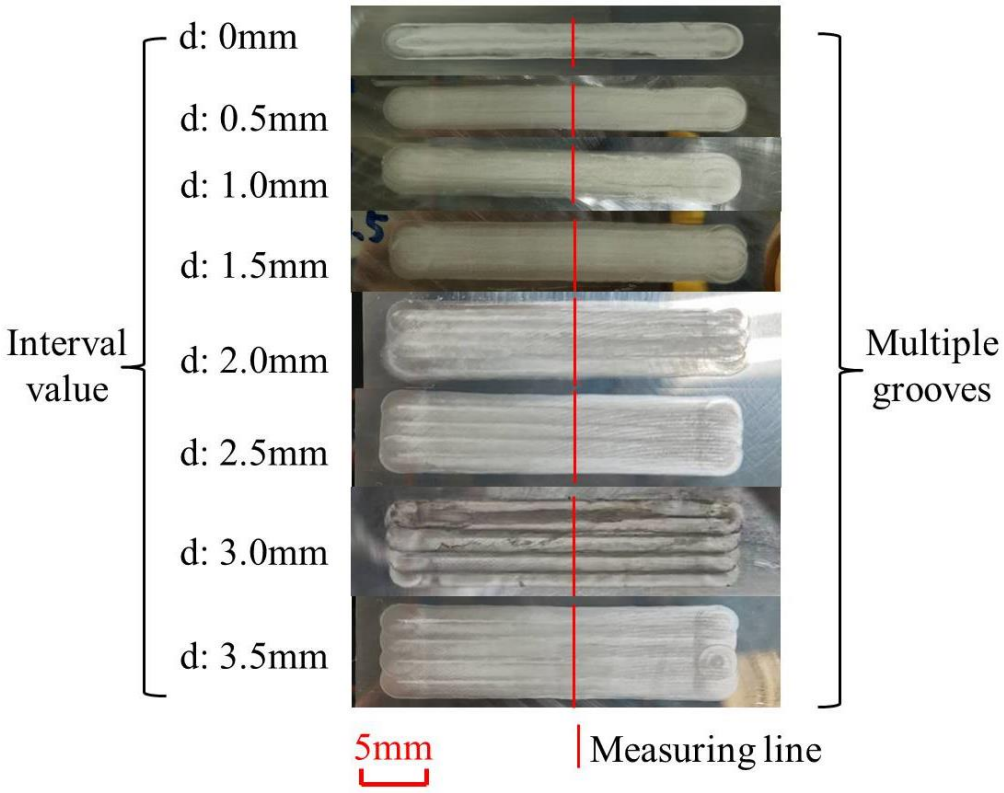

Figure 5.5 Photo of wide grooves.

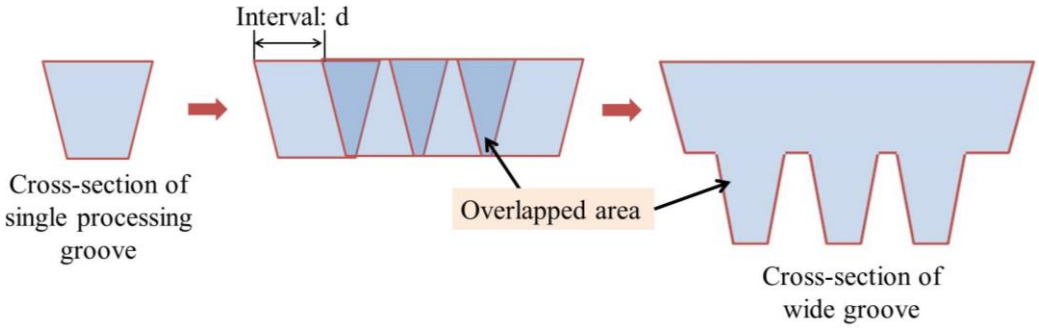

Figure 5.6 Schematic of cross-section calculating.

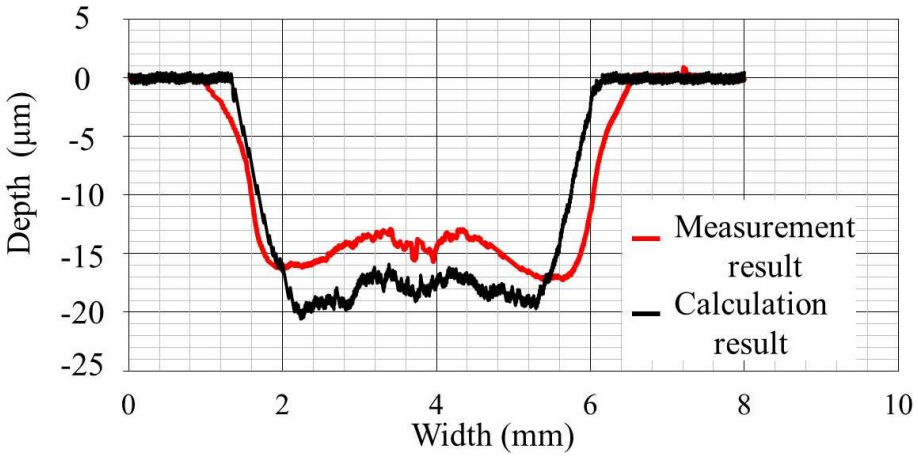

(a) Interval: 0 mm.

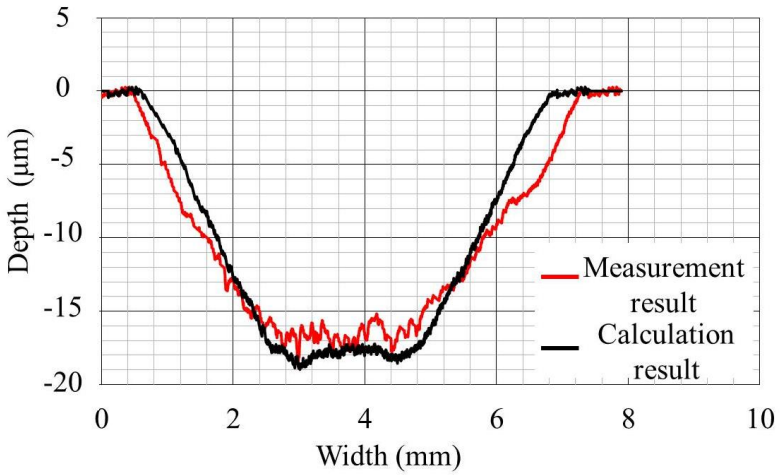

(b) Interval: 0.5 mm.

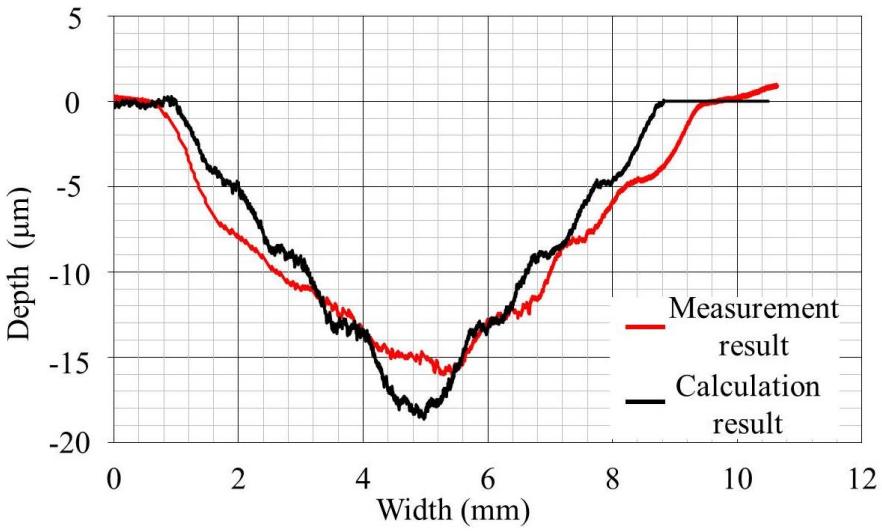

(c) Interval: 1 mm.

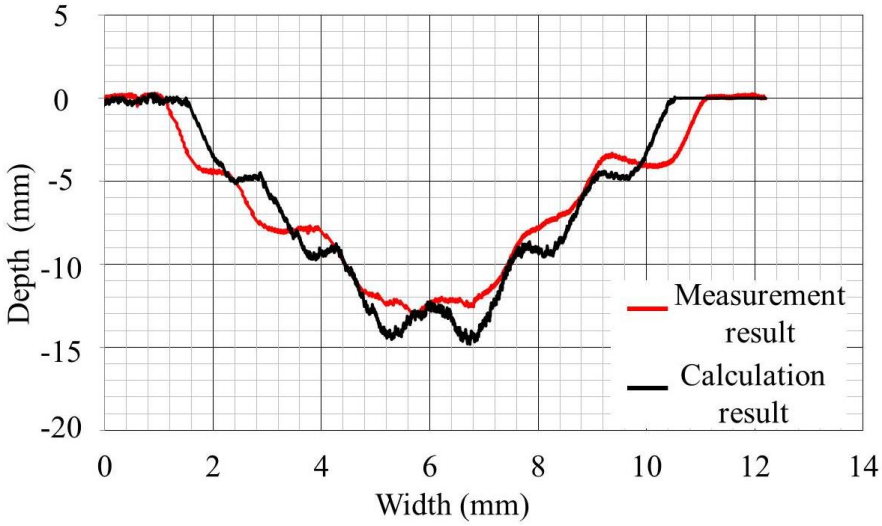

(d) Interval: 1.5 mm.

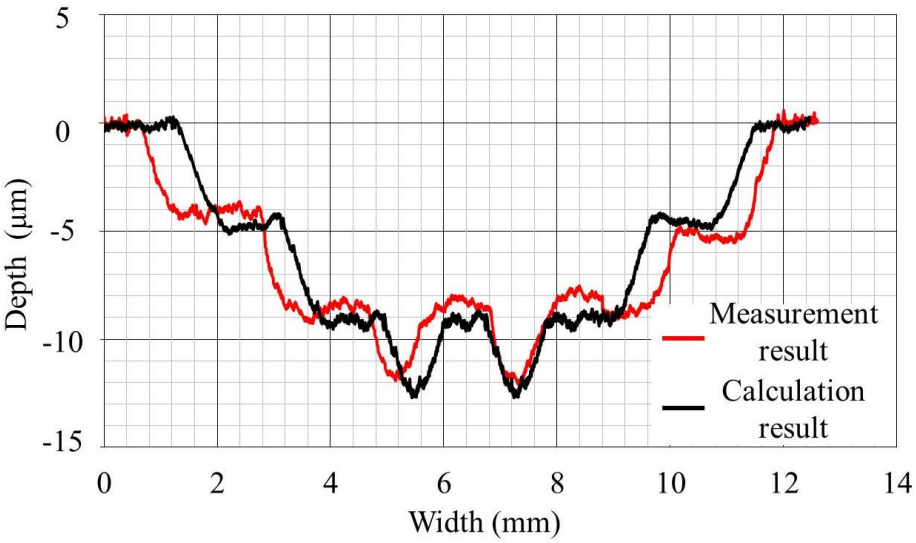

(e) Interval: 2 mm.

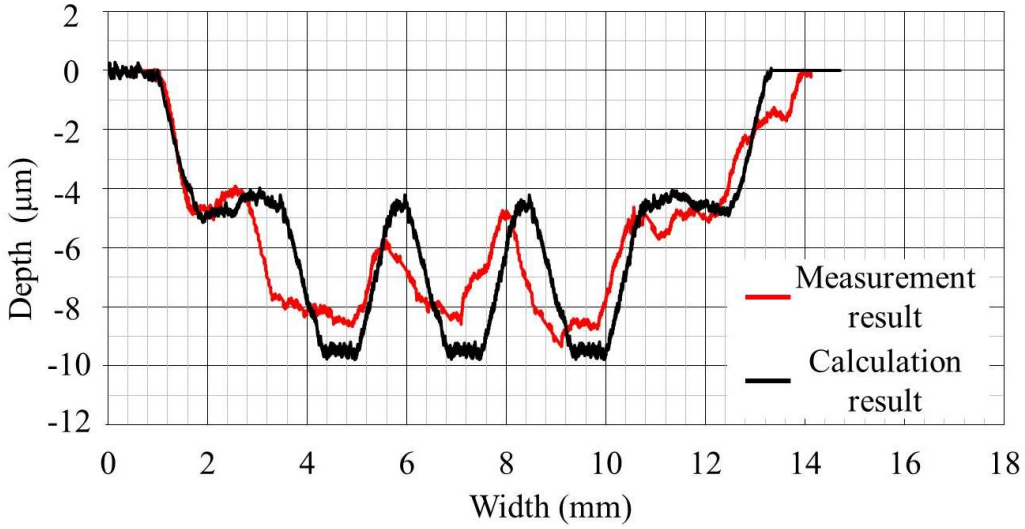

(f) Interval: 2.5 mm.

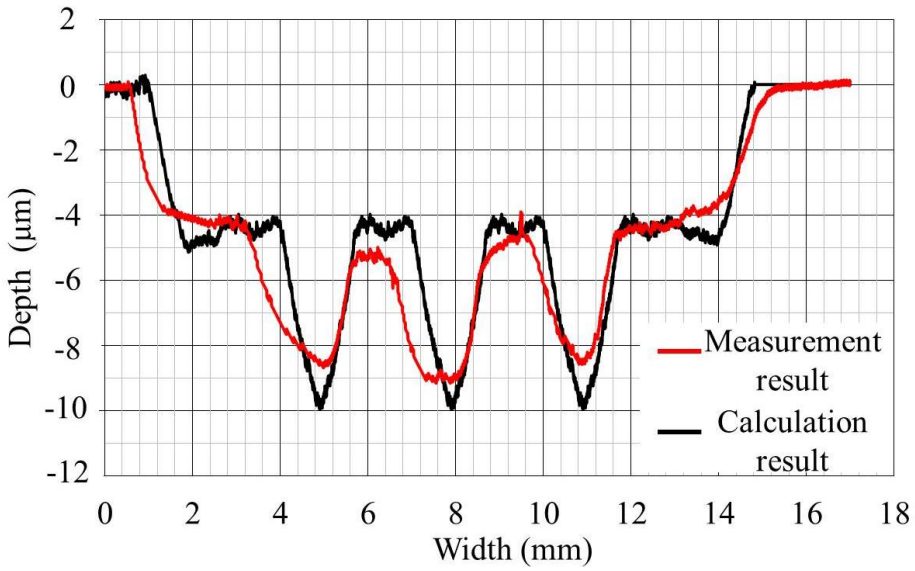

(g) Interval: 3 mm.

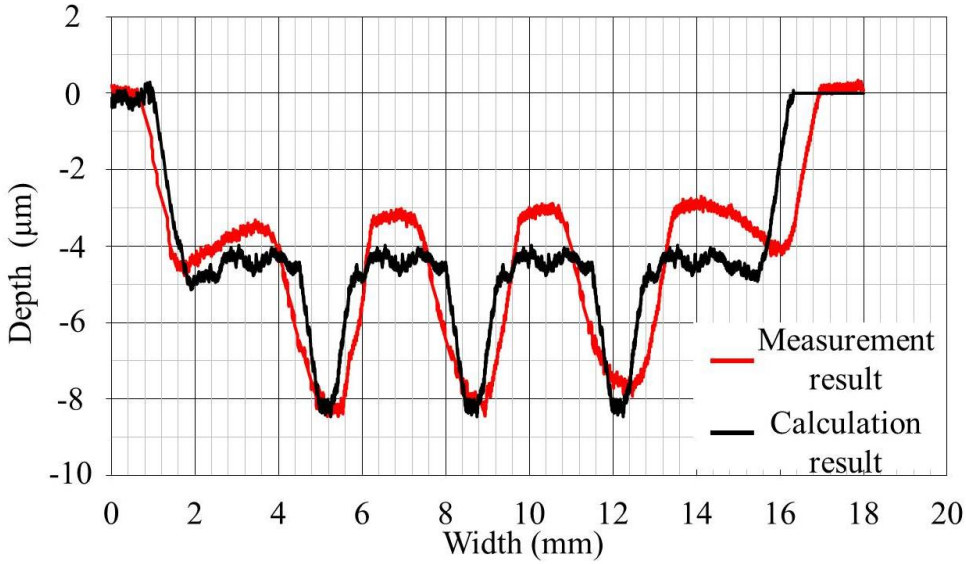

(h) Interval: 3.5 mm.

Figure 5.7 Cross-section profiles of measurement results and calculation results of wide grooves.

5.2.3 Comparison between wide groove measurement result and calculation result and analysis

From the comparison between wide groove's cross-section profiles of measurement results and calculation results in Figure 5.7, we can find that:

(1) For the same interval condition, the cross-section shapes of the processed results and the calculated result of wide groove are similar to each other roughly. It is thought that due to the MFS-ball can limit the electrolyte's distribution in ECM processing, material dissolutions only occur in the electrolyte existing areas. During the wide grooves processing, only the overlapping area was processed twice, while for the other areas, the formerly processed groove is hardly affected by the later processed trace except for the overlap position.

(2) Though the shape of the cross-section between the machining trace and the calculated result is the same as each other roughly, the black contour lines and the red contour lines of Figure 5.7 do not match completely. The reason is considered as the following.

As reported in chapter 4, if other experimental conditions can be maintained, the width and the depth of the processed groove increase as the ECM processing time increases. When the interval is 0mm, the total processing time of the wide grooves is equivalent to 400 s, which means that the ECM process is carried out continuously to 400 s, and the width of the processed groove increases. However, during calculating, only the depth of the processed area increases to become 4 times the depth of the single groove, while the width of the calculated result is kept constant during the calculation, which is equal to the width of a single groove whose processing time is only 100 s. Hence, the width of the actual machining trace is larger than the width of the calculated result.

(3) For other intervals, the reason why the contour lines do not match each other is considered that there is a size difference exists for MFS-balls. As recorded in the product introduction of

the MFS-ball, the size difference is about plus or minus 0.5mm. In chapter 4, we measured the diameters of MFS-balls, and there are dimensional differences that exist in the same MFS-ball and different MFS-balls. When the single groove is processed by using a bigger MFS-ball, the width of the processed groove may become wider than that of processing with a smaller MFS-ball.

5.3 Metal marking processing with universal moving unit

5.3.1 Introduction of metal marking

Metal is one of the most common materials in our daily life. Because of its features like conductive, reactive, cost-effective, etc., metal materials are dependent on and used in manufacturing, production, and consumerism. For most metal products, it is important to mark patterns such as product coding, product logos, graphics, etc. During metal marking, there are lots of processing methods which include dot peen marking, laser processing, and electrochemical marking are usually used.

(1) Dot peen marking

As shown in Figure 5.8, the dot peen marking method is a pin marking application, and it allows manufacturers to make deep, permanent impressions for identification and traceability on the surface of metal products. During which, by using a marking pin or stamping a series of small, closely spaced dots, target patterns are formed on the workpiece surface. These patterns make sure that the product is traceable, especially when the product does not meet the requirements of users' or has been damaged. While, as a kind of stress marking method, it is hard to be used in marking thin-walled products [46].

Figure 5.8 Photo of dot peen marking. [46]

(2) Laser marking

Laser marking is another effective marking method, the schematic of laser marking is shown in Figure 5.9. During processing, a focused laser beam [47] is used to mark permanent patterns on the workpiece surface. When the laser beam interacts with the workpiece, it alters the material's properties and appearance. This concentrated laser beam is distributed only in the specified area to create precise, high-quality, high-contrast marks that are easy to read or scan on the surface of the workpiece.

This feature makes the laser marking method for applications where high accuracy and permanence are critical to success. Besides that, this marking method is usable on various materials, not only metal materials but also plastics, woods, etc.

However, due to metal materials being removed by chipping or melting, some residual stresses and micro-cracks exist after laser marking.

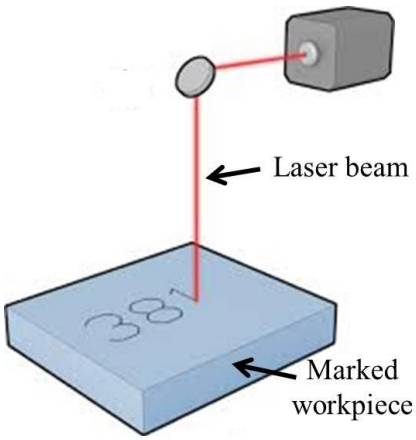

Figure 5.9 Schematic of laser marking. [47]

(3) Electrochemical etching

As a kind of etching method, electrochemical etching is usually used to process marks on the surface of products. Based on the processing principle of ECM, Electrochemical etching is a

process by which conductive metal surfaces are marked or etched with the help of electrical current and mild electrolytic fluids.

As reported in chapter 1, during ECM processing, the material of the workpiece is removed by electrochemical reaction at the level of atoms, there is no stress and melting occurs in the processing area. After ECM, the processed area is not affected by residual stresses or micro-cracks.

In this section, based on the research results before, we tried to explore using the ECM method with the MFS-ball used as the electrolyte absorption materials to process shallow patterns, which can be used as marks, on the workpiece surface.

5.3.2 Introduction of universal moving unit and processing principle

In our former research, the electrode where there is a V-shaped cross-section track used as the moving track of the MFS-ball was utilized. But by using that electrode, only the straight groove can be processed. Although the length of the groove can be controlled by adjusting the moving length of the workpiece and the MFS-ball, it is inconvenient to form patterns like English letters or numbers on the workpiece surface.

Hence, first of all, aiming at processing dimple textures and being inspired by the writing process of using a ball-point pen, the innovative experimental equipment called the universal moving unit was designed.

A photo and the schematic of the universal moving unit are shown in Figure 5.10, and a processing photo and the processing schematic are shown in Figure 5.11. The universal moving unit consists of an acrylic frame, used as the stand of the experimental equipment, four copper shafts, four stainless steel bearings, and an MFS-ball. The MFS-ball is placed in the cavity area surrounded by bearings. When being driven by the friction from the workpiece, the MFS-ball

can only roll freely instead of moving with the workpiece, because the movement of the MFS-ball is limited by bearings. With this universal moving unit, by controlling the moving trace of the workpiece with the CNC machine, it is convenient to process complicated target patterns on the metal workpiece surface.

The processing principle of using the universal moving unit is similar to that of using the electrode with a V-shaped cross-section track. Due to the capillary action, electrolytes are absorbed by the MFS-ball. At the ECM processing area, where the MFS-ball contacts with the workpiece, because of the surface tension of liquids, electrolytes spread on the workpiece surface, and a small area around the contact point is covered by electrolytes. Once machining currents are flowing from the workpiece to the electrode, electrochemical reactions will occur in the area covered by electrolytes. Besides that area, there is no electrochemical reaction occurs, and the other surface of the workpiece is not corroded by ECM. Hence, the ECM method of this research can limit the distribution of electrolytes and avoid the areas which should not be processed by ECM being corroded as much as possible.

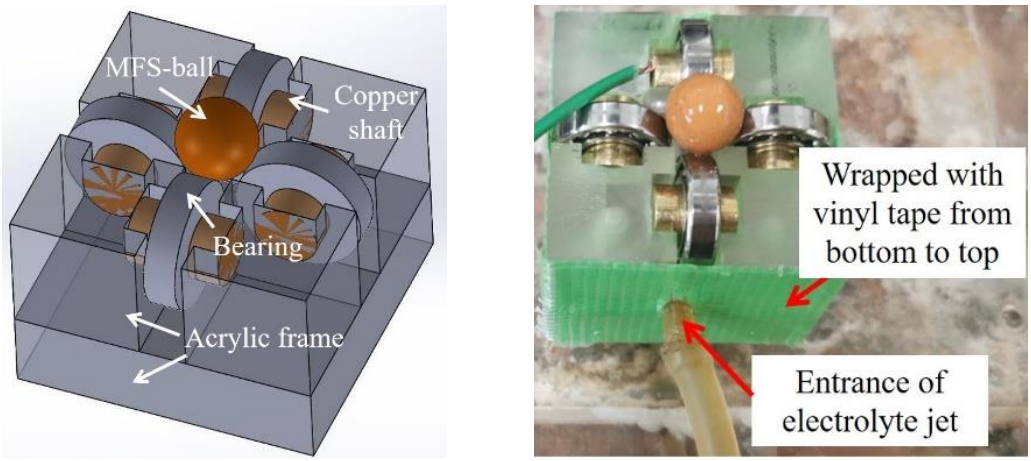

(a) Schematic of universal moving unit. (b) Photo of universal moving unit.

Figure 5.10 Schematic and photo of universal moving unit.

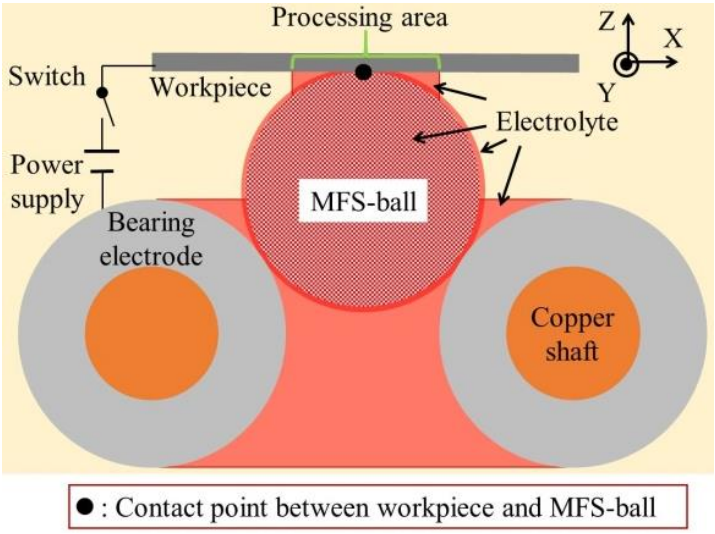

(a) Processing schematic of using universal moving unit.

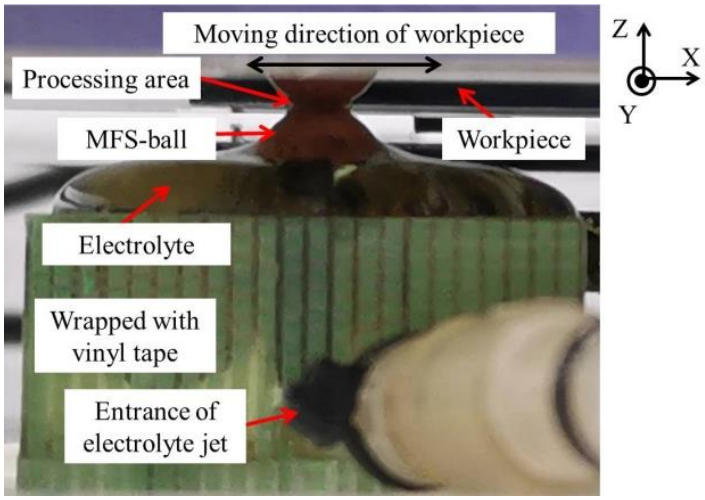

(b) Processing photo of using universal moving unit.

Figure 5.11 Processing schematic and photo of using universal moving unit.

In addition, as shown in Figure 5.11(b), the fresh electrolyte is supplied from the entrance of the electrolyte jet to replenish electrolytes for the MFS-ball and take away ECM by-products adhere to the surface of the MFS-ball, then the waste electrolyte flows out from gaps around the

MFS-ball and bearings. To avoid the electrolyte flowing out from side gaps of the acrylic frame, the acrylic frame are wrapped by vinyl tape from the bottom to the top of the sidewalls.

5.3.3 Processing method of metal marking

The whole experiment equipment of metal marking is shown in Fiugre 5.12. With the whole experiment equipment, the metal marking steps are as follows:

(1) Workpiece positioning and contact detection:

First, the MFS-ball was placed in the cavity of the universal moving unit. And then, the workpiece was moved downward along the –Z direction to contact with the MFS-ball. During this, the power supply remained turn-off. To make sure that the workpiece contacts the MFS-ball, the workpiece and one of the bearings were connected to probes of a digital multimeter separately. Once the workpiece contacts the MFS-ball, the electrical circuit of the digital multimeter is closed and a contact signal of beep will be emitted. Furthermore, to ensure that the MFS-ball ball was fully in contact with the workpiece during the whole process, the workpiece was moved downward 0.1mm further. The force between the workpiece and the ball produced due to the further movement was about 15N, according to the force measurement.

(2) Pre-scanning:

The electrolyte pump was switched on to provide fresh electrolytes to the MFS-ball and take away ECM by-products. Then, the workpiece moved along the pre-set trace under the control of the CNC system. During this step, the power supply was also turned off. This step in the experiment is referred to as pre-scanning. The purpose of the pre-scanning is to form a stable electrolyte film on the MFS-ball surface and accumulate electrolytes at the processing area. Otherwise, the whole ECM cannot be performed stably. The influence and necessity of the pre-scanning have been reported in detail in chapter 4.

(3) Metal marking:

After the pre-scanning period, the whole experimental equipment started to do metal marking as the pre-set program of the CNC machine. During which, the workpiece was driven by the CNC machine to move in the XY plane, moving traces of 'E', 'C', and 'M' are shown in Figure 5.13. Limited by the size of the workpiece and the maximum moving length of the CNC machine, these dimples were separately processed one by one. During processing, the constant current value is 40 mA, and the number of reciprocating processing is 16.

First, after the CNC machine sent an electric signal to the relay module through the R cable, the relay module was turned on. At the same time, the power supply was turned on, and electrochemical reactions occurred in the processing area. When the electric signal in the R cable was stopped, the relay module and the power supply were turned off, which led to the ECM process being stopped too.

The universal moving unit was fixed, and the workpiece, which moved in the XY plane, was controlled by the CNC machine based on the pre-set program. With the moving trace shown in Figure 5.13, dimple English alphabets of 'E', 'C', 'M' were processed. Limited by the size of the workpiece and the maximum moving length of the CNC machine, these dimples were separately processed one by one.

(4) Ending:

After the ECM, the power supply and electrolyte pump were turned off. The workpiece was moved up in the +Z direction, and then the CNC machine was switched off.

The common experimental conditions in Table 5.2 were used in metal marking.

Table 5.2 Common experimental conditions.

Item	Specification
Absorption material	MFS-ball
MFS-ball diameter	9.4 mm
Tolerance of MFS-ball diameter	+0.05 mm -0 mm
Workpiece	SUS304 plate
Electrode	SUS304 bearing
Electrolyte	10 wt.% NaCl solution
Number of reciprocating pre-scanning	8
Constant current value	40 mA
Number of reciprocating processing	16

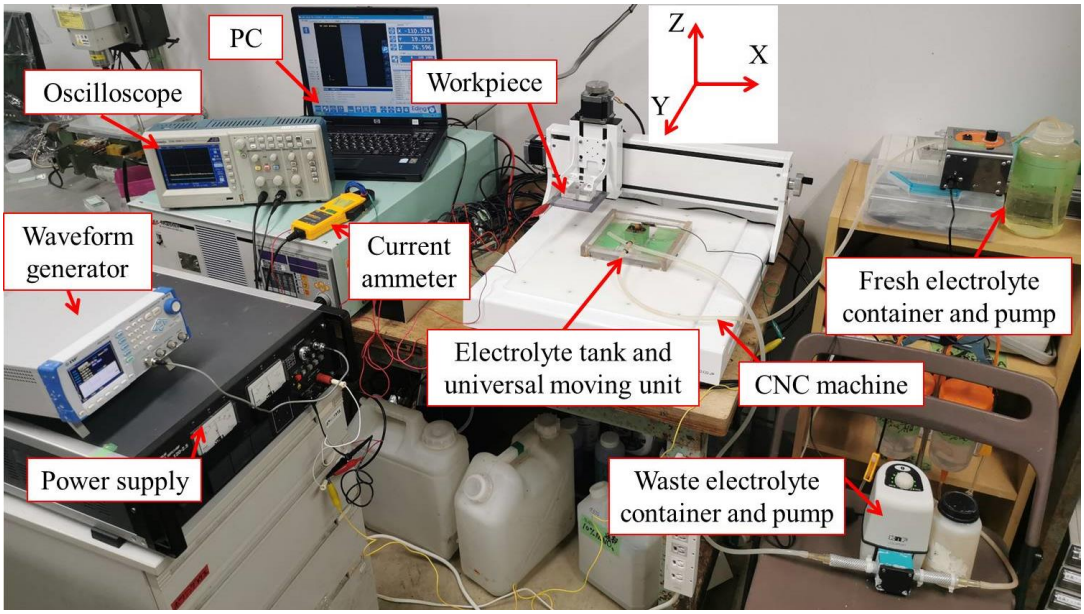

Figure 5.12 Photo of experimental equipment of metal marking.

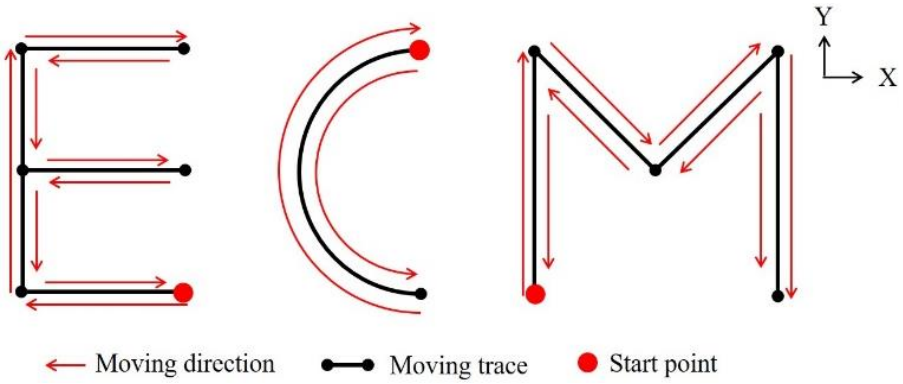

Figure 5.13 Moving trace of processing 'E' 'C' 'M'.

5.3.4 Processing result of metal marking

The photo of the marking processing result and the 3D measurement result are shown in Figure 5.14. From that, we can find that after marking processing, dimple English alphabets, 'E', 'C', 'M', with depths of about 7 μm were etched on the workpiece surface. Hence, it is verified that by using the ECM method of this research, metal marking can be achieved easily. And

because the distribution of the electrolyte is limited by the MFS-ball, besides the processed area, there is no material dissolved at other areas of the workpiece surface.

(a) Photo of marking processing results.

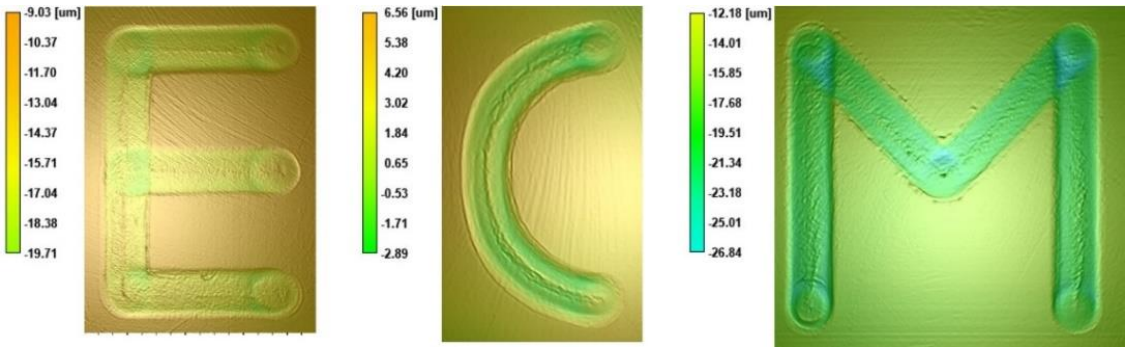

(b) 3D measurement results of marking processing results.

Figure 5.14 Photo and 3D measurement results of marking processing results.

5.3.5 Discussion about metal marking

In this research, limited by the CNC machine, only the workpiece which was fixed on the moving axis of the CNC machine can move during processing. However, in the actual production process, markings are usually processed in heavy workpieces, these workpieces are difficult to be moved and fixed on CNC machines.

Hence, in the following research, we plan to improve the ECM method and fix the universal moving unit on the moving axis of the CNC machine. In this way, heavy workpieces remain stationary during marking processing, and the target texturing can be processed only by controlling the movement of the universal moving unit.

In summary, the ECM method of this research is similar to writing with a ball-point pen, and it has a wide range of applicability, no matter how large and weight the workpiece is, and whether the processing surface is flat or curved.

5.4 Oil pocket processing

5.4.1 Introduction of oil pocket and its processing method

As discussed in the 1960s first [48], dimple texturing has emerged in recent decades as a viable means for enhancing tribological performance [49, 50]. Since dimple structures, like shallow grooves, can provide lubricant oils to form an oil film [51, 52] at the contact area of sliding surfaces, as shown in Figure 5.15, to reduce friction and improve the wear properties of mechanical components. As reported, dimpled structures used as oil pockets of the sliding surface can reduce friction by 30% or more [53].

However, as shown in Figure 5.16, if there is no oil pocket, supplying lubricating oil to the area between sliding surfaces becomes difficult. This causes wringing and stick-slip phenomena and thus leads to a drop in the movement smoothness and accuracy.

Figure 5.15 Photo of sliding surfaces of milling machine.

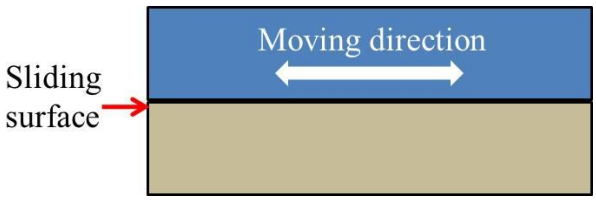

(a) Sliding surface without oil pockets.

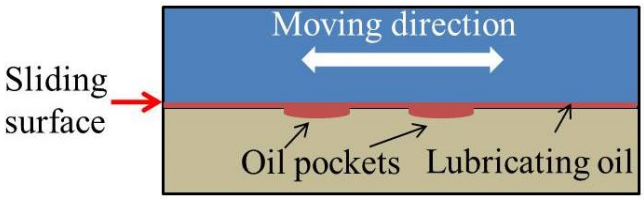

(b) Sliding surface with oil pockets.

Figure 5.16 Comparison of sliding surface without / with oil pockets.

Hence, various techniques have been employed for dimple texturing processing. Hand scraping [54] is a conventional method with a long history in oil pocket processing of sliding surfaces. A photo of hand scraping is shown in Figure 5.17. During which, skilled workers manually scrape shallow grooves, whose depth is about several micrometers usually. In the age of industrial automation, scraping with hands faces lots of shortcomings, which include that difficult operation, not conducive to skill transfer, and low processing efficiency [55].

Zhang et al. [49] have processed dimple surface texturing of carbon steel by using the photochemical machining method. With a prefabricated mask in the ECM, Chen et al. [56] and Shen et al. [57] processed micro-dimple texturing successfully. While, before processing by using these methods, micro-textures need to be made on the target area of the metal surface, which increases the cost and time.

Figure 5.17 Photo of hand scraping. [58]

In the paper of Ghaei et al. [59], a micro-dimple rolling apparatus shown in Figure 5.18 was developed to generate dimples with square cross-sections on metallic surfaces. Since these dimples are formed under the process of a mechanical machine, residual stress and deformation exist in the processing area. Also, this method is difficult to be used in hard-to-machined materials and thin-walled workpieces.

Besides the above-mentioned, laser surface texturing is another advanced method. It is widely used because the laser method is extremely efficient and leads to a short processing time. In addition, it is a kind of environmental processing method with excellent controllability of the shape and size of dimples [61]. However, surface heating by the laser beam leads to the creation of a heat-affected zone. In some cases, this disadvantage of laser processing is unacceptable, especially for coated sliding elements. In most cases, after laser processing, burrs occur around the dimple's edge and additional operation is required to remove them [61].

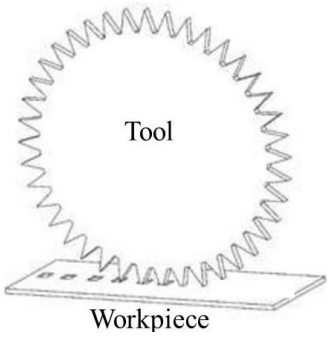

(a) Schematic of micro-dimple rolling apparatus.

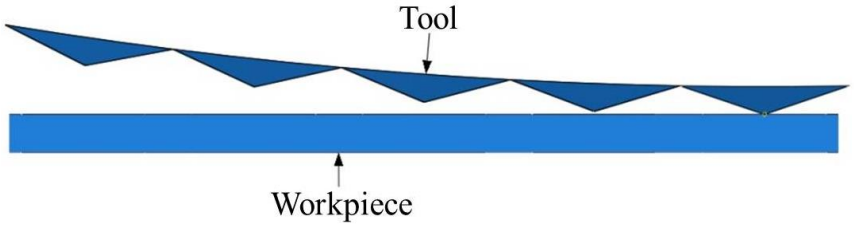

(b) Schematic of micro-dimple processing.

Figure 5.18 Schematic of micro-dimple rolling apparatus and processing. [61]

ECM is a well-known non-conventional processing method, based on the principle of electrochemical reactions in industrial processing. Takashima et al. [62] processed oil pockets by using the suction tool during ECM, the schematic of ECM processing with the suction tool is shown in Figure 5.19. Jung et al. [63] processed micro-dimple texturing with a micro-ECM method and performed a friction test on the sliding surface. The result showed a sliding surface with oil pockets has better properties in the overall frictional performance than that of a sliding surface without oil pockets. Liu et al. [64] used the electrolyte jet machining (EJM) method to process dimple texturing on the surface of Ti1023 titanium alloy, and dimples with small diameter and large depth were generated.

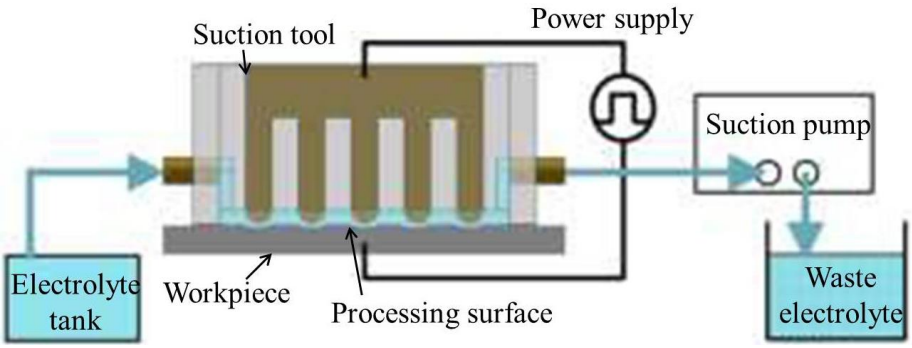

Figure 5.19 Schematic of oil pockets processing with suction tool. [62]

While in conventional ECM, the workpiece is immersed in electrolytes to let the processing area contact with flowing electrolytes. In this case, the fluidity of electrolytes causes the distribution of electrolytes and machining currents to become unlimited. Hence, unintended processed areas are easy to be corroded by the stray currents or rusted by electrolytes [65]. Because the sliding surface has been already processed by fine finishing, only shallow dimples need to be generated in the target area during dimple texturing. If the fine finishing sliding surface is corroded or rusted during ECM processing, the workpiece has to be reworked or even

scrapped. Hence, when using the ECM method to process dimple texturing, it is important to control the electrolyte distribution at the processing area only.

As mentioned in chapter 2, an MFS-ball was used as the electrolyte absorption material in ECM processing. Because of the principle of MFS-ball's electrolyte absorption, which includes the capillary action of the porous structure and the surface tension of the liquid, the distribution of electrolytes is limited only in the processing area of ECM. Since the workpiece is put above the electrolyte instead of immersed in the electrolyte container, the workpiece surface other than the processing area is not in contact with electrolytes. The stray-current corrosion and the rust can be avoided effectively. To overcome those shortcomings mentioned above and realize a stray-corrosion-free and rust-free dimple texturing with ECM, the ECM method with the MFS-ball used as the electrolyte distribution material is adopted in this research.

In this section, based on the research results before, we tried to explore using the ECM method with the MFS-ball to process shallow dimple texturing, which can be used as the oil pockets, in the target part of the metal workpiece surface.

5.4.2 Experimental equipment and groove processing method

Experimental equipment of groove processing, its electrical circuit diagram, and the relay module are shown in Figure 5.20. Based on experimental equipment of section 5.3, a relay module is added to be used as the switch of the ECM process.

As shown in the electrical circuit diagram, there are four control signal cables of the CNC machine, three of them are the X, Y, and Z signal cables used to control the movement of the experimental equipment along the XYZ axes. The fourth signal cable, originally used to control the spindle of the CNC machine, is used in this research to connect with the relay module to control the turn on/off of the power supply. This signal cable is hereinafter abbreviated as R

signal cable. Due to the power supply providing machining currents to keep electrochemical reactions occurring, the CNC machine can also start/stop the ECM process.

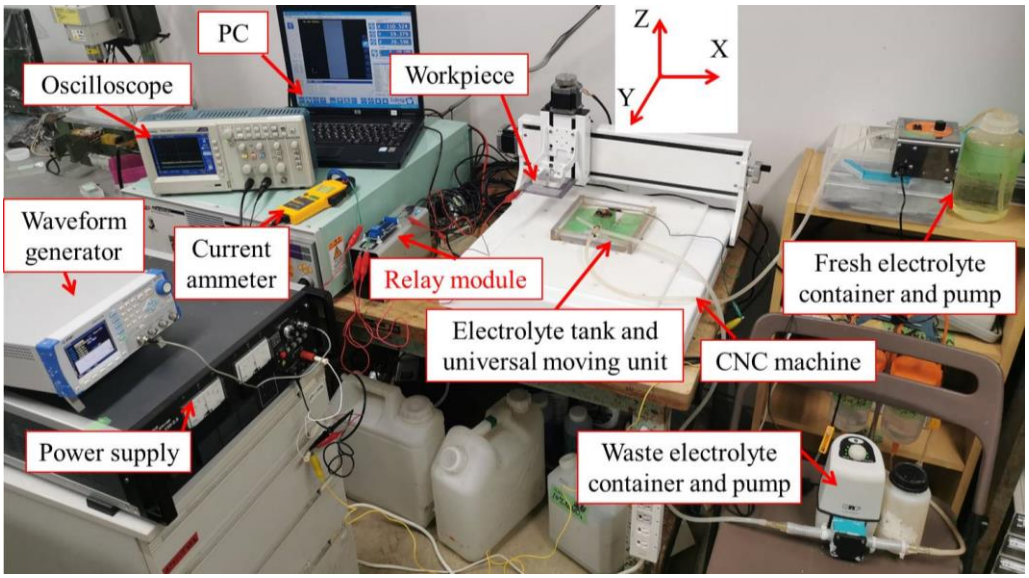

(a) Photo of experimental equipment of groove processing.

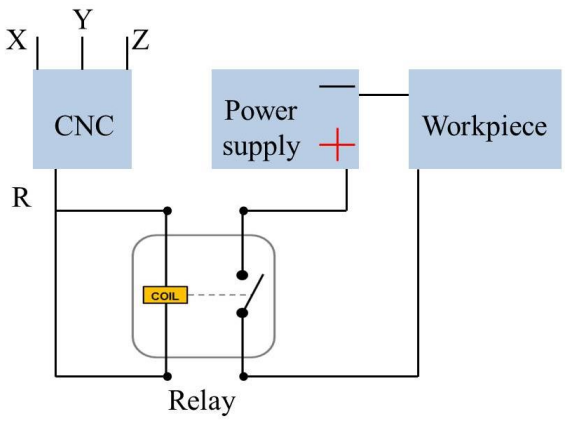

(b) Electrical circuit diagram.

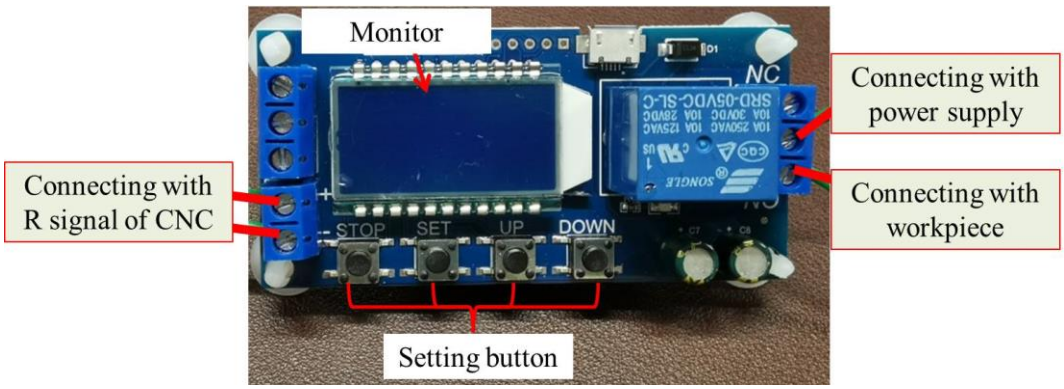

(c) Photo of relay module.

Figure 5.20 Photo of experimental equipment of groove processing, electrical circuit diagram and relay module.

The detailed experimental parameters are shown in Table 5.3. During ECM, the constant current value of 40 mA and the number of reciprocating processing 8 times were used.

The schematic of oil pocket processing is shown in Figure 5.21. To promote processing efficiency, target areas were processed repeatedly during the reciprocating movement between E and F of the workpiece. For easy presenting and understanding, we take the workpiece as the reference.

During the MFS-ball moving from E to F in Figure 5.21, at the start point of the red line's left side, the CNC machine starts sending the electrical signal to the relay to turn on the power supply. So that electrochemical reactions start occurring from the left start point. At the right side of the red line, the CNC machine stops sending the electrical signal, and the ECM is stopped at the same time. This area is called as ON region. After that, though the MFS-ball moves along the pre-set trace, there are no electrochemical reactions occur, and there is no pocket processed. This area of the black line is called as OFF region.

During the MFS-ball moving reversely, the process method is the same as above, but the ECM starts from the right endpoint of the red line to the left endpoint of the red line.

Table 5.3 Common experimental conditions.

Item	Specification
Absorption material	MFS-ball
MFS-ball diameter	9.4 mm
Tolerance of MFS-ball diameter	+0.05 mm -0 mm
Workpiece	SUS304 plate
Electrode	SUS304 bearing
Electrolyte	10 wt.% NaCl solution
Number of reciprocating pre-scanning	8
Constant current value	40 mA

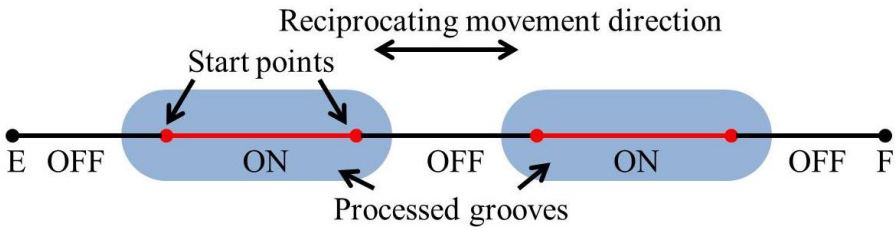

Figure 5.21 Schematic of processed oil pocket and moving trace.

5.4.3 Groove processing result of ON 10 mm / OFF 10 mm

As shown in Figure 5.21, for easy expression, we define the red line area as “ON + length” and the black line area as “OFF + length”.

With the moving speed of 10 mm/s, the number of reciprocating processing 8 times, and experimental conditions in Table 5.3, shallow pockets that can be used as oil pockets were processed by ECM. The photo of processed pockets and the cross-section are shown in Figure 5.22. The shape of the processed pocket looks like a capsule. From the measurement result of Figure 5.22(b), we can find that the area where electrochemical reactions occur was dissolved to about 4 μm, and the depth of the cross-section’s center is shallower than the depth of the cross-section’s edge.

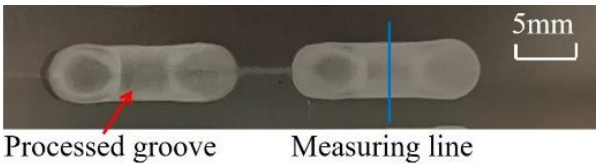

(a) Processed pockets.

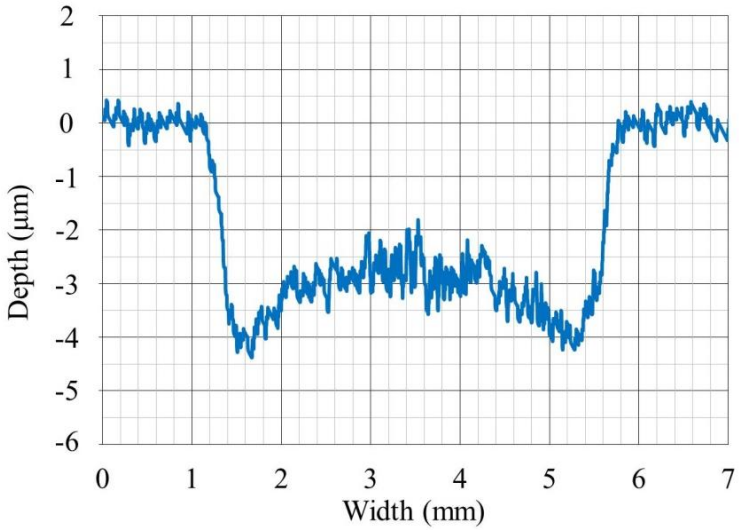

(b) Cross-section measurement result.

Figure 5.22 Processed pockets and cross-section measurement result of ON10 mm OFF10 mm.

5.4.4 Pocket processing result of different pocket lengths

In this section, by controlling the ON/OFF region with the CNC machine, by using the moving speed of 10 mm/s, the number of reciprocating processing 8 times, and experimental conditions in Table 5.3, we processed pockets with different lengths of the ON/OFF region. As shown in Figure 5.23(a), the lengths of ON /OFF regions are 5 mm, 10 mm, and 15 mm.

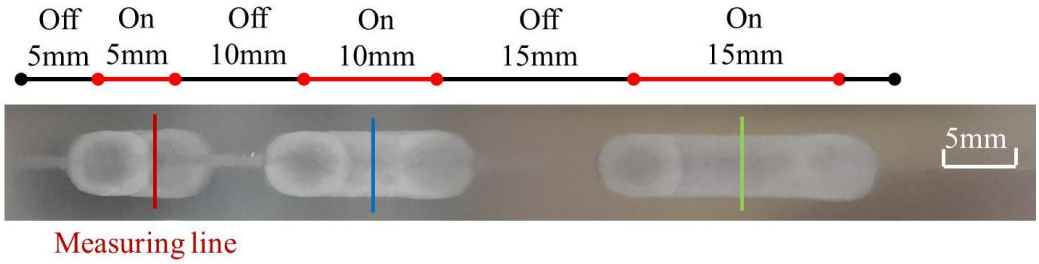

(a) Processed pockets.

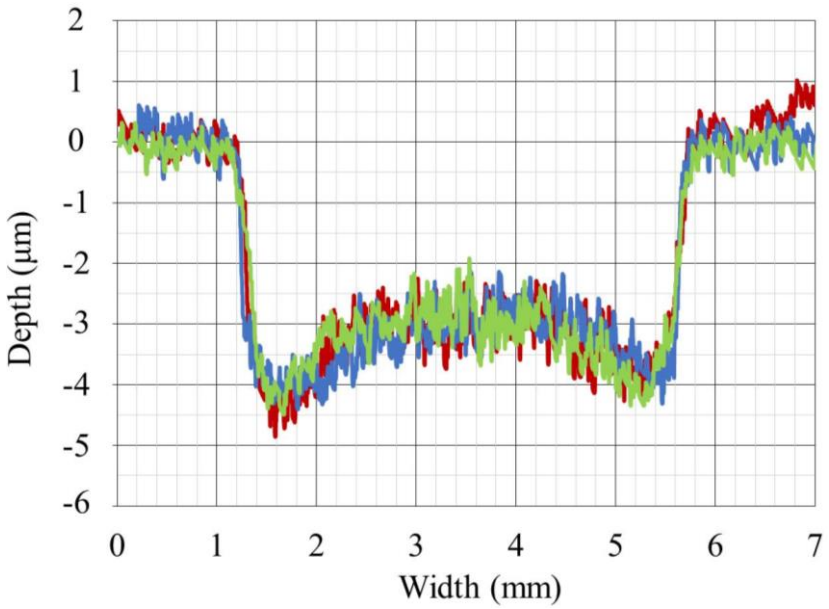

(b) Cross-section measurement results.

Figure 5.23 Processed pockets and cross-section measurement results of different pocket lengths.

From the measurement result of the cross-section in Figure 5.23(b), it is found that these pockets have a similar cross-section shape. Hence, by using this processing method, the processed pocket's length can be controlled, and dimple pockets with different lengths and depths in one moving trace can be achieved easily.

5.4.5 Pockekts processing result of different moving speed

In the experiments above, the same moving speed of 10 mm/s was used. When the length of the ON region is equal to each other, by using the different moving speeds, the processing time of each processed trace is different.

In this section, the ON 10 mm processing length and the constant current value of 40 mA were used, and the other experimental conditions are listed in Table 5.3. The processed traces and moving speeds of them are shown in Figure 5.24. The measurement result of the cross-section and the 3D measurement result are shown in Figure 5.25. From the measurement results, it can be found that the depth of processed traces increases as the moving speed decreases because the processing time of different processed traces increases at the same time. In addition, the depth of the center of the green cross-section is deeper than the red cross-section and the blue cross-section. The reason for this result will be considered in section 5.4.6.

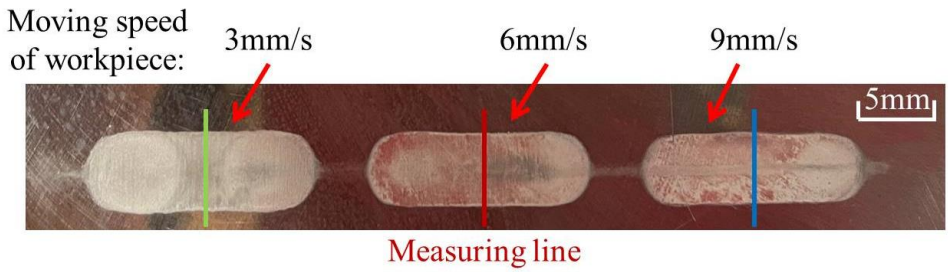

Figure 5.24 Processed pockets using different moving speeds.

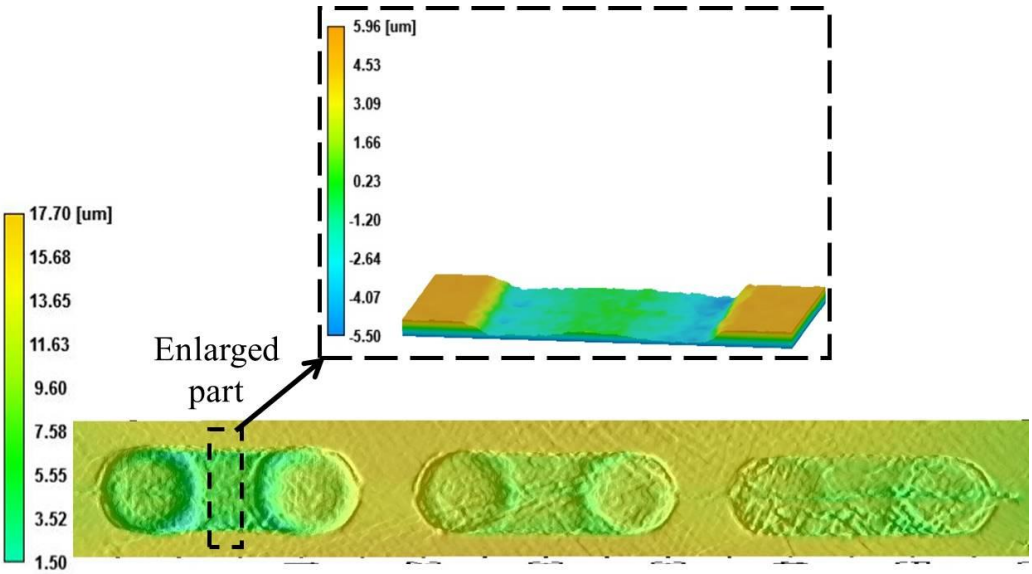

(a) Cross-section measurement results.

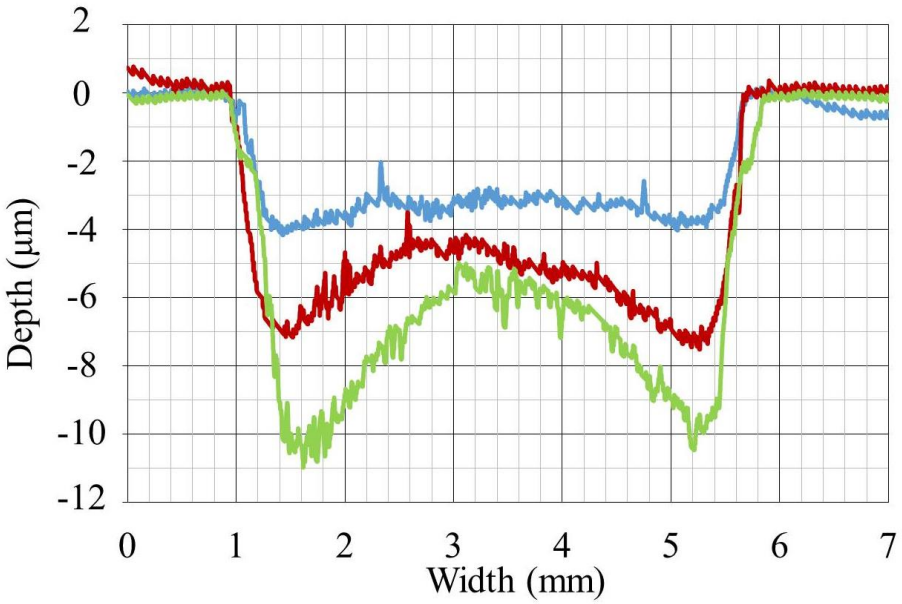

(b) 3D measurement result.

Figure 5.25 Cross-section measurement results and 3D measurement result using different moving speeds.

5.4.6 Discussion of pocket processing

After that, by using the moving speed of 9 mm/s, a pocket was processed. The maximum depth of the pocket processed in 9 mm/s is equal to that of the pocket processed in 3 mm/s, as shown in Figure 5.26. The other experimental conditions are shown in Table 5.3.

From the comparison of Figure 5.27(c), we can find that the depth of the center area of the pocket processed at 9mm/s is smaller than the groove processed at 3mm/s.

The reason is thought that, when using the slower moving speed of 3 mm/s, first of all, the proving speed of electrolytes to the processing area becomes slower than that of the moving speed of 9mm/s. As the ECM goes on, the electrolyte distributed around the contact point of the workpiece and the MFS-ball is used up, while the fresh electrolyte cannot be provided immediately, the ECM processing speed and the amount of the corroded materials on the workpiece surface decrease. At the same time, at the edge area of the processing area, though no fresh electrolytes are being provided too, due to there being much more electrolytes existing, the ECM processing speed is not affected obviously, lots of materials can be processed away still.

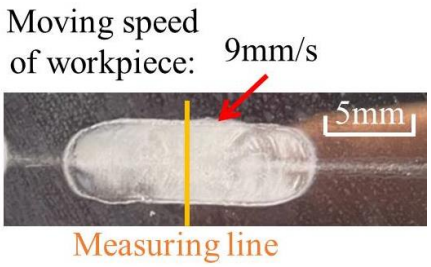

(a) Photo.

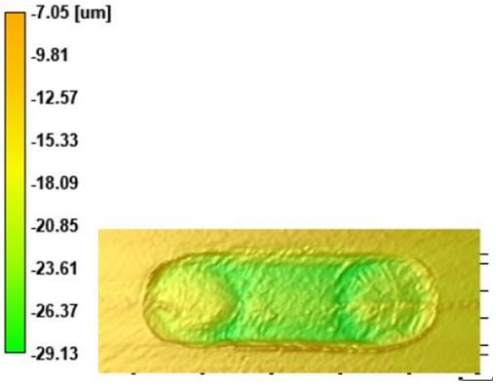

(b) 3D measurement result.

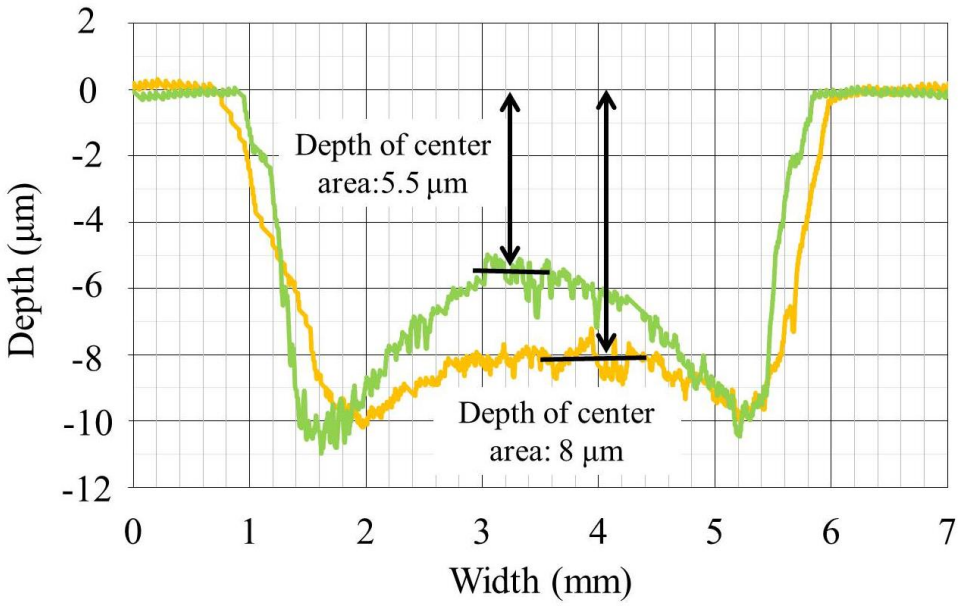

(c) Cross-section measurement results.

Figure 5.27 Photo, 3D measurement result, and cross-section measurement results of processed are using moving speed of 9 mm/s.

For the ECM result when using the moving speed of 9 mm/s, no matter the area around the contact point or the edge area of the processing area, fresh electrolytes can be provided fast, and the processing speed of ECM at the whole processing area will not be limited. Finally, when the maximum depth of the green cross-section and the orange cross-section are equal to each other, the depth of the center area of the orange cross-section is deeper than that of the green cross-section.

5.5 Conclusions

In this chapter, three applications of this ECM method were explored through actual experiments.

First, the wide grooves with different cross-section shapes were processed by changing the interval between every two single grooves. And through the comparison result of the cross-section profile between the processed wide grooves and the calculation results, it is found that though they have similar cross-section shapes when the interval is the same condition, the contours are not overlapped with each other well due to there are size differences existing of the MFS-ball.

To achieve metal marking, a new tool, called the universal moving unit, was designed and machined to replace the previously used electrode where there is a V-shaped cross-section track. When using the universal moving unit, the MFS-ball only rolls inside of the cavity area surrounded by bearings instead of moving along the workpiece. Finally, by controlling the moving trace of the workpiece, which is controlled by the CNC system, the corresponding pattern of dimple English alphabets were processed by the MFS-ball through ECM on the workpiece surface.

When being used in oil pockets processing, to process shallow pockets by using the ECM method of this research, the experimental equipment combined with a relay module used as the switch of the power supply was used. By controlling the turn on/off, the moving speed of the workpiece, and the length of the processed area, shallow pockets with different depths, and different lengths were obtained.

Chapter 6 Shortcomings, future issues and conclusions

6.1 Shortcomings and future issues

In this study, a kind of porous solid ball, the MFS-ball was used as the electrolyte absorption material in ECM processing to limit the electrolyte distribution and avoid the stray-current corrosion beside the target processing area. And the processing mechanism, processing features, applications in the future were reported in detail.

However, due to the limitation of experimental materials and devices, the other research content, which cannot be ignored, is not involved and explored until now. It is that the stray-current corrosion leading to the processing accuracy of the ECM method is difficult to be improved.

Hence, because of the excellent limitation for the electrolyte distribution of the ECM method with the MFS-ball, future research on how to improve the processing accuracy is essential and necessary to be involved.

Besides that, it is worth trying not only the porous solid like the MFS-ball but also the other materials with the porous structures inside being used in the ECM process. And these attempts can both gradually improve the ECM method of this research, and the applications can also be expanded to meet much more demands.

6.2 Conclusions

In this paper, first of all, the principle, background, and processing method of ECM were introduced. And the research purpose of this study is proposed.

Then, through the comparison of using the water absorption materials of diatomaceous earth chip and the MFS-ball, the MFS-ball is selected for the following research. And the MFS-ball and its electrolyte-absorbed principle of capillary action in detail, thanks to the MFS-ball's porous structures consisting of abundant micro holes, the electrolyte is absorbed into the MFS-ball and forms an electrolyte film on the MFS-ball surface driven by a physical phenomenon of capillary action. During ECM, the MFS-ball can take the electrolyte to the ECM processing area, and due to the limitation of the MFS-ball, electrolytes cannot flow at the workpiece surface, which eliminates the effects of the stray-current corrosion.

Besides that, from the experimental results, it is verified that the stray-current corrosion can be eliminated due to the distribution of the electrolyte being limited by the MFS-ball, and only the area where there exist electrolytes was dissolved to become a shallow groove. And the depth of the groove's edge area is deeper than that of the groove's center area. In addition, it is understood that during ECM of this research, machining currents flow through both the inside electrolyte and the electrolyte film of the MFS-ball, and the value of the machining current flowing through the electrolyte film is greater than that of flowing through the MFS-ball's inside electrolyte.

After that, according to the actual experiment, we have 2D modeled for the processing area. And by using the software of COMSOL Multiphysics, the potential between the workpiece and the electrode, the current density distribution at the processing area, and the cross-section profile of the processed area were simulated. By comparison between the simulation results and the actual experiment results, the simulation results are confirmed.

During experiments before, it is found that the processing results are influenced by lots of experimental parameters. Hence by changing the experimental parameters which include the pressure between the workpiece and the MFS-ball, the flow rate of the electrolyte, the pre-scanning, the machining current, the machining times, the moving speed of the workpiece, and the size difference of the MFS-ball, reasons and effects of those parameters are cleared and summarized.

Aiming at expanding the application, the ECM method of this study was used in wide groove processing, metal marking processing, and oil pockets processing respectively. And it is confirmed that this ECM method is suitable for those applications.

Conclusions for every chapter of this study are shown as follows:

Chapter 1

In this chapter, the principle, background, and processing method of ECM were introduced first.

Chapter 2

In this chapter, first of all, by using two kinds of water absorption materials, the diatomaceous earth chip, and the MFS-ball, ECM experiments were carried out tentatively. According to experiment results, it is found that though the diatomaceous earth chip has superior electrolyte absorption, due to its poor water resistance and soft texture, the diatomaceous earth chip is easily dispersed in electrolytes and broken during ECM. Compared with the diatomaceous earth chip, when it is used in experiments, the MFS-ball has good water resistance and absorption, and the strength of the MFS-ball is good enough to be used for a long time. In ECM processing, the distribution of the electrolyte is controlled well too. Hence, the MFS-ball is selected as the electrolyte absorption material in ECM for the following research.

After that, we introduced the MFS-ball and its electrolyte-absorbed principle of capillary action in detail. Thanks to the MFS-ball's porous structures consisting of abundant micro holes, the electrolyte is absorbed into the MFS-ball and forms an electrolyte film on the MFS-ball surface driven by a physical phenomenon of capillary action. During ECM, the MFS-ball can take the electrolyte to the ECM processing area, and due to the limitation of the MFS-ball, electrolytes cannot flow at the workpiece surface, which eliminates the effects of the stray-current corrosion.

Before processing with the MFS-ball, several main devices the experimental equipment and the electrode were introduced. Then, experimental procedures of using the experimental equipment in ECM were listed.

And through the photo of ECM and the processing schematic, we summarized that, due to capillary action, the MFS-ball can absorb electrolytes to its inside and form an electrolyte film on its surface. As rolls of the MFS-ball in ECM, the MFS-ball provides fresh electrolytes to the processing area and takes away ECM by-products continuously. At the processing area, limited by the MFS-ball, the electrolyte distributes to a small area around the contact point between the workpiece and the MFS-ball.

Besides that, from the experimental results, it is verified that the stray-current corrosion can be eliminated due to the distribution of the electrolyte being limited by the MFS-ball, and only the area where there are electrolytes existing was dissolved to become a shallow groove. And the depth of the groove's edge area is deeper than that of the groove's center area.

It is understood that during ECM of this research, machining currents flow through both the inside electrolyte and the electrolyte film of the MFS-ball, and the value of the machining current flowing through the electrolyte film is greater than that of flowing through the MFS-ball's inside electrolyte.

Chapter 3

In this chapter, according to the actual experiment, we have 2D modeled for the processing area. And by using the software of COMSOL Multiphysics, the potential between the workpiece and the electrode, the current density distribution at the processing area, and the cross-section profile of the processed area were simulated.

Through the simulation, the discussion and the verification of this chapter, and combined with the groove processing result of chapter 2 and the simulation results of section 3.4, conclusions about the reasons for the occurrence of the depth difference of cross-sections can be summarized as follows:

(1) Due to the limitation of the electrolyte distribution by the MFS-ball, the amount of the electrolyte at the edge area of the electrolyte distribution is more than that in the center area of the electrolyte distribution, and the value of the machining current flowing through the electrolyte film is greater than that of flowing through the inside electrolyte of the MFS-ball. Differences in the electrolyte distribution and the value of the machining current lead to the depth difference occurring in the processed area.

(2) During ECM processing, the machining current density distribution at the edge area of the electrolyte distribution is greater than that of the center area, and the greater the machining current density, the more materials are corroded from the workpiece surface. Finally, the processed depth of the edge area is deeper than the center area.

(3) Since the groove processing can be regarded as the process in which countless point processing is carried out and overlapped with a tiny interval, and the simulation results of section 3.4 are suitable for the point processing, the simulation results of chapter 4 also can be used to explain the experimental results of groove processing.

Chapter 4

This chapter summarized the influences of several main experimental parameters in this ECM method.

Although the pressure between the workpiece and the MFS-ball does not affect the processing results during ECM processing, to ensure that the workpiece and the MFS-ball contact with each other for the whole process and make the ECM process being carried out stably, the pressure value is selected as 15 N.

Due to the flowing electrolyte not working directly on the processing area of the workpiece surface, it is used to take away ECM by-products of the MFS-ball surface and the V-shaped cross-section track. Hence, a suitable electrolyte flow rate of 3 ml/s was selected for the following experiments.

According to experiments of this method, a necessary operation called Pre-scanning was summarized. The pre-scanning operation can accumulate electrolytes at the processing area in advance, and ensure the smooth progress of ECM. In addition, we found that when the pre-scanning time is less than 250 s, the width of the electrolyte distribution at the processing area increases as the time of the pre-scanning increases when the pre-scanning time is more than 250 s, the width of the electrolyte distribution will not be affected by the pre-scanning.

During the ECM processing of this method, the machining current value influences the processed groove directly. When using the same experimental parameters, the depth and the width of the processed groove increase as the machining current value increase. While, when the value of the machining current is larger than 50 mA, because the electrolyte supplied by the MFS-ball is not enough to be used in processing, the ECM cannot be carried out.

When using the same experimental parameters, except for the machining time, the depth and the width of the processed groove increase as the machining time.

Besides that, it is found that the depth of the processed groove increases and the width of the processed groove decreases as the moving speed of the workpiece increases. It is considered that a faster moving speed of the workpiece promotes the rotation and the movement of the MFS-ball, hence the refresh rate of the electrolyte at the processing increases. This is helpful for ECM processing.

Finally, it is found that size differences are exiting of MFS-balls' diameters, and it is turn out be that the size differences of processed grooves are caused by the size differences of MFS-balls, and the larger the MFS-ball's size difference, the greater the size difference in the processed groove. After being eliminated by the hemispherical grinding tool, size differences of the MFS-ball's diameter and the processed groove's width were decreased obviously.

Chapter 5

In this chapter, three applications of this ECM method were explored through actual experiments.

First, the wide grooves with different cross-section shapes were processed by changing the interval between every two single grooves. And through the comparison result of the cross-section profile between the processed multiple grooves and the calculation results, it is found that though they have similar cross-section shapes when the interval is the same condition, the contours are not overlapped with each other well due to there are size differences existing of the MFS-ball.

To achieve metal marking, a new tool, called the universal moving unit, was designed and

machined to replace the previously used electrode where there is a V-shaped cross-section track, and the processing method is the same as that of being reported in chapter 2. When using the universal moving unit, the MFS-ball only rolls inside of the cavity area surrounded by bearings instead of moving along the workpiece. Finally, by controlling the moving trace of the workpiece, which is controlled by the CNC system, the corresponding pattern of dimple English alphabets was processed by the MFS-ball through ECM on the workpiece surface.

When being used in oil pockets processing, to process shallow grooves by using the ECM method of this research, the experimental equipment combined with a relay module used as the switch of the power supply was used. By controlling the turn on/off, the moving speed of the workpiece, and the length of the processed area, shallow grooves with different depths, and different lengths were obtained.

Renference

[1] J. F. Wilson. Practice and theory of electrochemical machining, John Wiley & Sons, Inc, 1971.

[2] K. P. Rajurkar, D. Zhu, J. A. McGeough, et al. New developments in electro-chemical machining. CIRP Annals-Manufacturing technology, 1999, 48(2): 567-579. https://doi.org/10.1016/S0007-8506(07)63235-1

[3] A. Spieser, A. Ivanov. Recent developments and research challenges in electrochemical micromachining (μECM). International Journal of Advanced Manufacturing Technology; 2013, 69(1): 563-581. https://doi.org/10.1007/s00170-013-5024-8

[4] J. McGeough. Principles of Electrochemical Machining. 1974, Chapman & Hall, London.

[5] 佐藤敏一，電解加工と化学加工，朝倉書店, 1970.

[6] 木本康雄，電気・電子応用精密加工，オーム社, 1982.

[7] C. Y. Zhang, Y. J. Zhang, X. L. Chen, W. Li, G. X. Liu. Investigation of the electrochemical dissolution behavior of tungsten during electrochemical machining. The International Journal of Advanced Manufacturing Technology, 2018, 97: 3575-3582. https://doi.org/10.1007/s00170-018-2142-3

[8] M. Zohoor, S. Jalili, A. Alipour, R. Mosallanejad. Effect of electrolyte type on electrochemical machining of 304 steel, International Journal of Applied Engineering Research, 2016, 12(3): 20-39.

[9] O. Ralph, S. Max. The Faraday-Whewell correspondence concerning electro-chemical terms. The Scientific Monthly. 1937, 45 (6): 535-546. https://www.jstor.org/stable/16304

[10] A. E. Debarr, D. A. Oliver. Elelctrochemical machining. Macdonald, 1968.

[11] M. Kumar, P. K. Mahto, D. Kushwaha, N. K. Singh. Electrochemical machining: review of historical and recent developments, International Journal of Advance Research in Science and Engineering. 2016, 5(3): 217-227.

[12] Aero-engine: https://www.mistral-engines.com/node/2

[13] B. Bhattacharyya. Experimental investigation on the influence of electrochemical machining parameters on machining rate and accuracy in micromachining domain. International Journal of Machine Tools and Manufacture, 2003, 43(13): 1301-1310. https://doi.org/10.1016/S0890-6955(03)00161-5

[14]W. Han. Research on Micro Electrochemical Machining Using Electrostatic Induction Feeding Method. 東京大学博士学位論文, 2016.

[15] R. J. Leese, A. Ivanov. Electrochemical micromachining: an introduction. Advances in Mechanical Engineering, 2016, 8(1): 1-13. https://doi.org/10.1177/1687814015626860

[16] A. Lesch, G. Wittstock, C. Burger, B. Walther, J. Hackenberg. External control of anodic dissolution mechanism of 100Cr6 in nitrate/chloride mixed electrolytes. Journal of Electrochemical Science and Engineering, 2011, 1(1): 39-54. https://doi.org/10.5599/jese.2011.0004

[17] R. Świercz, D. Oniszczuk-Świercz. Investigation of Surface Layer Properties of High Thermal Conductivity Tool Steel after Electrical Discharge Machining. Metals, 2017, 7, 550: 1-16. https://doi.org/10.3390/met7120550

[18] Y. B. Zeng, H. J. Ji, X. L. Fang, Y. F. Wang, N. S. Qu. Analysis and Reduction of Stray-Current Attack in Reciprocated Traveling Wire Electrochemical Machining. Advances in Mechanical Engineering, 2014, 6: 11-21. https://doi.org/10.1155/2014/505932

[19] G. D. Liu, Y. Li, Q. C. Kong, H. Tong, H. Zhong. Silicon-based tool electrodes for micro electrochemical machining. Precision Engineering, 2018, 52: 425-433. https://doi.org/10.1016/j.precisioneng.2018.02.003

[20] M. Kunieda, M. Yoshida, Y. Akamatsu. Influence of Micro Indents Formed by Electro-chemical Jet Machining on Rolling Bearing Fatigue Life. ASME PED, 1993, 64: 693-699.

[21] W. Natsu, T. Ikeda, M. Kunieda. Generating Complicated Surface with Electrolyte Jet Machining. Precision Engineering, 2007, 31(1): 33-39. https://doi.org/10.1016/j.precisioneng.2006.02.004

[22] K. Yoneda, M. Kunieda. Numerical analysis of cross sectional shape of micro-indents formed by the electrochemical jet machining. JSEME, 1996, 29(62): 1-8. [In Japanese].

[23] M. Hackert, G. Meichsner, A. Schubert. Generating micro geometries with air assisted jet electrochemical machining. Proceedings of the 10th Anniversary,

International Conference of the European Society for Precision Engineering and Nanotechnology, 2008: 420-424.

[24] X. D. Wang, N. S. Qu, X. L. Fang. Reducing stray corrosion in jet electrochemical milling by adjusting the jet shape. Journal of Materials Processing Technology, 2019, 264: 240-248. https://doi.org/10.1016/j.jmatprotec.2018.09.017

[25] K. Endo, W. Natsu. Proposal and Verification of Electrolyte Suction Tool with Function of Gap-width Detection. International Journal of Electrical Machining, 2014, 19: 34-39. https://doi.org/10.2526/ijem.19.34

[26] G. X. Liu, Y. J. Zhang, W. Natsu. Influence of electrolyte flow mode on characteristics of electrochemical machining with electrolyte suction tool. International Journal of Machine Tools and Manufacture, 2019, 142: 66-75. https://doi.org/10.1016/j.ijmachtools.2019.04.010

[27] S. Q. Qian, D. Zhu, N. S. Qu, H. S. Li, D. S. Yan. Generating micro-dimples array on the hard chrome-coated surface by modified through mask electrochemical micromachining. International Journal of Advanced Manufacturing Technology, 2010, 47: 1121-1127. https://doi.org/10.1007/s00170-009-2246-x

[28] K. Zhai, L. Q. Du, Y. K. Wen, S. X. Wang, Q. Cao, X. Zhang, J. S. Liu. Fabrication of micro pits based on megasonic assisted through-mask electrochemical micromachining. Ultrasonics, 2020, 100, 105990. https://doi.org/10.1016/j.ultras.2019.105990

[29] N. S. Qu, X. L. Chen, H. S. Li, Y. B. Zeng. Electrochemical micromachining of micro-dimple arrays on cylindrical inner surfaces using a dry-film photoresist.

Chinese Journal of Aeronautics, 2014, 27(4): 1030-1036. https://doi.org/10.1016/j.cja.2014.03.012

[30] X. L. Chen, N. S. Qu, H. S. Li, Z. N. Guo. Removal of islands from micro-dimple arrays prepared by through-mask electrochemical micromachining. Precision Engineering, 2015, 39: 204-211. https://doi.org/10.1016/j.precisioneng.2014.09.002

[31] H. L. Costa, I. M. Hutchings. Development of a maskless electrochemical texturing method. Journal of Materials Processing Technology, 2009, 209(8): 3869-3878. https://doi.org/10.1016/j.jmatprotec.2008.09.004

[32] W, Natsu, J. F. He, Y. Iwanaga. Experimental study on electrochemical machining with electrolyte confined by absorption material. Procedia CIRP, 2020, 87: 263-267. https://doi.org/10.1016/j.procir.2020.02.106

[33] Introduction about ball-point pen. https://stationery.wiki/Ballpoint_pen

[34] F. Akhtar, Y. Rehman, L. Bergtrom. A study of the sintering of diatomaceous earth to produce porous ceramic monoliths with bimodal porosity and high strength. Powder Technology, 2010, 201(3): 253-257. https://doi.org/10.1016/j.powtec.2010.04.004

[35] Product introduction of Maifan stone ball. https://www.ceramic-kouseki.com/product/62

[36] Product introduction of Maifan stone. https://www.ceramic-kouseki.com/product/419

[37] G. K. Batchelor. An Introduction to Fluid Dynamics. Cambridge University Press (1967) ISBN 0-521-66396-2.

[38] Manuscripts of Léonardo de Vinci (Paris), vol. N, folios 11, 67, and 74.

[39] B, David. ed., Edinburgh Encyclopaedia (Philadelphia, Pennsylvania: Joseph and Edward Parker, 1832, 10： 805–823.

[40] M. J. Clerk, S. J. William (1911). "Capillary Action". In Chisholm, Hugh (ed.). Encyclopædia Britannica. Vol. 5 (11th ed.). Cambridge University Press. 256-275.

[41] J. U. Lloyd, (1902) References to capillarity to the end of the year 1900, Archived 2014-12-14 at the Wayback Machine Bulletin of the Lloyd Library and Museum of Botany, Pharmacy and Materia Medica, 1 (4): 99-204.

[42] T. Young, (January 1, 1805) An essay on the cohesion of fluids, Archived 2014-06-30 at the Wayback Machine Philosophical.

[43] P. S. Laplace, T. M. Céleste, volume 4, (Paris, France: Courcier, 1805), Supplément au dixième livre du Traité de Mécanique Céleste, pages 1-79 Archived 2016-12-24 at the Wayback Machine.

[44] A. Einstein, (1901) "Folgerungen aus den Capillaritätserscheinungen" Archived 2017-10-25 at the Wayback Machine (Conclusions [drawn] from capillary phenomena), Annalen der Physik, 309 (3): 513-523.

[45] H. J. Kuepper, "List of Scientific Publications of Albert Einstein". Einstein-website.de.

[46] Introduction about dot-peen marking.

https://www.pannier.com/stamping/dot-peen/what-is-dot-peen-marking/

[47] Introduction about laser-marking.

https://www.manufacturingguide.com/en/laser-marking

[48] D. B. Hamilton, J. A. Walowit, C. M. Allen. A theory of lubrication by micro irregularities. Journal of Basic Engineering, 1966, 88(1): 177-185.

[49] J. Y. Zhang, Y. G. Meng. A study of surface texturing of carbon steel by photochemical machining. Journal of Materials Processing Technology, 2012, 212: 2133-2140. https://doi.org/10.1016/j.jmatprotec.2012.05.018

[50] D. Gropper, L. Wang, T. J. Harvey. Hydrodynamic lubrication of textured surfaces: a review of modeling techniques and key findings. Tribology International, 2016, 94: 509-529. https://doi.org/10.1016/j.triboint.2015.10.009

[51] I. Etsion, Y. Kligerman, G. Halperin. Analytical and experimental investigation of laser-textured mechanical seal faces. Tribology Transactions, 1999, 42 (3): 511-516. https://doi.org/10.1080/10402009908982248

[52] Q. Wang, D. Zhu. Virtual texturing: Modeling the performance of lubricated contacts of engineered surfaces. Journal of Tribology, 2005, 127 (4): 722-728. https://doi.org/10.1115/1.2000273

[53] A. A. G. Bruzzone, H. L. Costa, P. M. Lonardo, D. A. Lucca. Advances in engineered surfaces for functional performance. Annals of the CIRP, 2008, 57 (2): 750-769. https://doi.org/10.1016/j.cirp.2008.09.003

[54] K. Hirata, 2008. Hand finish processing. Nikkan Kogyo Shimbun. 56. (In Japanese)

[55] K. Ai, 2009. A point of hand finish processing. Nikkan Kogyo Shimbun. 7. (In Japanese)

[56] X. L. Chen, N. S. Qu, H. S. Li, Z. Y. Xu. Electrochemical micromachining of micro-dimple arrays using a polydimethylsiloxane (PDMS) mask. Journal of Materials Processing Technology, 2016, 229: 102-110. https://doi.org/10.1016/j.jmatprotec.2015.09.008

[57] Y. Shen, Y. T. Lv, B. LI, R. X. Huang, B. J. Yu, W. W. Wang, C. D. Li, J. J. Xu. Reciprocating electrolyte jet with prefabricated-mask machining micro-dimple arrays on cast iron cylinder liner. Journal of Materials Processing Technology, 2019, 266: 329-338. https://doi.org/10.1016/j.jmatprotec.2018.11.009

[58] Introduction about hand scraping. https://www.sakurai-net.co.jp/en/tool-6/

[59] A. Ghaei, M. Khosravi, M. Badrossamay, H. Ghadbeigi. Micro-dimple rolling operation of metallic surfaces. The International Journal of Advanced Manufacturing Technology, 2017, 93: 3749-3758. https://doi.org/10.1007/s00170-017-0790-3

[60] I. Etsion. State of the art in laser surface texturing. Journal of Tribology, 2005, 125: 248-253. https://doi.org/10.1115/1.1828070

[61] W. Slawomir, K. Waldemar, P. Pawel. Selected Methods and Applications of Anti-Friction and Anti-Wear Surface Texturing. Materials, 2021, 14 (12): 3227. https://doi.org/10.3390/ma14123227

[62] Y. Takashima, W. Natsu. Study on electrochemical machining of oil pockets on sliding surface with electrolyte suction tool. Procedia CIRP, 2016, 42: 112-116. https://doi.org/10.1016/j.procir.2016.02.203

[63] J. W. Byun, H. S. Shin, M. H. Kwon, B. H. Chu. Surface Texturing by Micro ECM for Friction Reduction. International Journal of Precision Engineering and Manufacturing, 2010, 11 (5): 747-753. https://doi.org/10.1007/s12541-010-0088-y

[64] W. D. Liu, Z. Luo, M. Kunieda. Electrolyte jet machining of Ti1023 titanium alloy using NaCl ethylene glycol-based electrolyte. Journal of Material Processing Technology, 2020, 283, 116731. https://doi.org/10.1016/j.jmatprotec.2020.116731

[65] Y. B. Zeng, H. J. Ji, X. L. Fang, Y. F. Wang, N. S. Qu. Analysis and Reduction of Stray-Current Attack in Reciprocated Traveling Wire Electrochemical Machining. Advances in Mechanical Engineering, 2014, 6: 11-21. https://doi.org/10.1155/2014/505932

Acknowledgements

This thesis is a summary of the research results accomplished in Natsu Laboratory at Tokyo University of Agricultural and Technology from 2019 to 2022.

Foremost, I would like to express my sincere gratitude to my supervisor, Prof. Wataru Natsu, for the continuous support of my Ph.D. study, and research, for his greatest supervision, motivation, and encouragement. I greatly appreciate his immense knowledge and serious attitude to research and his assistance in writing papers and this thesis. His attitude to the research work will be an example in my whole life, and prompt me to try my best to do any research mission well in the future.

Great thanks to Assitant Prof. Shuhei Kodama, Ms. Minako Sano, and everyone in Natsu Laboratory for their kind advice on my research at the research meeting and my entertainment life.

Besides, I would like to thank the other members of my thesis committee: Prof. Hiroyuki Sasahara, Prof. Keichi Nakamoto, Prof. Toshihiko Kuwabara, and Associate Prof. Kentaro Iwami from the Tokyo University of Agricultural and Technology for their kindness in taking the time out from their busy schedule and their insightful comments and valuable questions to the thesis.

I must acknowledge Prof. Hiroshi Iizuka, my supervisor during my master period in Yamagata University. I also need to thank Prof. Takahisa Masuzawa and Prof. Masanori Kunieda for their suggestions for my research in the conferences.

Sincerely thanks for scholarships, including the Tohoku Mirai scholarship from Yonezawa Kougyokai, JEES scholarship from Japan Educational Exchanges and Services, Yoneyama Rotary scholarship from Rotary International District 2800 Yamagata and Yonezawa Chuo Rotary Club, FLOuRISH Support for Pioneering Research Initiated by the Next Generation from Tokyo University of Agricultural and Technology, to let me finish my study and research. And thanks to the support for our research from JKA (the Japan Keirin Autorace Foundation) and its promotion funds from KEIRIN RACE.

At last, I would like to thank my parents: Yinhai Wang and Pingxia Hu, my elder sister: Yue Wang, and everyone who loves me and who I love for their great love and support throughout my life.

Published papers related to this dissertation

Peer-reviewed Journal Paper

1) J, K, Wang. W, Natsu. Mechanism and characteristics of electrochemical machining using electrolyte absorbed in solid porous ball. Precision Engineering, 2022, 7: 307-319. https://doi.org/10.1016/j.precisioneng.2022.06.012

2) J, K, Wang. W, Natsu. Stray-corrosion-free dimple texturing through electrochemical machining with an electrolyte absorbed in a porous solid ball, Journal of Manufacturing Processes. (Submitted)

3) 王 建康、夏 恒: 多孔質ボールによる電解液領域制限の電解加工法の実用化に向けた検討, 電気加工学会誌、2022. (Submitted)

International Conference Paper

Peer-reviewed International Conference Paper：

1) Jiankang Wang, Wataru Natsu: Investigating characteristics of electrochemical machining through electrolyte absorbed with porous solid material, Proceedings of 21st International Conference and Exhibition, pp.169-172, 2021.

2) Jiankang Wang and Wataru Natsu: Pattern machining by using the electrochemical machining through electrolyte absorbed with porous material, Proceedings of the 10th International

Conference on Leading Edge Manufacturing in the 21st Century (LEM21), pp.313-317, 2021.

3) Jiankang Wang and Wataru Natsu: Simulation and verification of electrochemical machining with electrolyte collected and confined by a porous solid ball, the 18th International Symposium on Electrochemical Machining Technology (INSECT), 2022. (Submitted)

International Conference Paper without Peer-review：

1) Jiankang Wang, Wataru Natsu: Exploratory study about limitation of electrolyte contact area by using porous solids in ECM process, Proceedings of 6th Symposium for International Cooperation on Micro and Precision Electrical Machining (SICMPEM), pp.43-46, 2021

2) Jiankang Wang, Wataru Natsu: Design and application of electrochemical machining through electrolyte absorbed with porous solid ball, Proceedings of International Workshop on Non-traditional Machining 2022, pp.37-40, 2022.

Domestic Conference Paper

1) 王 建康、夏 恒: Exploratory study about limitation of electrolyte contact area by using porous solids in ECM process, 2020 年度精密工学会秋季大会学術講演会講演論文集、pp.210-211, 2020. https://doi.org/10.11522/pscjspe.2020A.0_210

2) 王 建康、夏 恒: Influence factors of the ECM process by using Maifan stone balls to limit the electrolyte distribution areas, 電気加工学会全国大会（2020）講演論文集、pp.53-56, 2020.

3) 夏 恒、王 建康：保水性材料の利用による液域限定電解加工に関する研究、電気加工技術, 2021, 45 (139), 1-7.

4) 王　建康、夏　恒：Elucidation of machining mechanism of ECM through electrolyte absorbed with porous solids、2021 年度精密工学会秋季大会学術講演会講演論文集、pp.512-513, 2021. https://doi.org/10.11522/pscjspe.2021A.0_512

5) 遠部 多聞、王　建康、小玉 脩平、夏　恒：保水機構を有する液域限定電解加工の加工持続性に関する研究、2021 年度精密工学会秋季大会学術講演会講演論文集、pp.508-509, 2021. https://doi.org/10.11522/pscjspe.2021A.0_508

6) 王　建康、夏　恒：Study on ECM of oil pocket by using a porous solid ball as the electrolyte absorption material、2022 年度精密工学会春季大会学術講演会講演論文集、pp.435-436, 2022. https://doi.org/10.11522/pscjspe.2022S.0_435

7) 王　建康、夏　恒：Metal marking by using stray-corrosion-free ECM method with a porous solid ball used as the electrolyte absorption material、2022 年度精密工学会秋季大会学術講演会講演論文集、 pp.10-11, 2022.

8) 王 建康、夏 恒: 多孔質ボールによる電解液領域制限の電解加工法の実用化に向けた検討, 電気加工学会全国大会（2022）講演論文集、2022. (Submitted)